2006

Remote sensing of montane forest structure and biomass : a canopy relectance model inversion approach

Soenen, Scott

Lethbridge, Alta. : University of Lethbridge, Faculty of Arts and Science, 2006

REMOTE SENSING OF MONTANE FOREST STRUCTURE AND BIOMASS: A CANOPY REFLECTANCE MODEL INVERSION APPROACH

SCOTT SOENEN
BSc.(Honours), University of Lethbridge, 2003

A Thesis
Submitted to the School of Graduate Studies
of the University of Lethbridge
in Partial Fulfillment of the
Requirements for the Degree

MASTER OF SCIENCE

Department of Geography
University of Lethbridge
LETHBRIDGE, ALBERTA, CANADA

ABSTRACT

The multiple-forward-mode (MFM) inversion procedure is a set of methods for indirect canopy reflectance model inversion using look-up tables (LUT). This thesis refines the MFM technique with regard to: 1) model parameterization for the MFM canopy reflectance model executions and 2) methods for limiting or describing multiple solutions. Forest stand structure estimates from the inversion were evaluated using 40 field validation sites in the Canadian Rocky Mountains. Estimates of horizontal and vertical crown radius were within 0.5m and 0.9m RMSE for both conifer and deciduous species. Density estimates were within 590 stems/ha RMSE for conifer and 310 stems/ha RMSE for deciduous. The most effective inversion method used a variable spectral domain with constrained, fine increment LUTs.

A biomass estimation method was also developed using empirical relationships with crown area. Biomass density estimates using the MFM method were similar to estimates produced using other multispectral analysis methods (RMSE = 50 t/ha).

ACKNOWLEDGEMENTS

I would like to acknowledge the people and institutions that have given their support during this research project:

I would like to thank my thesis supervisor, Dr. Derek Peddle, who provided support, encouragement and many very unique opportunities throughout the course of my program. Working with Derek has been a very intellectually stimulating and rewarding experience. I would like to thank Dr. Craig Coburn, whose door was always open when I had questions and who was always happy to kick around an idea. I would also like to thank Dr. Ronald Hall who provided essential guidance during the field component of this study and whose comments and ideas have greatly improved the direction of the thesis.

I also gratefully acknowledge Dr. Danielle Marceau who provided commentary and helpful final suggestions for the thesis.

I would also like to acknowledge my field assistants, Sam Lieff (2003) and Adam Minke (2004). Their skill, perseverance, and capacity to carry the larger pieces of equipment in the field were invaluable. I would also like to thank all of the support staff, in particular Judy Buchannan-Mappin and Kristin Yaehne, at the University of Calgary Kananaskis Field Stations (Barrier Lakes) who provided lodging and support.

This research was generously supported by grants held by Dr. Derek Peddle from NSERC (Operating and Equipment), the Alberta Ingenuity Centre for Water Research (AICWR), the Prairie Adaptation Research Collaborative (PARC), the Water Institute for Semi-arid Ecosystems (WISE), Natural Resources Canada and the Alberta Research Excellence program, and this research has contributed to those funded research programs. Additional financial support was made available through the School of Graduate Studies and the Dean of Arts and Science at the University of Lethbridge.

Computing resources were supplied by the Department of Geography and Department of Mathematics and Computer Science at the University of Lethbridge and the Westgrid high performance computing collaborative (www.westgrid.ca).

TABLE OF CONTENTS

LIST OF FIGURES

LIST OF TABLES

LIST OF EQUATIONS

CHAPTER 1

Introduction

1.1 Introduction

Forests play a critical role in the global climate owing to the atmospheric-biospheric exchange of carbon and energy. Quantifying forest stand physical structure and carbon stored within forested areas is important as it contributes to sustainable development strategies in countries committed to international protocols such as the Kyoto Protocol stemming from the Intergovernmental Panel on Climate Change (UNFCCC, 1997). Carbon in forests is constantly in flux in the form of carbon dioxide (CO_2) through natural and anthropogenic processes (Dong et al, 2003). Canada, for example, contains about 310.1 Mha of forest lands, approximately 10% of the global total (Natural Resources Canada, 2006). Of this area, 293 Mha may potentially be used for commercial forest activities and between 1 Mha and 2 Mha has been reported burned each year in the past three years (Natural Resources Canada, 2005; 2006).

Determining the amount of stored carbon within Canada's forested land is a complex process that requires, among other things, accurate estimates of aboveground biomass (Brown, 2002). Aboveground biomass carbon stocks, and their temporal dynamics, are of interest in the context of afforestation, reforestation, and deforestation (ARD) and the clean development mechanism (CDM) within articles 3.3 and 12 of the Kyoto protocol (Rosenqvist et al., 2003). There is currently an interest in remote sensing methods for forest inventory and biomass estimation as these data could provide systematic, repetitive observation at local to global scales, as well as archived data well

before the 1990 Kyoto baseline (Patenaude et al., 2005). Furthermore, given the volume of forests and inaccessibility of some forested areas, remote sensing estimates are the only practical means of assessment. These fundamental advantages become very important when considering the data needs of global climate change research.

This research builds on the lineage of past success with canopy reflectance model and remote sensing data integration to produce estimates of forest structural parameters including biomass and volume (Peddle et al. 2003c; Pilger, 2002; Peddle et al., 1999; Wu and Strahler, 1994). Canopy reflectance modelling produces estimates of reflectance based on an abstraction of the biophysical properties of the canopy (Strahler, 1997). Geometric-optical (G-O) canopy reflectance models are particularly useful within a biomass estimation context as they use a simplified three dimensional, crown level abstraction of the canopy and can provide a linkage between physical forest stand structure and satellite image spectral response. The satellite image to G-O canopy reflectance model link is based on the premise that image pixel-level reflectance is influenced by three primary spectral components in forest images: sunlit canopy, sunlit background and shadow. The abundance of each component within a pixel is directly related to the physical structure and density of the trees on the ground and can be modeled using G-O canopy reflectance models. Thus, the reflectance data within the imagery can be related to physical structure through the model. If the average physical structure of a forest stand can be estimated, then it is also possible to estimate forest biomass density and total biomass, as biomass will be a function of the physical dimensions of the stem and canopy, and biomass density will be a function of physical dimensions of individual trees and stand density (Parresol, 1999).

A significant part of this research dealt with the improvement and application of G-O modelling methods including the Multiple-Forward-Mode (MFM), an indirect inversion method for complex models where mathematical inversion is impossible or requires excessive computation (Peddle, 1999). Two significant new features have been added to the MFM application base, which already includes physical parameter estimation and classification (Peddle et al., 2006), stand volume estimation (Pilger et al., 2005), and topographic correction (Soenen et al., 2005). The first new feature was a suite of procedures for dealing with multiple solutions to the indirect inversion problem, where the MFM procedure returns multiple matches (§ 3.6.4). The second new feature was an integrated pixel-level biomass density estimation procedure (§ 3.6.5) based on MFM estimates of forest stand structure. The biomass calculation was based on empirical models relating biomass to crown surface area for tree species native to the study area. This estimation procedure is presented here as another unique test application of the MFM canopy reflectance model inversion method.

1.2 Research Objectives

The primary research objectives for this thesis were twofold. The initial primary objective was to create a method for estimation of primary stand-level biophysical parameters based within the existing MFM indirect inversion framework using moderate spatial resolution (>10m) satellite imagery. To apply this method at the regional scale, it needed to conform to the following criteria: 1) the method must be highly automated; 2) it must be applicable over variable topography; 3) it should not be sensor-specific; 4) it must utilize pre-defined empirical biomass models; 5) it should require minimal *in situ*

structural data. However, to realize this goal it was necessary to first identify the extent to which uncertainty and the potential for multiple solutions affect the outcome of the inversion. It was also necessary to develop a set of methods to reduce the multiple solutions to a single solution set that could be used in the subsequent biomass estimation application.

A two-stage validation was necessary to evaluate these primary objectives. In the first stage, the combination of structural parameters that constituted the solution to the inversion problem was compared to field measured parameters for 40 forest stand test plots within the study area. In the second stage, the biomass density predicted using the canopy reflectance model-based method was compared to stand-level biomass predicted using the field data collected at the 40 forest stand test plots. The efficacy of the canopy reflectance model-based method was compared against two other multi-spectral biomass estimation methods using empirical relationships with satellite image derivatives (spectral mixture analysis endmember fractions and vegetation indices).

Two secondary objectives were identified: 1) to evaluate of the ability of the canopy reflectance model to predict pixel level reflectance, and 2) to further refine the MFM processing suite. The first objective included a test of the fundamental assumption of any model inversion is that there is a connection between the radiative-transfer assumptions within the model and the observable result of those principles in reality. The second involved creation of a proven, rigorous "black-box" method for use in future studies. This required the transition of the MFM indirect inversion stage from a hands-on, query method to automated software. This black-box method is a first step towards

creating a method that can be adapted for use in forest inventory or for application within the forest industry.

An ancillary objective for this study was to increase the knowledge base for the Kananaskis study area by measuring new field parameters and increase the spatial extent of the study area from the 75km^2 covered in previous field campaigns (Pilger, 2004). By increasing the spatial extent, more topographic and canopy physical structural variability may be added to the data set.

1.3 Thesis Structure

This thesis is organized into six chapters beginning with this chapter, where the thesis and research objectives have been introduced. The second chapter includes a review of the pertinent literature regarding the subjects of global climate change and the carbon cycle, field mensuration, allometric theory, remote sensing principles, preprocessing methods for rugged terrain, canopy reflectance models, reflectance model inversion, and current methods for obtaining biomass using remote sensing analysis techniques.

The third chapter begins with a description of the study area, field data, and image data set. A description of all data pre-processing used in this research follows. Next, the canopy reflectance model methods and indirect inversion are described, including a summary of software created for the inversion. Following this, Image-based biomass estimation procedures are discussed including the canopy reflectance based method, spectral mixture analysis based methods, and empirical methods using vegetation indices.

The fourth chapter contains results from the canopy reflectance model inversion for canopy structure. The indirect inversion estimates of primary canopy structural parameters are presented according to the procedure used for refining the multiple solutions. The problem of multiple solutions is quantified for a number of field sample plots.

The fifth chapter includes a description of a new application of the MFM inversion method for estimating forest biomass density. Estimates of biomass density from MFM inversion are compared to estimates produced using empirical relationships between satellite image derivatives and measured structural information. Finally, the biomass density estimates are compared to field estimates. The predictive accuracy of each technique is critically compared and discussed.

The final chapter includes major conclusions drawn from the research. Specific advantages of the methods presented within this thesis are highlighted along with contributions to biomass estimation research and canopy reflectance model indirect inversion research. Suggestions for future research are presented within the areas explored by this thesis.

CHAPTER 2

Literature Review

2.1 Introduction

Literature pertaining to the topic of satellite image analysis and the use of remote sensing data for forest stand structure and biomass estimation is reviewed in this chapter. A brief treatment of global climate change, the carbon cycle and forest management sets the context for the current study. A review of forest mensuration and satellite image data pre-processing provides background on many methods used in the thesis methodology. The linkage between digital imagery and modeled canopy reflectance and inversion methods similar to those used in this research are discussed focusing on the geometric optical mutual shadowing model (GOMS). Biomass estimation techniques are reviewed, including those that use canopy reflectance model outputs, to provide a comparison and background for subsequent chapters where a new biomass estimation method is presented. While a number of these biomass estimation techniques do not use multi-spectral satellite image inputs and are not tested within this study, they are still reviewed here to note their availability.

2.2 Global Climate Change, the Carbon Cycle, and Monitoring

2.2.1 Global Climate Change and the Carbon Cycle

Climate change is considered one of the most pressing issues facing society today (Butler and Schiermeier, 2005). Average global temperatures are projected to increase between 1.0 and 4.5 °C under a projected doubling of atmospheric CO_2 (Stennes et al.,

1998). The increase in global temperature is attributed to the greenhouse effect, where GHGs reflect outgoing radiation back to the earth surface. It is generally accepted that there is an increase in GHG release, in particular CO_2, as a result of anthropogenic disruption of the natural carbon cycle. Some studies predict that atmospheric CO_2 levels could increase from present levels of about 370 ppm to as much as 700 ppm in the next 100 years (Malhi et al., 2003).

Forests factor highly in the carbon cycle as they have the potential to sequester significant amounts of CO_2 through photosynthesis and release significant amounts of CO_2 through deforestation and fire. For example, Canadian boreal forest biomass, and soil contain approximately 15% (200 Pg) of the total C stored in the terrestrial biosphere (Banfield et al., 2002). Sequestration of C is directly related to the rate of photosynthesis and respiration. These two processes control the rate at which C is stored as biomass in the form of carbohydrates (Malhi et al., 2003). Studies have also shown that there is an increase in standing, soil, and litter biomass in temperate forests. As a result, it has been suggested that there exists a total sink of 1.2PgC yr^{-1} for temperate forest (Malhi et al., 2003). This storage accounts for a substantial part of the total terrestrial carbon sink (3.2PgC yr^{-1}). In the short term it is likely that anthropogenic CO_2 emission will increase. Therefore, it is important to try to mitigate these effects through monitoring and responsible management of forested areas.

2.2.2 Forest Monitoring and Climate Change

While the link between anthropogenic CO_2 emissions and climate change has not yet been definitively established, many governments have taken steps to mitigate emissions (UNFCCC, 1997). To do so it is necessary to measure and report the amount of

stored carbon within forested areas as forest sequestration potential has a direct influence on emissions allowances. Canada has ratified the Kyoto protocol, an amendment to the United Nations Framework Convention on Climate Change (UNFCCC). By ratifying this protocol, Canada has committed to reduce emissions of carbon dioxide and other GHGs so that the collective emissions are cut by 5.2% compared to the baseline year of 1990 (UNFCCC, 1997). The overall goal of this protocol is to stabilize GHG concentrations in the atmosphere at a level that prevents anthropogenic interference with the climate system (UNFCCC, 1997). To ensure that this goal is achieved it is necessary to monitor GHG emissions as well as sequestration potential of carbon stores, including live biomass in forests.

An increasing number of tools have become available for monitoring biomass and canopy structural conditions in forests, including remote sensing techniques and methods involving geographic information systems (GIS). These tools allow for two critical activities to be completed. The first is to establish a baseline level of carbon stocks for 1990, the Kyoto Protocol baseline year. The second is to monitor changes in land use through ARD (Patenaude et al., 2005). Remote sensing and GIS tools can be used in an estimation context as well as a validation context (Rosenqvist et al., 2003; Patenaude et al., 2005). To ensure that remote sensing and GIS-based estimates are accurate it is important to validate the estimates using forest mensuration.

2.3 Forest Mensuration and Allometry

Forest mensuration, in a broad sense, deals with the determination of dimension, form, weight, volume and age of trees or stands of trees as well as other variables that

relate to forest, wildlife, and watershed management (Helms, 1998; Husch et al., 2003). Within the context of carbon stock estimation and canopy modelling, the primary mensurational parameters are height, canopy size, diameter at breast height (DBH), and stand density (Li and Strahler, 1992; Fournier et al., 2003; Peddle et al., 2003b). These first order parameters can be related to tree and stand volume and standing biomass via allometric transforms (Parresol, 1999; Peng, 2001). These measures of volume and mass are directly related to the carbon storage potential of a given tree or stand of trees.

2.3.1 Height

Tree height, or the distance along the axis of the tree stem between the ground and top of the tree, is a critical parameter in the assessment of tree biomass. The distribution of heights within a particular area and height to the center of the tree crown are also important input parameters for canopy reflectance models (Li and Strahler, 1992). Total height can be measured using a number of techniques. In-situ measurements of height, such as those conducted in this study, typically rely on distance and angle measurements taken with a hypsometer, clinometer, or laser range finder. The height of a tree (h) is obtained from the tangent of the inclination angle (α_1) to the top of the tree and declination to the base of the tree (α_2) at a set horizontal distance (d) (Husch et al., 2003):

$$h = d(\tan \alpha_1 + \alpha_2) \qquad \text{(Equation 2.1)}$$

Tree height has also been estimated from aerial photographs through differential parallax and using the relationship between height and the measurement of shadow length at a known solar zenith angle (Avery and Berlin, 1985). A third, more economical height estimation technique involves the inversion of canopy reflectance models as discussed in a later section (§2.5.2).

2.3.2 Crown and Bole Dimensions

Canopy size and DBH are typically measured directly in the field. Crown diameter and area are measured using the average of the diameter of the crown at the widest point and a measurement at a right angle to the first measurement (Husch et al., 2003). The horizontal extent of the crown can be determined by using a vertical-looking device like a right angle densiometer or observing the extent of leaf or needle litter (drip-line). DBH is measured using either calipers or measuring tape around the bole at a height of 1.3m above ground (Bond-Lamberty et al., 2002; Snell and Brown, 1978). The measuring tape most commonly used by foresters is at intervals of π units, permitting direct readings of diameter (Husch et al., 2003).

2.3.3 Density

Stand density is usually described as the number of trees, basal area, or volume per unit ground area (Husch et al., 2003). Stand density is related to crown closure (CC), or the vertical projection of crown area per unit ground area (Rudnicki et al., 2003). Crown closure can be estimated using a number of techniques, the most predominant being point estimates using a spherical densiometer (Buckley et al., 1999; Bunnell and Vales, 1990) or hemispherical photography (Frazer et al., 2001). However, there can be bias and significant differences between estimation techniques due to differences in the area sampled resulting from the basic geometric principles of the technique in question (e.g. the hemispherical projection). In general, the crown closure estimate will increase with increasing viewed area in a point sample (Bunnell and Vales, 1990). Estimates of crown closure using optical devices may also be affected by topography in a manner similar to the effect of topography on LAI estimation (Walter and Torquebiau, 2000). For example, a uniform slope of 54° can obscure 30% of the viewing hemisphere for a

hemispherical photography system. In this case, vegetation will also appear denser upslope and less dense downslope. Estimates of crown closure using optical devices will also be dependant upon sky and illumination conditions, camera type, and image storage and analysis methods (Frazer et al., 2001).

2.3.4 Allometry

Allometric functions rely on the simple presumption that the size or proportion of one aspect of an organism can be correlated with the proportion of other constituent parts (Gould, 1966). Allometric relationships can be applied to all organisms and are thought to be related to the capacity for essential materials transported through branching networks (West et al., 1997). The most pertinent example of this principle is the vascular system of free standing plants. As the plant grows vertically, or as leaf diameter increases, the plant requires more stem diameter and volume to contain the vascular system that supports this growth. Thus, it is possible to relate volume, and subsequently, mass to simple biophysical parameters like height and DBH.

2.3.5 Forest Biomass

Forest biomass is the mass of organic material, live or dead, from root tips to leaf or needle tips (Singh, 1982). In the above ground component, biomass is often divided into woody, bole, or stem biomass and foliage biomass (Kaufmann and Troendle, 1981; Singh, 1982). There are also below ground components including root biomass and soil biomass. These variables are difficult, or impossible, to retrieve with remote sensing methods and, therefore, are outside of the scope of this study. Stand biomass is an aggregation of the above ground biomass for all individual trees within the stand (Parresol, 1999). Biomass density is the total stand biomass per unit area. In forestry, the

basic management unit is biomass density (e.g. Mg/ha) at the forest stand. This study focuses on aboveground biomass density.

2.3.6 Stand Level Biomass Prediction

Individual tree biomass prediction equations have generally been based upon one of the following general regression models: linear (additive error) and non-linear (additive error and multiplicative error). These models commonly utilize DBH, DBH^2, height (h), $DBH^2 \cdot h$, diameter at the base of live crown and sapwood area or combinations of these variables (Kendall Snell and Brown, 1978; Kaufmann and Troendle, 1981; Paressol, 1999; Bond-Lamberty et al, 2002; Hall et al., 2006). These variables are related via one of the aforementioned regression models with the mass of harvested tree components.

The most used and accurate models for tree species of the front range of the Canadian Rocky Mountains are of the log-linear form (Hall et al., 2006). Often, biomass exhibits a non-linear relationship with tree structure parameters, so it is useful to transform nonlinear relationships into a form where equation parameters can be estimated using a least squares procedure. When using an equation of this form for prediction, it is important to remember that converting to arithmetic units using the anti-logarithm can result in a systematic underestimation of biomass (Baskerville, 1971). Thus it is necessary to apply a correction factor based on skewness of the arithmetic distribution of biomass.

It is also important to record and deal with error whenever developing biomass prediction models. Error can be introduced due to measurement, model form, parameter estimation, and spatial variation. Woods et al. (1991) showed that, the most significant

error sources were due to spatial variability and fitting of regression model parameters. They recommend that error analysis be used to determine the most effective way to increase model precision.

2.4 Remote Sensing Theory and Pre-processing Methods

2.4.1 Radiometric Calibration

Radiometric calibration is traditionally based upon a fundamental model, referred to as the Sun-Terrain-Sensor model (STS) (Hugli and Frei, 1983; Colwell, 1983). The STS model represents radiation interaction as a function of incident solar irradiance (E_0), and reflective properties and orientation of the surface. The incident solar irradiance may also be scattered and attenuated by atmospheric effects and is generally not equivalent to the irradiance incident on a target. The irradiance incident upon a target is in fact a combination of two components, the direct irradiance component and the diffuse irradiance component.

The direct irradiance component can be given as the total incident solar irradiation (E_0), moderated by an atmospheric attenuation factor (T_{a0}), and multiplied by the cosine of the incidence angle relative to the terrain surface to account for foreshortening effects (θ_{i0}) (Hugli and Frei, 1983).

$$E_D = E_0 \, T_{a0} \cos\theta_{i0} - E_A \qquad \text{(Equation 2.2)}$$

The diffuse atmospheric irradiance component is composed of light reflected from atmospheric particles and is considered a hemispherical source of illumination. The diffuse irradiance component can be mathematically represented as:

$$E_A = \sigma^{2\pi}_{\phi=0}\sigma^{\pi/2}_{\theta=0} L(\theta_0, \theta, \phi)(\cos\theta_i)(\sin\theta)(d\theta)(d\phi) \qquad \text{(Equation 2.3)}$$

Where $L(Z_0, Z, \phi)$ is the downward radiance from the direction defined by the zenith angle and azimuth, θ and ϕ are zenith and azimuth angles respectively and θ_0 is the sun elevation angle (Temps and Coulson, 1977; Kimes and Kirchner 1981; Proy et al., 1989). This expression, however, does not fully explain the interactions in areas of moderate to high relief, as the diffuse solar irradiance does not originate from a proper hemisphere.

A diffuse terrain component (E_T) must also be considered. This component originates from diffuse and direct solar radiation that is reflected from a terrain element to the target. A calculation of radiance received by a target M from a point P is given by Proy et al (1989) as:

$$E_T = L_{PM} = (L_P \, dS_M \cos T_M \, dS_P \cos T_P)/r^2_{MP} \qquad \text{(Equation 2.4)}$$

Where dS_M and dS_P are the areas of the target pixel, point M, and point P respectively, T_M and T_P are the angles between the terrain normal and the line MP, L_P is the luminance of P, and r^2_{MP} is the squared distance of line MP. This computation relies upon a Lambertian surface assumption that has been shown to be invalid for most montane cover types (Teillet et al., 1982; Meyer et al. 1993). The total irradiance incident on a pixel is essentially a combination of the direct and diffuse components mentioned previously.

The terrain component of the STS model can be regarded as a combination of the target orientation as well as its inherent reflective characteristics. Most terrain correction methods require the use of a digital elevation model (DEM), or digital terrain model (DTM) to compute the slope and aspect for a given pixel. The slope and aspect of a pixel are used to calculate the surface normal and consequently the angle of incidence of solar irradiance. This angle of incidence θ_I can be calculated using the equation:

$$\cos \theta_I = \cos\theta \cos\alpha + \sin\theta \sin\alpha \cos\varphi \qquad \text{(Equation 2.5)}$$

where α and φ are the target slope and relative azimuth between the slope aspect and solar azimuth respectively (Gu and Gillespie, 1998).

The radiometric signal received at a sensor is also dependant on the reflective properties of a surface. The reflectance of a target is wavelength dependant, and is also dependant upon physical structure and texture (Hugli and Frei, 1993; Schaff et al. 1994). A surface is occasionally assumed to have isotropic reflectance behavior when computational efficiency is a priority. Isotropic (Lambertian) reflectance assumes that light incident on a horizontal surface will be reflected equally in all directions. In reality, most natural surfaces have a preferred direction of scattering, and are termed anisotropic reflectors. Anisotropic reflectance can be described by the Bi-directional Reflectance Distribution Function (BRDF). Montane ground cover generally exhibits anisotropic reflectance due to complex physical structures that yield a complex BRDF (Abuelgasim and Strahler, 1994; Schaaf and Strahler, 1994). Interest in characterizing forest BRDF led to the development of canopy BRDF G-O models (Li and Strahler, 1985; 1986) that were subsequently refined into the GOMS mode used in this study (Li and Strahler, 1992).

2.4.2 Topographic Correction

Topographic correction of remotely sensed imagery received considerable attention in the early 1980s through the development of a variety of photometric techniques (Smith et al., 1980; Justice et. al, 1981; Kimes and Kirchner, 1981; Teillet et al., 1982; Hugli and Frei, 1983; Civco, 1989). These methods were applied and tested in a series of studies that followed (Meyer et al., 1983; Proy et al., 1989; Itten and Meyer, 1992; Conese et al., 1993; Ekstrand, 1996; Colby and Keating, 1998; Tokola et al.,

2001;), however, no fundamentally new approaches were forthcoming until the introduction of a physical-structural basis to topographic correction by Gu and Gillespie (1998) for forested terrain, variations to that approach (Gu et al., 1998; Johnson et al., 2000; Peddle et al., 2003a) and follow-up studies (Soenen et al., 2003, 2005).

2.4.2.1 Cosine Correction

By applying a simple photometric function, a reduction in the topographically induced variation can be partially realized (Teillet et al., 1982). The cosine correction (Justice et al., 1981) is one such approach that, in the case of illumination not originating from the zenith, normalizes the reflectance of any pixel based on the assumption that the total irradiance received at a pixel is directly proportional to the cosine of the incidence angle (i) (defined as the angle between the normal to the pixel surface and the solar zenith direction (Teillet et al., 1982)) as:

$$L_n = L \frac{\cos \theta}{\cos i} \qquad \text{(Equation 2.6)}$$

where L_n is the normalized reflectance, L is the uncorrected reflectance, and θ is the solar zenith angle (SZA). However, areas that are weakly illuminated by direct irradiance can still receive a considerable proportion of diffuse radiation and are therefore brightened excessively by the cosine correction (Kimes and Kirchner, 1981; Proy et al., 1989; Meyer et al., 1993, Conese et al., 1993).

2.4.2.2 Minnaert Correction

The cosine correction relies upon the Lambertian assumption (perfectly diffuse reflector), which is not applicable to most natural surfaces (Teillet et al., 1982; Meyer et al., 1993). The Minnaert (1941) constant (k) has been used in topographic corrections to represent the extent to which a surface is non-Lambertian. The value of the Minnaert

constant will range from 0 (specular reflector) to 1 (Lambertian surface). The Minnaert constant k is applied to the cosine equation, as (Colby, 1991):

$$L_n = L\left[\frac{\cos\theta}{\cos i}\right]^k \qquad \text{(Equation 2.7)}$$

In several studies, the Minnaert correction has provided improved results compared to the simple cosine correction (Justice et al., 1981; Colby, 1991; Itten and Meyer, 1992; Meyer et al., 1993; Ekstrand, 1996; Colby and Keating, 1998; Tokola et al., 2001;).

2.4.2.3 Statistical Empirical Correction

Past studies have demonstrated that some correlation exists between the predicted illumination derived from a digital elevation model and the measured illumination of a target (Teillet et al., 1982; Meyer et al., 1993). Based on this correlation, a statistical approach can be used with a linear regression to correct or normalize observed data:

$$L_n = L - \cos i\, b - a + L_{avg} \qquad \text{(Equation 2.8)}$$

where L_n is the normalized radiance, a and b are the y-intercept and slope of the regression line, respectively, and L_{avg} is the average of the measured radiance data. The rotation of the data makes an object's radiance independent of cos *i*. While this technique is dependent on the strength of the correlation between modeled and measured illumination, it has provided image corrections similar to the Minnaert correction (Meyer et al., 1993).

2.4.2.4 C - Correction

Teillet et al. (1982) proposed the addition of a semi-empirical moderator (C) to the cosine correction. Based on an examination of image data, a linear relationship exists between L and cos *i* in the form:

$$L = a + b\cos(i) \qquad \text{(Equation 2.9)}$$

The parameter C is a function of the regression slope (b) and intercept (a):

$$C = \frac{a}{b} \qquad \text{(Equation 2.10)}$$

and is introduced to the cosine correction model as an additive term:

$$L_n = L \frac{\cos \theta + C}{\cos i + C} \qquad \text{(Equation 2.11)}$$

The parameter C is said to be analogous to the effects of diffuse sky irradiance, although the analogy is not exact (Teillet et al., 1982). The C correction has been shown to retain the spectral characteristics of the data and improve overall classification accuracy in areas of rugged terrain (Meyer et al., 1993; Riano et al., 2003).

2.4.2.5 SCS Correction

The SCS correction improves on the cosine correction by normalizing the illuminated canopy area, which is one of the main factors contributing to pixel level reflectance in forested scenes (Gu and Gillespie, 1998, 1999; Dymond and Shepard, 1999). The SCS correction is equivalent to projecting the sunlit canopy from the sloped surface to the horizontal, in the direction of illumination (Figure 2.1). Assuming that the reflected radiation from the sunlit canopy is largely independent of topography due to the geotropic (vertical) nature of tree growth, the integrated reflectance from the sunlit canopy is proportional to its area:

$$L_n = L \frac{\cos \alpha \cos \theta}{\cos i} \qquad \text{(Equation 2.12)}$$

where a is the terrain slope (Gu and Gillespie, 1998). By formulating the SCS model to be as generally applicable as possible, the effect of diffuse irradiance is neglected resulting in overcorrection for slopes facing away from the source of illumination.

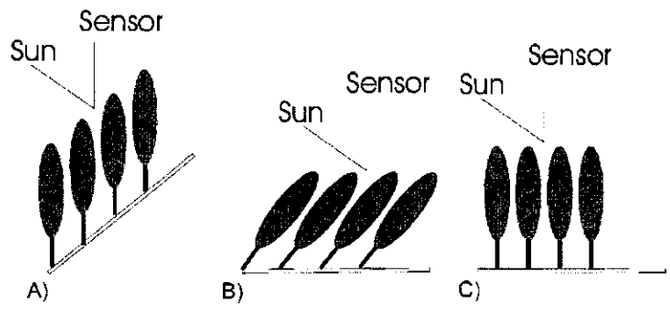

Figure 2.1 - Visual representation of sun terrain sensor (STS) geometry and sun-canopy sensor (SCS) geometry: a) forest stand on sloped terrain; b) STS: terrain rotated to horizontal with illumination geometry compensation based on photometric function; c) SCS: forest stand on horizontal terrain with forest structure and orientation preserved.

2.4.2.6 SCS+C Correction

The SCS+C correction includes the moderator C to account for diffuse irradiance but is set within the improved physical context of the SCS model. The formulation for this new SCS+C correction is:

$$L_n = L \frac{\cos \alpha \cos \theta + C}{\cos i + C} \qquad \text{(Equation 2.13)}$$

The parameter C was chosen due to its past success in moderating the cosine correction (Meyer et al., 1993; Riano et al., 2003) and also because of its computational simplicity (Teillet et al., 1982).

2.5 Forest Canopy Reflectance Modelling Methods

2.5.1 Canopy Reflectance Modelling

The intrinsic reflectance of a surface media such as a stand of trees can be characterized by a physical model of light scattering, interception and transmission through an abstraction of said media at a given view and illumination angle (Strahler et al., 1986). For the most part, computational canopy reflectance models can be separated

into three categories: Radiative Transfer (RT), Geometric-Optical (G-O), and hybrids of the two (Chen et al., 2000). These models are characterized by the level of abstraction of the media through physical principles. For example, RT models treat vegetation canopy as a randomly distributed assemblage of elements (Suits, 1972; Shabayanov, 2002), or turbid media (Knyazikhin and Marshak, 1991) which have fixed properties of reflectance and transmittance; whereas G-O models (Li and Strahler, 1985; Cavayas and Teillet, 1985) treat the canopy as an assemblage of discrete three dimensional objects (tree crowns) set on a spectrally contrasting background.

The G-O approach models illumination as a purely linear geometric phenomenon, ignoring diffraction and polarization (Chen et al., 2000). G-O models represent trees as simplified shapes such as cylinders (Jasinski and Eagleson, 1990), cones (Li and Strahler, 1985; Cavayas and Teillet, 1985), and spheroids (Li and Strahler, 1992). The model output is based on the area-weighted sum of the radiance of sub-pixel components of sunlit canopy (c), shadow (s), and background (b).

The Li-Strahler (1985) G-O model assumes a Poisson model random spatial distribution of cones at a user defined density (λ) with a log-normal height distribution (dh) on a spectrally contrasting background. It also assumes that the size of the modeled pixel is greater than the size of an individual cone. The model uses parallel-ray geometric calculations to determine the proportion of shadow cast on the ground. The reflectance of a pixel (ρ_{pix}) can then be calculated in forward mode as the sum of the reflectance of scene components sunlit canopy (ρ_c), sunlit background (ρ_b), and shadow (ρ_s) as weighted by their areas (A_c, A_b, A_s) within the pixel (Li and Strahler, 1985) where the reflectance values have been independently predetermined:

$$\rho_{pix} = (A_c\rho_c + A_b\rho_b + A_s\rho_s)/A \quad \text{(Equation 2.14)}$$

where A is the total pixel area. The ground-projected scene component areas for a tree crown with radius r are related to one another for a given θ and crown apex angle (τ):

$$A_c = (\mu/2 + (\sin^{-1}(\tan\tau / \tan\theta))r^2 \quad \text{(Equation 2.15)}$$

$$A_s = (\cot(\sin^{-1}(\tan\tau / \tan\theta))+(\sin^{-1}(\tan\tau / \tan\theta))+\mu/2)r^2 \quad \text{(Equation 2.16)}$$

$$A_b = A- (A_c + A_s) \quad \text{(Equation 2.17)}$$

In subsequent versions of the model, the ability to model the proportion of shadow cast on neighboring trees was included and the element shape was changed to a spheroid (Li and Strahler, 1992). This later version is referred to as the geometric optical mutual shadowing model (GOMS). The model also saw the input parameter list for forward mode runs increase to include vertical (b) and horizontal crown radius. The spheroid shape is generally applicable for conifer (prolate spheroid) and deciduous (oblate spheroid) species (Li and Strahler, 1992). As a result of the additions, it became possible to model the preferential obscuring of adjacent crowns and crown shadows to properly depict the BRDF "bowl-shape" effect at large solar zenith angles. The model also includes a representation of the "hotspot" effect, where the view angle and illumination angle are similar and the visible portions of the scene are not shadowed (Li and Strahler, 1986).

The effect of topography on the areal abundance of scene components within a forested scene was included in a later version of the model (Schaff et al., 1994). In a forested scene, topography will cause the projected area of shadow to be elongated or shortened as it is projected on a sloped surface (Soenen et al., 2003; 2005). Mutual shadowing between crowns will also be altered. Upslope crowns facing the direction of

illumination receive more illumination as they remain geotropic and are raised above downslope canopy as slope increases. To account for this, the spheroids are transformed into spheres which project the equivalent shadow area and the scene is converted to slope coordinates where the z-axis is the slope normal. The illumination geometry inputs are then recalculated for the slope coordinate system. Woodcock et al. (1997) also included a brightness correction for the background component based on the cosine of incidence. The sunlit canopy spectral value is not corrected as its position in coordinate space is topographically invariant (i.e. it is always aligned with gravity).

2.5.2 Canopy Reflectance Model Inversion

Canopy reflectance models are useful because they provide the linkage between biophysical structure of the forest overstory and its spectral response recorded by a satellite or airborne imaging system. Canopy models are capable of providing information about species type, physical dimensions, and leaf area through inversion. There are two types of model inversion: direct and indirect. Direct inversion typically involves the use of an optimization algorithm to minimize the difference between image reflectance and model reflectance (Kimes et al., 2000). Typically, a canopy reflectance model is formulated such that the spectral response for a given band (L_λ) is a function (f) of θ, solar azimuth (ψ), view zenith (θ_v), view azimuth (ψ_v), canopy physical structure (C_s), and element reflectance (ρ):

$$L_\lambda = f(\theta, \psi, \theta_v, \psi_v, C_s, \rho) \qquad \text{(Equation 2.18)}$$

Direct model inversion iteratively solves equation 2.18 using variable values for C_s. The optimization algorithm adjusts canopy reflectance model input variables until error between modeled reflectance and image reflectance reaches a lower bound. At this stage

the input parameters are deemed "best" estimates of surface parameters. In some cases though, models are difficult to invert due to high levels of complexity and potential for indeterminate systems of equations. However, high levels of complexity and sophistication are needed for viable model output, especially in areas of complex terrain and canopy physical structure.

The look-up table inversion method is an obvious solution to the computational inefficiency of direct inversion methods. The LUT method involves pre-computation of model reflectance, the most computationally expensive aspect, prior to the inversion. Then, the inversion is simply a matter of searching the LUT for a model reflectance value which matches an input image reflectance value (Kimes et al., 2000). However, there are a number of unique issues involved in this approach, including search method, LUT constraints, and input parameter distribution.

The LUT inversion method is based on: 1) a space of observed canopy reflectance (D); 2) a space of all possible canopy realizations (modeled inputs, P); and 3) a relationship (F) between the spaces such that a member of D (d) corresponds to a member of P (p) so that the inversion problem can be stated as (Kimes et al., 2000):

$$F(p) = d \qquad \text{(Equation 2.19)}$$

However, there is uncertainty inherent in both the modeled and measured values. This uncertainty is due to model generalizations and typical geometric and radiometric remote sensing error sources. Thus, there exists a domain of uncertainty (O) around both d and F(p). The "true value" of p may exist at any point within the overlap of these areas of uncertainty. It is also possible to find a number of p that satisfies the inversion equation (2.19). This is often termed multiple solutions or multiple matches, and is discussed

further below. Thus the true LUT inversion problem is as follows: given d and O_d find all p in the space P for which F generates canopy reflectance comparable with measured data.

The Multiple Forward Mode (MFM) inversion method is an example of an indirect LUT inversion method. It was created to account for inversion problems such as those mentioned above and to create a process whereby models like the Li and Strahler (1992) GOMS model could yield inversion output in a computationally efficient manner (Peddle, 1999).

MFM involves a number of forward mode model runs where elements of p (i.e. the structural, illumination, topographical and spectral inputs) are varied over a specified range of values. The number of model runs (n_m) is a function of the number of parameters, minimum and maximum values and the increment size used to step through them. Each model run represents one of the n possible canopy realizations, P (Peddle et al., 2000). Each model run produces a set of scene component fractions and pixel level reflectance that are stored in a look-up table along with the structural, illumination and terrain inputs for the model run. The look-up table records (n_m results over the full set of model runs) can be matched with the satellite image using either the scene component fractions (Johnson, 2001) or reflectance values (Peddle et al., 2000; Pilger et al., 2002; Peddle et al., 2003b; 2003c).

There are two primary advantages to using the MFM inversion parameterization. The first is that it possesses the same ease of use and user flexibility as standard forward mode (Johnson et al., 2000). Secondly, it allows for full characterization of forest structure with no *a priori* field knowledge. MFM allows for a range of each input

parameter, extending beyond the range of possible field measurements (Peddle et al., 2000). If these large ranges create excessively large LUTs, then a multi-stage filtering process can be used to narrow the range of possible input parameter values to increase computational efficiency. This process involves running the model once with a broad range of input parameters and a course increment size to determine the general range of structural parameters (Peddle et al., 2004). A second run using the range of values determined in the first run but with a finer increment size will yield a higher precision LUT.

There is one critical issue to consider when applying the MFM inversion technique, the ill-posed inversion problem. A problem is ill-posed if a solution doesn't exist or if there are multiple solutions (Combal et al., 2002). MFM inversion is inherently ill-posed due to the fact that there is not necessarily a unique solution to the inversion problem. In other words, it is possible for dissimilar structural input combinations to produce similar reflectance values. This situation is most common with high input precision and large LUTs. As a result, there may be multiple LUT record matches ("multiple matches") for a given image pixel. In the past there have been options for dealing with these multiple matches: 1) average the structural outputs within a specified threshold; 2) create a distribution for each structural parameter within the multiple matches and output the most frequent occurrence; 3) use spatial context to determine the most likely match within a specified pixel window of structural values; 4) add more ancillary information to better constrain the matching framework (Peddle et al., 2000). These methods, however, have not been explicitly evaluated for their ability to improve structural estimates.

2.6 Biomass and Biophysical Parameter Estimation

Previous studies in the remote sensing literature identify many different methods of canopy structure and biomass estimation including: 1) aerial photo interpretation 2) active sensor estimates (radar, LiDAR, and microwave), 3) empirical relationships with visible and NIR wavelength radiance/reflectance, 4) empirical relationships with subpixel scene components, 5) empirical relationships with vegetation indices, and 6) empirical relationships with structure estimates using canopy reflectance models (Brown, 2002; Rosenqvist et al., 2003; Patenaude et al., 2005).

2.6.1 Aerial Photo Interpretation

In the past, aerial photo interpretation has been a primarily analog analysis technique for high spatial resolution airborne data to derive forest stand attributes (Avery and Berlin, 1985). Photo interpreters relate characteristics such as the tone, texture, and pattern of a forest stand represented within the airphoto to stand attributes such as crown closure and stand density (Hall, 2003). Stand height can be measured through using image parallax through stereoscopic analysis and aerial triangulation in dense canopy forests (Okuda, 2004). The interpretation process has been moving into the automated digital domain with the development of algorithms for the estimation of crown closure, height, and volume (Wulder, 1998; Hall, 2003) applied to digitized aerial photographs or very high spatial resolution airborne or satellite imagery. These algorithms can be applied at the stand level and at the individual tree level with crown delineation methods (Gougeon, 1995).

2.6.2 Active Sensor Biomass Estimates

Unlike the majority of remote sensing systems, active sensors transmit and receive their own electromagnetic energy. These systems are designed to send and receive specific wavelengths, instead of ranges of wavelengths, and usually operate in areas of the electromagnetic spectrum beyond the range of human sight. For terrestrial imaging, the use f microwaves for radar imaging and infrared wavelengths for Light Detection and Ranging (LiDAR) sensors are most commonly used. Active sensors are particularly suitable for estimating forest biophysical parameters as the returned radiation is generally a function of the physical and structural conditions on the ground.

SAR data can be used in single wavelength and polarization instances or with interferometry principles where interferometric coherence is used to determine the spatial distribution of scattering mechanisms composing a target and to reduce the influence of terrain on the radar signal (Baltzer, 2001). Common wave bands for forest applications are X-band, C-band, L-band, and P-band. Radar backscatter is generally correlated in a non-linear way with forest biomass (Tsolmon et al., 2002; Kuplich et al., 2000; Lucas et al., 2004) and linearly with stem volume (Fransson et al., 2001). The relationship is based on wave band, polarization, cover type and moisture. C-band, L-band, and to some extent, P-band backscatter is dominated by scattering from woody biomass components with increasing wavelength dominated by larger size woody components (Tsolmon et al., 2002). Interpretation of how backscatter is affected in each waveband by canopy components can be aided by radiative transfer models (Picard et al., 2004).

Neural network analysis can be used with multi-frequency and multi-polarization backscatter as an alternative to linear empirical models (Del Frate and Solimini, 2004). SAR data can also be incorporated with optical remote sensing data to improve biomass

estimate accuracy. SAR data has been fused with hyperspectral data (Treuhaft et al., 2004) and multispectral data to improve estimates of foliage area volume density and biomass by fusing reflectance derivatives with SAR backscatter. However, the backscatter saturates at around 200 t/ha for non-tropical forests (Baltzer, 2001) and significant error can enter SAR-based biomass estimates through volume decorrelation as a result of canopy movement between subsequent SAR acquisitions as a result of wind (Gaveau, 2002).

Average canopy height can also be measured by comparing SAR scattering information from the canopy with "bare-earth" elevation models. The difference between the estimated elevation from the SAR data and the elevation model equates to canopy height. This type of estimate has been done at a regional scale using data from the Shuttle Radar Topography Mission (SRTM). An added benefit of using SRTM data is that volume decorrelation is reduced due to simultaneous, spatially offset acquisitions. High quality image and DEM spatial registration is essential for this approach.

LiDAR instruments can measure canopy vertical structure by measuring the return time of a laser pulse from the canopy objects it intercepts within the sensor footprint. The intensity of pulse returns from the canopy can be used to derive crown cover density, stand height, biomass and volume (Lefsky et al., 2002). LiDAR systems can return either the full intercept waveform or discrete intercept points. Both canopy height and crown closure can be measured using either type of LiDAR system through calculating the difference between first and last returns within a three-dimensional return point cloud or prominent modes in the full intercept waveform (Lim et al., 2003). Height is thought to be a function of the vertical distribution of leaf area following a quantile –

quantile relationship (Lim and Treitz, 2004). The full waveform data may be used to estimate crown bulk density (Riano et al., 2004).

Total biomass can be derived from LiDAR derivatives either through empirical relationships including height and crown density (Lefsky et al., 2002) or basal area derived from height (Patenaude et al., 2004). Foliage biomass may also be estimated using small footprint LiDAR where each return corresponds to an element within a crown. The abstract dimensions of a crown can then be reconstructed. These data along with the spatial coordinates of the crowns are of use in fire management where canopy biomass can be used to model fire propagation and fuel use (Morsdorf et al., 2004; Riano et al., 2004).

2.6.2 Radiance and Reflectance Relationships with Forest Structure

Stand structure and biomass are related to radiometric response in select areas of the electromagnetic spectrum, and typically at visible and near infrared wavelengths. The underlying principle of the biomass-radiometric response relationship is that as photosynthetic material (biomass) increases, chlorophyll a and b will absorb more radiation in the blue and red wavelengths. In the NIR wavelengths, biomass is positively correlated with radiometric response as a result of increased NIR scattering by the increase in spongy mesophyll cells (Jensen and Hodgson, 1985). Jensen and Hodgeson (1985) and Shaw et al. (1998) both found strong linear reflectance-crown cover and reflectance-biomass relationships for scots (*Pinus sylvestris L.)* and loblolly pine (*Pinus Taeda*).

While the previous two studies made use of high spectral resolution data, Franklin et al. (2003) examined the relationship between coarser bandwidth Landsat-5 TM

imagery and crown closure, height, and age. A moderate to strong (r = 0.4 to 0.8) relationship between jack pine (*Pinus Banksiana* Lamb.) crown closure and Landsat response was found. There was also a significant inverse relationship with stand height. These results were similar to those in an earlier study by Gerylo et al. (2002) where jack pine stand crown closure (r = 0.76, TM4) and height (r = -0.62, TM4). In this study, a stepwise multiple regression resulted in a model with adjusted $r^2 = 0.46$ for stand height and $r^2 = 0.55$ for crown closure. Hall et al. (2006) reported similar results for multivariate regressions with Landsat TM data. In this case, the adjusted r^2 for stand height was 0.65 and $r^2 = 0.57$ for crown closure. Using the stand height and crown closure estimates, Hall et al. (2006) were then able to estimate conifer biomass with a validation RMSE of 37.6 t/ha. Hame et al. (1997) found that biomass could be related to spectral values via stem volume. In that case, stem volume displayed a weak inverse relationship with Landsat bands 3,4 and 5.

A number of other studies involving different forest types and cover types have shown similar linear relationships (De Jong et al., 2003; Roy et al, 1996; Thenkabail et al., 2004). However, these relationships between reflectance and stand characteristics can be adversely influenced in areas of high topographic variation (Gemmell, 1995) or where other surface features such as exposed rock and soil can lead to mixed pixels which can confound the relationship with biomass (Elvidge et al., 1985).

2.6.3 Vegetation Indices

The relationship between biomass and vegetation indices is based on the same fundamental principles underlying the raw radiance/reflectance-biomass relationship. Essentially, vegetated surfaces will reflect and absorb radiation differently depending on

water content, chlorophyll content, and other plant physiological factors. Thus, vegetation indices are potentially related to the proportion of living vegetation in the form of biomass.

The most commonly used vegetation index is the normalized difference vegetation index (NDVI). NDVI creates a normalized index of values between -1 and 1 by ratioing the difference and sum of NIR and red wavelengths (Chen, 1996). The NDVI was originally developed as an indicator of green leaf biomass (Rouse et al., 1974; Tucker, 1979). Typically, the NDVI value is used as a surrogate for scene vegetation content and is empirically related to canopy structure parameters like LAI and biomass (Wulder, 1998).

NDVI has been related to biomass to varying degrees depending on location and conditions within the study. These studies range from urban areas (Nichol and Lee, 2005), where biomass was related to NDVI estimates of cover ($r^2 = 0.16$) and density ($r^2 = 0.24$), to tropical forests (Atkinson, et al., 2000) where biomass was somewhat related to NDVI ($r^2 = 0.28$). NDVI has also been used extensively in coniferous forest studies to estimate above ground biomass and biomass density (Zheng et al., 2004; Peddle et al., 1995; 1999; 2001a; De Jong et al., 2003; Hame et al., 1997). These studies generally report inconsistent, weak to moderate relationships ($r^2 < 0.55$) between NDVI and biomass with the exception of Zheng et al.(2004) who report a strong relationship ($r^2 = 0.86$) using a corrected non-linear empirical model. Weak relationships are attributed to the influence of standing litter (van Leeuwen and Huete, 1998), background vegetation or shadow (Gao et al., 2000), soil (Huete, 1985), or a saturation effect in high density stands (McDonald et al., 1998).

A number of other vegetation indices have been developed that attempt to improve the relationship between specific vegetation characteristics by using different areas of the electromagnetic spectrum or by trying to minimize the undesirable influence of background contamination. A number of studies reviewing and evaluating the applicability, advantages and disadvantages of using alternative vegetation indices have been conducted (Bannari et al., 1995; Chen, 1996; Peddle et al., 2001a). Some of these refined vegetation indices show improved relationships with biomass in forested terrain. For example, the WDVI and GEMI indices showed a higher predictive ability for biomass in a Rocky Mountain forest study (Peddle et al., 2001a), while shadow fractions from SMA performed considerably better than all ten vegetation indices tested. While NDVI has been most widely used, it is possible that empirical relationships between VIs and biomass can be improved with these more specialized indices.

2.6.4 Subpixel Scene Components

Subpixel scene components, or endmembers, are the constituent parts that contribute to pixel level reflectance. In a forested scene these are typically generalized as three primary components within a coarse spatial resolution pixel: sunlit canopy, understory background, and shadow. These subpixel components are estimated through use of a linear (Adams et al., 1993) or non-linear mixture model (Shimabukuro and Smith, 1994) and can be based on actual physical canopy models (Hall et al. 1995).

Mixture models rely on the assumption that the spectra of these fundamental scene components can be combined based on their abundance within the pixel to resemble pixel-level spectra (Adams et al., 1993). The unknown scene fractions can be solved for as a function of pixel-level and endmember reflectance. Subpixel scene

components are of use in biophysical parameter estimation due to the first-order physical relationship with the canopy. In other words, the canopy structure has a direct effect on the proportions of these generalized subpixel components.

Subpixel components are typically related to forest physical structure either directly through empirical means or through canopy reflectance model inversion (§ 2.6.5). There has been some success in relating these subpixel components to standing biomass. Hall et al. (1995) reported a strong relationship ($r^2 = 0.76$) between biomass density and the derived shadow abundance at low solar zenith angles ($< 30°$). A subsequent study by Hall et al. (1996) that used canopy reflectance models based on a conical shape to derive subpixel scene components also concluded that the subpixel shadow abundance was moderately to strongly related ($r^2 = 0.51$ to 0.81) to biomass density. Peddle et al. (1999) reported similar results in a boreal forest setting and in a comparison with vegetation indices by Peddle et al. (2001a) who concluded that subpixel shadow component abundances were strongly related ($r^2 = 0.74$) to biomass density. Hall et al. (1997) also reported that sunlit crown area could be related to biomass density based on the relationship between biomass density and crown volume as well as sunlit canopy fraction with canopy volume, based on a conical tree model. It was also possible to improve the relationship between subpixel components and biophysical parameters in mountainous terrain by applying a topographic correction as an extension to linear mixture modelling (Johnson et al., 2000).

2.6.5 Canopy Reflectance Model Inversion Studies

Canopy reflectance models provide an explicit linkage between forest physical structure and reflectance data from remotely sensed imagery (§ 2.5). In biomass and

structural parameter estimation studies, these canopy reflectance models are inverted to provide canopy structure information. There are two basic types of inversion: direct and indirect (Chen et al., 2000). Direct inversion typically involves the mathematical inverse of the model, whereas indirect inversion uses tools such as neural networks and LUT search routines to achieve a solution. The Li and Strahler (1985) reflectance model can be inverted using a direct optimization technique. However, direct computational inversion studies have not been particularly successful due to the models inability to relate the image variance with the density and crown radius within a given pixel (Franklin et al., 1991, Woodcock et al., 1997). One suspected cause is that image reflectance variance resulting from topography is more prevalent than variance from structural differences (Gemmell, 1998). Gemmell (1998) found a correlation ($r = 0.76$) between measured density and model predicted density in a Rocky Mountain forest when terrain slope and aspect were included within the inversion procedure. In a similar study, Gemmell (2000) found that the use of multi-angle data improved this direct model inversion procedure. Other studies have also reported some success in estimating forest physical parameters using inversion procedures for the Li and Strahler (1985) model in both temperate and Eucalypt forests (Wu and Strahler, 1994; Woodcock et al., 1997; Scarth et al., 2000).

Indirect inversion techniques have also been developed that are model-independent. These indirect techniques can be applied when direct inversion techniques are impossible or unavailable. There are two similar indirect inversion methods found in the literature: one developed by Knyazikhin et al. (1998b) and another developed by Peddle et al. (1999) detailed in § 2.5 and §3.6.2. Both of these indirect inversion procedures rely on matching image reflectance with reflectance values created by canopy

reflectance modeling stored in a look-up table. Knyazikhin et al. (1998a; 1998b) show that it is possible to estimate LAI and fPAR using this inversion method given that these variables can be derived from model structural inputs. Peddle et al. (2004) used a LUT-based indirect inversion method with the 5-Scale model canopy reflectance model (Leblanc and Chen, 2000) to estimate LAI, a parameter related to biomass, in a Northern Boreal forest setting. In that study, they were also able to predict LAI to within an overall average difference of 0.53 LAI.

As mentioned above, it is possible to estimate physical-structural parameters as long as they can be calculated as a function of primary model parameters. Thus, it is possible to predict biomass from models with height and density input parameters. Wu and Strahler (1994) used structural information from model inversion to predict stand level biomass using allometric equations. These allometric equations relied on estimates of crown radius, which was related to dbh, and height. This method demonstrated some success with error ranging between 2t/ha and 1500t/ha. The larger error was likely due to model inadequacy and heterogeneity in canopy cover (Wu and Strahler, 1994). A similar method for mapping biomass relied on the use of species specific biomass calculations taken from structural estimates derived by Landsat TM cluster labeling using MFM (Peddle et al., 2003c). In this case, density and height were estimated using a canopy reflectance model approach for cluster labeling and used with allometric equations developed by Fournier et al. (2003). A test case of this estimation method was successfully used to estimate forest biomass in Newfoundland (Guindon et al., 2003).

The method developed by Peddle et al. (2003c), as well as the method described in this thesis, fit within a general strategy for mapping Canada's biomass, described by

Luther et al. (2003). Within that strategy canopy reflectance model inversion played a role in estimating forest inventory parameters that were related to biomass through allometric equations developed using baseline data. These techniques, based on cluster labeling and using forest biophysical inventory information were implemented at the stand level. However, it is possible to extract biomass information at the pixel level, which can avoid constraints introduced by the inherent heterogeneity of clusters (Peddle et al., 2005).

2.7 Summary

Estimation of biomass and biophysical parameters requires knowledge of a wide range of principles and methodologies. While the goal of this research is the development of a new canopy reflectance model-based remote sensing methodology, knowledge of proper field mensuration, allometric principles, and radiometric calibration of remotely sensed data, presented in this chapter, is of key importance due to the need for data integrity and proper validation from field measurement. It is also important to be aware of the other biomass and biomass density estimation methods reviewed in this chapter to understand how the canopy reflectance model method compares in terms of not only error, but also data requirements, efficiency, and suitability to large areas.

CHAPTER 3

Methods

3.1 Introduction

This chapter presents the methods used to estimate canopy structural parameters and biomass density, including new additions to the multiple forward mode canopy reflectance model inversion method. A description of the study area defines the location and ecotype for which the inversion method was applied. Image pre-processing techniques are described, including orthographic and topographic correction methods, both of which are of critical importance in study areas that include sloped terrain. Other multispectral image analysis methods (SMA, NDVI) used for estimating biomass density through empirical relationships with image derivatives were also used as a comparison to the canopy reflectance model inversion method. The measured structural data are also described as they apply to validating the estimates from the inversion method.

3.2 Study Area

The study area included part of a Montane/Sub-alpine forest ecoregion in Kananaskis Country Provincial Park, Alberta, Canada. The study area (Figure 3.1), centered at 51° 1' 13"N, 115° 4' 20"W, was located on the eastern slopes of the front range of the Canadian Rocky Mountains. The area covers approximately 180 km^2 and ranges in elevation from 1400 m to 2100 m. Slopes ranging from 0° to 55° and a full range of terrain aspect are included within the study area.

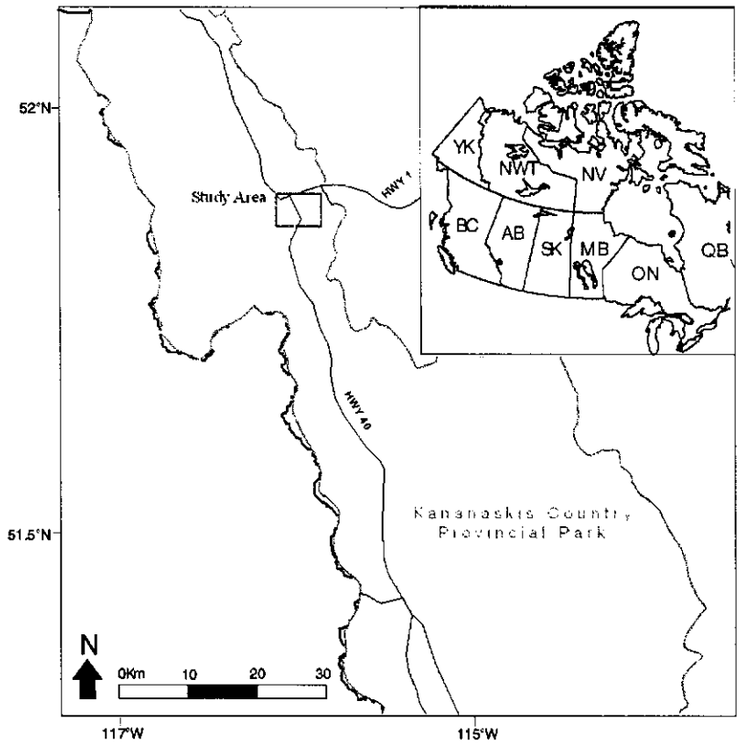

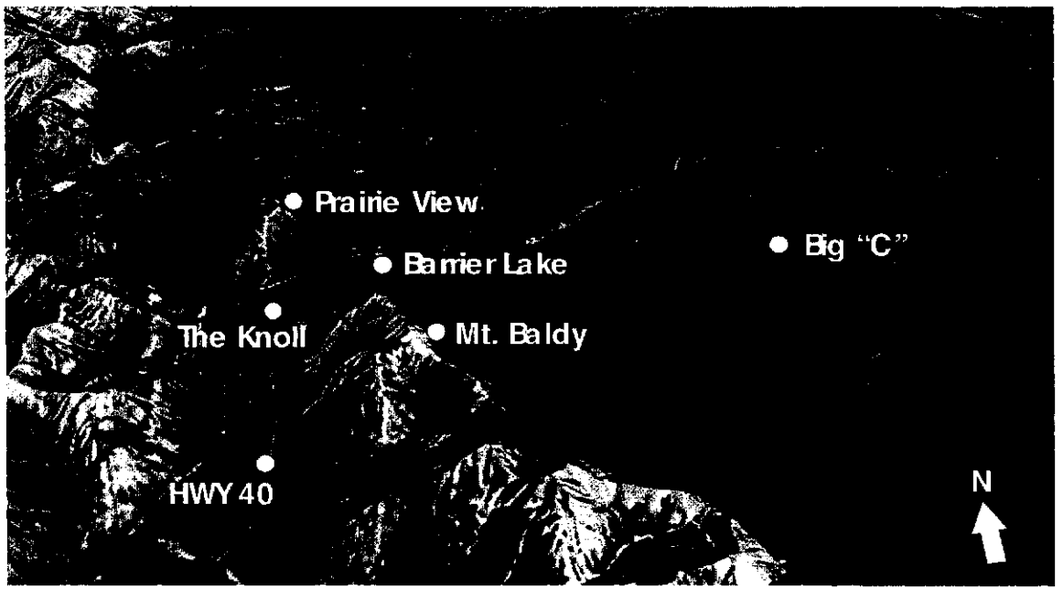

Figure 3.1 – Barrier lake study area. The study area is shown in relation to the province of Alberta. The main study areas were located along Barrier Lake, on the South slopes of Prairie View, on the Knoll, South of Barrier along highway 40, on the Eastern slopes of Mt. Baldy, and along the interior of the big "C". This area is within Kananaskis Provincial Park.

The study area includes both Montane and Sub-Alpine vegetation zones. Both zones in this particular area (Barrier Lake) are dominated by stands of lodgepole pine (*Pinus contorta* Loudon; Figure 3.2), which prefer the dryer microclimatic conditions prevalent in the area. Trembling aspen (*Populus tremuloides* Michx.; Figure 3.3) is another dominant species found primarily at lower elevations in areas of fine-silty glacial or alluvial soils (Hallworth and Chinappa, 1997). Stands consisting of Engelmann Spruce (*Picea engelmannii* Parry Ex Engel.) and White spruce (*Picea glauca* (Moench) Voss) are also found in moist microclimatic areas near drainage channels and on shade dominant slopes. Some scattered douglas fir (*Pseudotsuga menziesii* (Mirb.) Franco) and balsam poplar (*Populus balsamifera* L.) have also been documented within the study area.

Figure 3.2 – A lodgepole pine stand (*Pinus contorta* Loudon). Oblique (top) and horizontal (bottom) views.

The climate in the area is cool and moist in the summer and cold with snow in the winter. The growing season (June – August) daily average temperature based on data from years 1971 to 2000 is 13°C with a mean monthly precipitation of 77.1mm (Environment Canada, 2004). The annual temperature range falls between -14°C and 22°C while the mean annual precipitation is 637mm. However, due to orographic influence in the study area, it is not uncommon for temperature and precipitation to vary with elevation and orientation of the terrain.

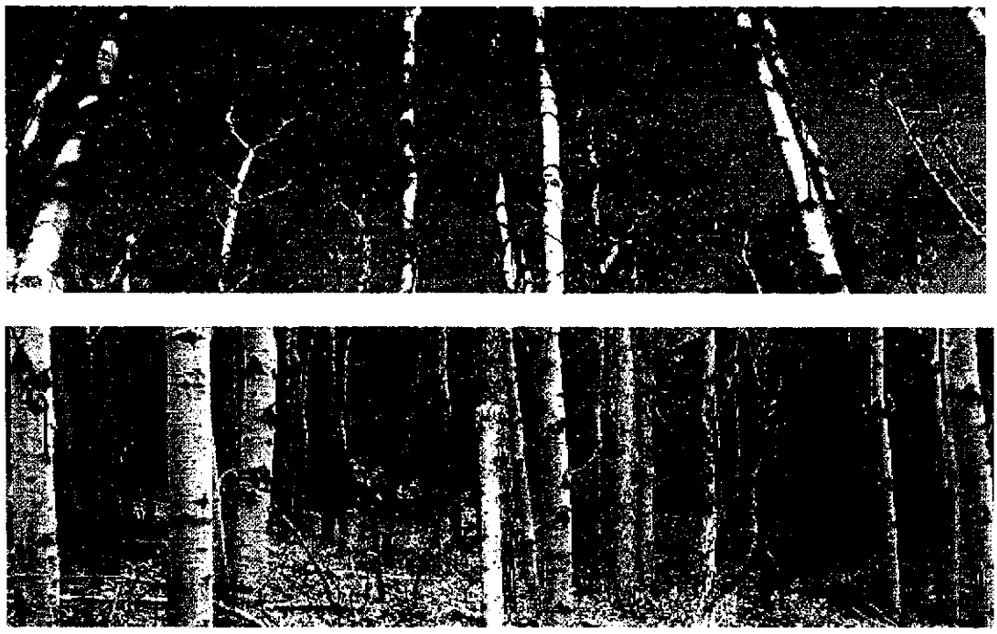

Figure 3.3 – A trembling qspen (*Populus tremuloides* Michx;) stand. Oblique (top) and horizontal (bottom) views.

3.3 Field Data Collection

In situ field data were collected during two consecutive field seasons in 2003 and 2004 between the months of June and August. During these two seasons data were collected within 40 field plots. These data can be divided into three primary categories: 1)

mensurational data, including biomass for each tree, 2) spectral data, and 3) data obtained from devices using optical principles (e.g. LAI-2000).

3.3.1 Plot Location

A total of 40 plot locations were selected within the study area based on species composition, terrain orientation and stand density. This stratification scheme was created to capture variability in both forest stand structure and terrain. Of the 40 plots, 20 plots were dominant (> 80%) lodgepole pine, 15 plots were dominant trembling aspen, and 5 plots were primarily white spruce, engelmann spruce or mixed conifer (dominant species <80%). The plot size was set at 400 m^2 to satisfy two requirements. The first was to ensure that at least one pixel from the SPOT imagery (pixel size = 20 m x 20 m) would spatially coincide with each plot and the second was to ensure adequate field measurement coverage within a limited time frame. Each plot was aligned to true North with each corner and the center point referenced using a Trimble Pathfinder® Pro-XRS GPS receiver.

The positional data for each plot were differentially corrected and converted to a spatial point feature for use with geometrically corrected image data. Differential correction was applied using Trimble Pathfinder Office™ software and base station positional data recorded with a second Trimble receiver at the Kananaskis field station. Further, a modification to the GPS setup was applied for reducing multiple GPS signal returns (multi-path error) that often occur within forest stands (§ 3.4.1). Slope and aspect data were also recorded for each plot using a Suunto Clinometer for slope and a compass for terrain aspect.

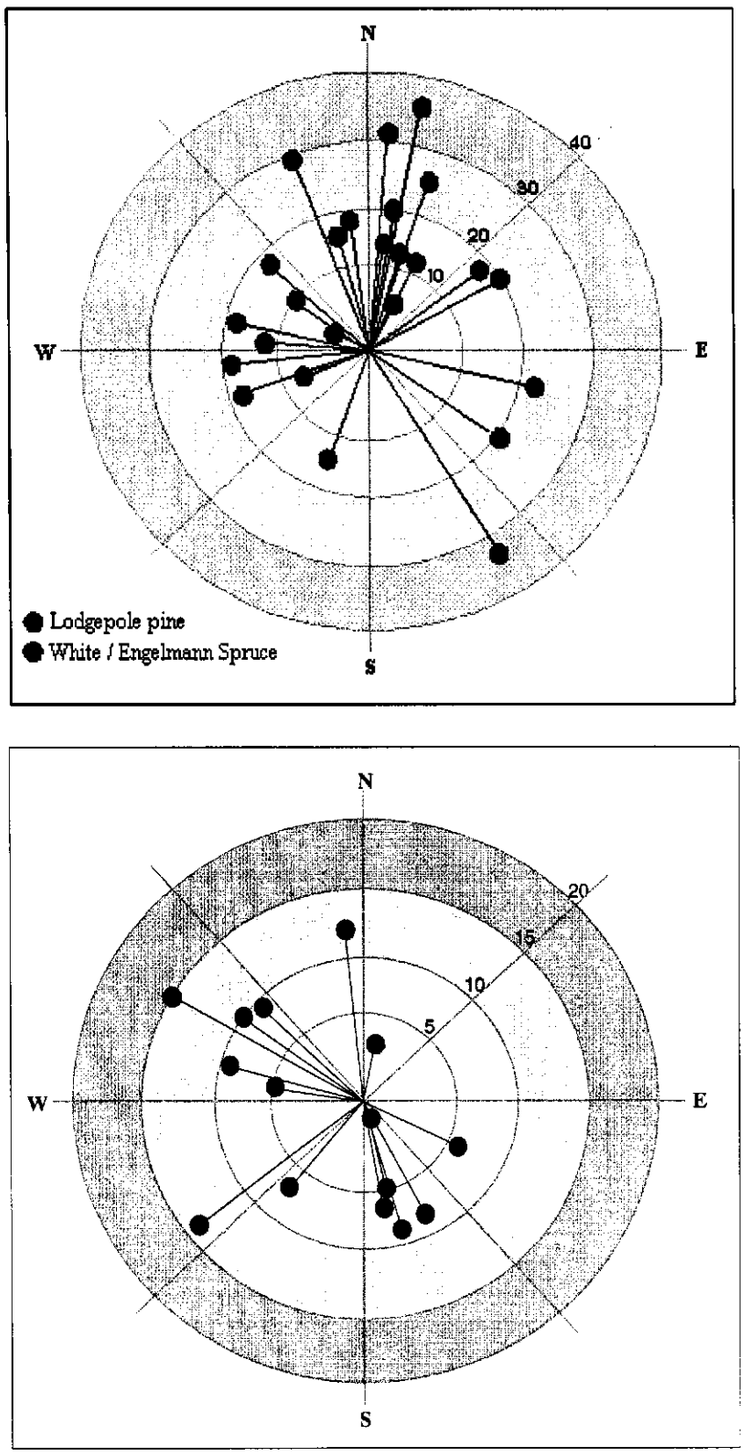

Figure 3.4 – Field plot slope and aspect values. Lines extend in the direction of terrain aspect and slope is indicated by concentric coloured rings. Conifer (top) and deciduous (bottom) dominant plots are represented.

3.3.2 Physical Measurements

Overstory trees were enumerated and the species and relative positions mapped within the 400 m^2 field plot. Physical canopy dimensions and tree height measurements were recorded for association with canopy information derived from remote sensing and canopy modelling techniques. The first measurements, tree height and height to center of crown (*htc*) were measured using two methods. The first involved the use of a digital clinometer at a 20 m distance. The second method used of a digital hypsometer also at a 20 m distance from the measured tree. Height to center of the crown was determined by subtracting the height to the base of the canopy (a parameter more easily and accurately measured than HTC) from the total height, dividing in half, and adding the height to the base of the canopy. The diameter 1.3 m above the base of the trunk was measured using a diameter-at-breast-height tape. The horizontal canopy diameter for each tree was measured using a GRS densiometer to determine the vertical projection of the edges of the crown to the ground (i.e. the drip line). The distance back to the trunk was then measured using a measuring tape. This process was repeated perpendicular to the first measurement in an attempt to characterize variation in horizontal crown dimensions.

3.3.3 Biomass Calculation

Biomass was calculated for each tree within the field plots using predefined allometric equations for tree species in Alberta based on DBH and tree height (Singh, 1982). Above ground total tree Biomass ($AGTB_{tree}$) was calculated for each tree within plot boundaries using the formula:

$$ln(AGTB_{tree}) = b_0 + b_1 ln(DBH) \qquad \text{(Equation 3.1)}$$

Values for b_0 and b_1 can be found in table 3.1. When converting from the logarithm of tree biomass to biomass it is necessary to apply a correction factor to account for the skewness in the distribution in arithmetic units (Baskerville, 1971). These correction factors (CF) for each tree species are also displayed in table 3.1. The $AGTB_{tree}$ ($kg \cdot tree^{-1}$) was then summed for each plot and divided by the plot area to give total biomass (kg) within the plot and total standing biomass density ($tonnes \cdot ha^{-1}$).

Table 3.1 – Tree level biomass model parameters[1]

Species	b_0	b_1	CF
Trembling Aspen	-2.763	2.524	1.022
Lodgepole Pine	-2.021	2.274	1.019
White Spruce	-2.464	2.366	1.033

3.3.4 Field Spectroradiometer Measurements and Data Processing

Spectral properties of vegetation are a key link between image data and field based measurements. Spectral signatures allow for the extraction of individual scene component information from image data. An Analytical Spectral Devices (ASD) Field Spec spectroradiometer was used to record the spectral properties of sunlit and shadowed forest vegetation samples and pseudo-invariant features (PIFs) in the study area (Figure 3.5). The vegetation samples included the four main overstory vegetation species: lodgepole pine, trembling aspen, white spruce and engelmann spruce, as well as a mixed background consisting of understory vegetation and litter. The measurements occurred near the expected satellite overpass time on two cloudless dates in June and July, 2004. The spectroradiometer measures reflected radiance between 350 and 2500 nm using three sensors calibrated for visible and NIR wavelengths, IR, and SWIR radiation (ASD, 1995). The sensors are attached to a fiber-optic cable that is connected to a fore-optic

[1] Personal communication with R.J. Hall (2004)

lens. The field of view (FOV) can be adjusted by raising or lowering the height above target or adjusting the fore-optic lens. For this study, a 5° fore-optic lens was kept at 1.5 m above the ground at a nadir viewing angle. This yielded a FOV with a diameter of 13.1 cm. Vegetation targets were arranged in a 20 cm diameter optically thick stack to ensure a pure target measurement (Peddle, 1998). Shaded vegetation spectra were measured by intercepting the incoming solar radiation for the target with a wooden panel, creating cast shadow over the target and surrounding area.

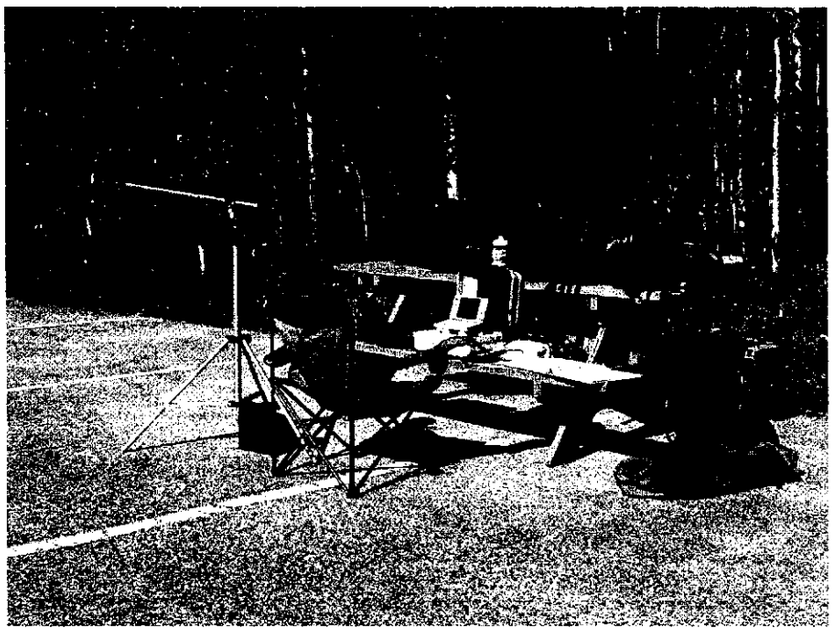

Figure 3.5 – A portable field spectroradiometer setup at the Barrier Lake PIF calibration site

To ensure a high signal to noise ratio, the spectroradiometer was configured to acquire 10 measurements within a 60 second time frame. These measurements were then averaged for each sample. A dark current measure and white reference calibration measurement were also taken prior to each measurement. These measurements were used to account for any internal signal noise and illumination variations during measurement.

Measurements were taken for both raw digital number (DN) and reflectance. The internal reflectance calibration required a measurement of incident irradiance prior to the reflectance calculation. This was accomplished by taking spectral readings of a Spectralon white reference panel.

The Spectralon panel is a near-Lambertian surface that reflects approximately 98% of incident irradiation. However, to derive surface reflectance of the target (Figures 3.6 and 3.7) it was necessary to use a calibration process (Peddle, 1998). In order to account for the two percent of incident irradiation not represented in the white reference panel measurement, a calibration procedure using known spectral properties of the Spectralon panel was employed. The calibration value was integrated into the traditional reflectance calculation as follows (Peddle, 1998; Labsphere, 2001):

$$\text{Reflectance } (\rho) = \frac{\text{Target Radiance}}{\text{Panel Radiance}} \text{ x Calibration Factor} \quad \text{(Equation 3.2)}$$

This procedure was repeated for each acquired spectra. The spectra were then averaged for each target. To incorporate the field spectra in subsequent satellite image data processing it was necessary to reduce the spectral dimensionality by integrating the reflectance across a range of wavelengths to a single "band" value based on published spectral response functions (Figure 3.8) for the satellite sensor.

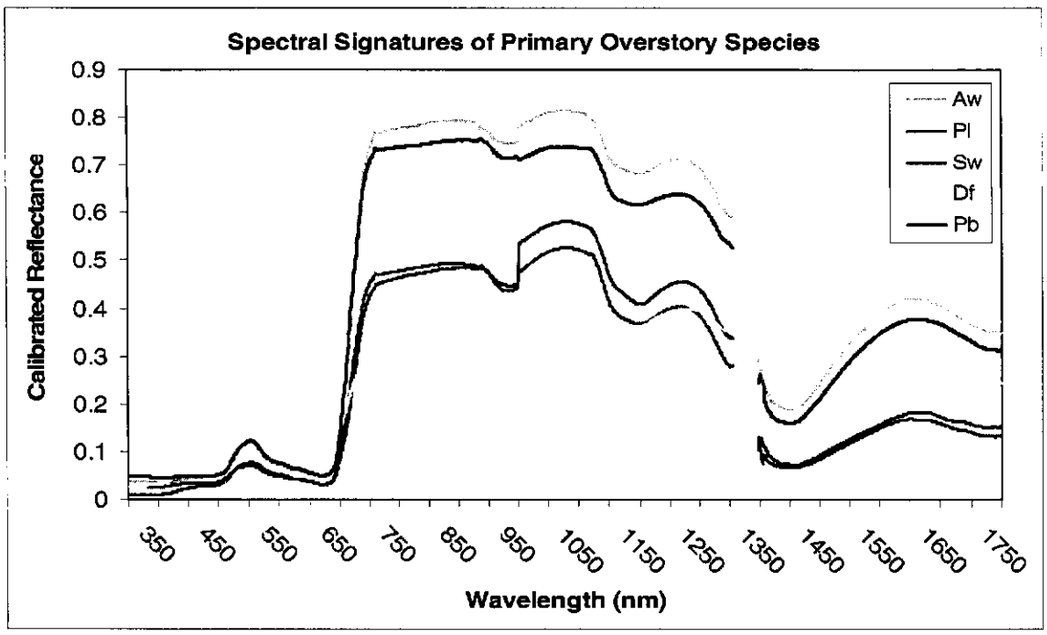

Figure 3.6 – Spectral signatures of trembling aspen (Aw), lodgepole pine (Pl), white spruce (Sw), Douglas fir (Df), and balsam poplar (Pb) species within the Kananaskis study area. Spectral data is displayed between 300 and 1750 nm, corresponding to SPOT spectral resolution. Some data were removed due to high noise at sensor borders.

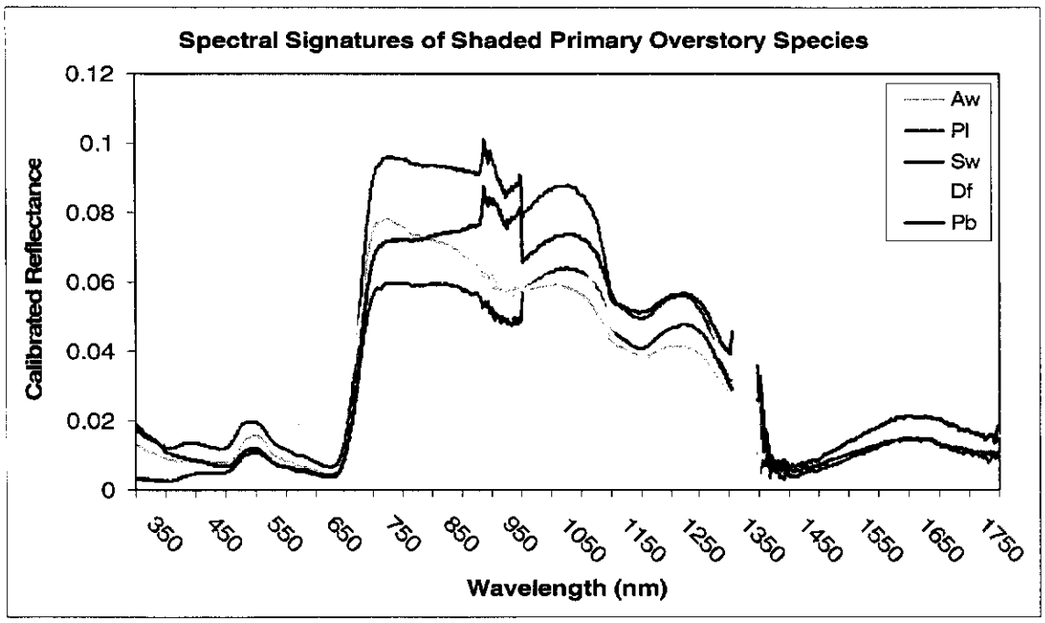

Figure 3.7 – Spectral signatures of the shaded primary overstory species within the Kananaskis study area. Spectral data is displayed between 300 and 1750 nm, corresponding to SPOT spectral resolution.

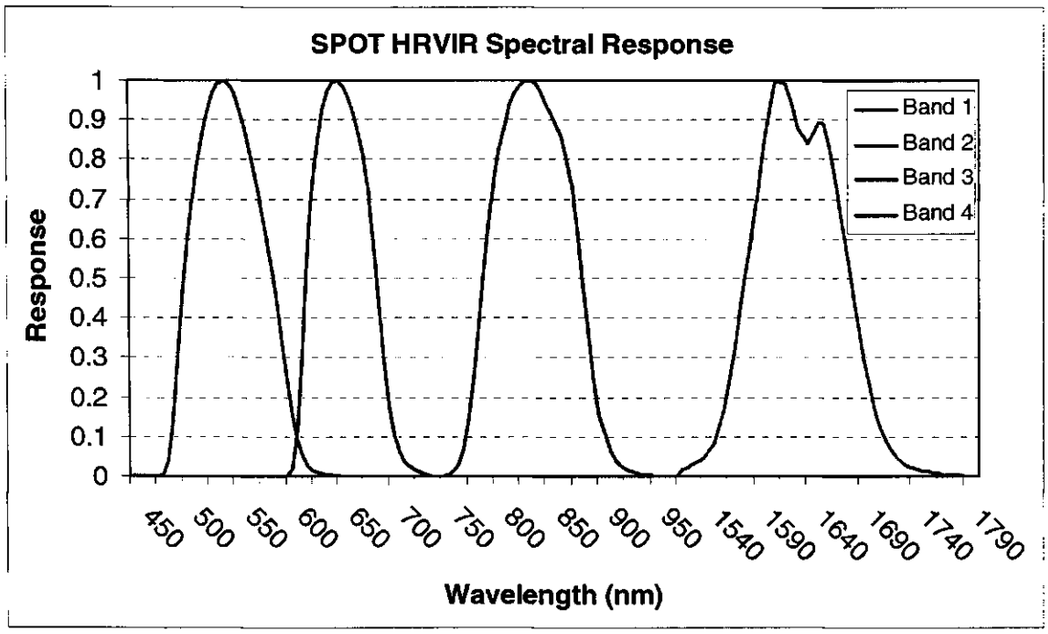

Figure 3.8 – Spectral response functions for the SPOT 5 sensor

3.4 Satellite Image Data and Pre-Processing

Satellite image data covering the study area were collected on August 12th by the High Geometric Resolution (HGR; SPOT 5) sensor aboard the Système pour l'Observation de la Terre (SPOT) satellite. The SPOT satellite platform was chosen due to the spatial coverage of the imagery, the vegetation-centric location of the spectral bands and the potential to obtain multi-resolution imagery from a single sensor. The data collected on August 12th consisted of cloud free 2.5 m spatial resolution panchromatic data and 10 m multispectral data. The multispectral data collected with the HGR sensor comprised four bands: green, red, near-infrared, and short-wave-infrared (Table 3.2). The SPOT sensor has the capability to acquire imagery at off-nadir view angles and for the August 12th acquisition was pointing -7.3° off nadir.

Table 3.2 – SPOT sensor details

Sensor	Band	Spatial Resolution (m)	Band minima (nm)	Band maxima (nm)
Spot 5	Panchromatic	2.5	480	710
	B1 - Green	10	500	590
	B2 - Red	10	610	680
	B3 - NIR	10	780	890
	B4 - SWIR	20	1580	1750
Spot 4	B1 - Green	20	500	590
	B2 - Red	20	610	680
	B3 - NIR	20	780	890
	B4 - SWIR	20	1580	1750

3.4.1 Geometric Correction

The SPOT imagery was calibrated to correct for sensor calibration error. No geometric processing was done prior to image delivery. Geometric correction is critical in studies relating image data to ground data sources. Positional error can be a substantial contributor to overall error in studies linking *in situ* and sensor data. Thus, substantial effort was undertaken to ensure the highest possible level of positional accuracy in the field and with image processing. In this case, the acceptable positional accuracy was considered to be one half of the highest resolution multispectral pixel or 5 m so that the majority of the field plot fell within the image pixel at co-incident geographic coordinates.

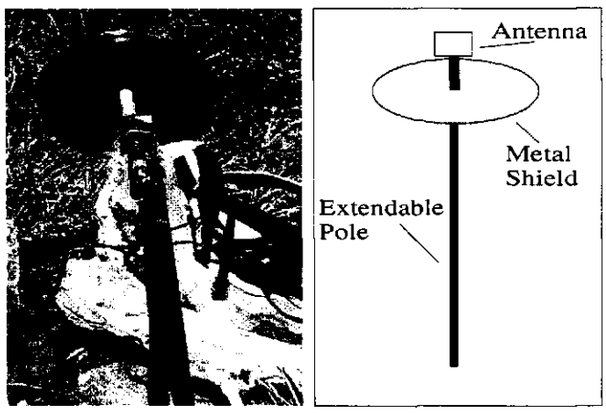

Figure 3.9 – A system to reduce multi-path GPS signal returns

A number of steps were taken to ensure that a high level of positional accuracy was obtained. The first step was to reduce the amount of multi-path GPS signal returns from the canopy to the GPS unit by raising the receiving unit and antenna high into the canopy while shielding the receiver's underside from canopy induced multi-path signals. A shield[2] was constructed using a 30 cm diameter metal disk mounted below the GPS antennae and secured on a 5 m extendable pole (Figure 3.9). The system was raised a further 2 m into the canopy by the operator.

The second step involved recording a number of ground control points (GCPs) throughout the spatial extent of the image which could be used in the geometric correction process. While the geometric correction using the GCPs was effective in areas of low topographic relief, there was still considerable positional error (> 20 m) in high relief areas. To correct for the image distortions in areas of high relief, a 30 m digital elevation model (DEM) was used with the GCPs to orthorectify the SPOT imagery using the SPOT orthorectification routine within the Environment for Visualisation of Images (ENVI, 2002) software. The resulting corrected image showed an average positional error of less than 5 m when checked against a number of spatially distributed GCPs reserved for validating the positional accuracy of the corrected image. The positional error was assessed by comparing the coordinates of GCP features within the orthorectified 2.5 m resolution panchromatic imagery with their field recorded positions (Table 3.3). It should be noted that there was still some potential for error due to the fact that image resolution was larger than feature size in some cases.

[2] Personal communication with C. Coburn (2004)

Table 3.3 – Positional accuracy assessed from independent, mutually exclusive validation GCPs collected in the study area. Coordinates are Universal Transverse Mercator (UTM N11 NAD '83).

	Field GCP location		
Feature	Northing (m)	Easting (m)	Image Positional Error (m)
1	5657412	636015	7
2	5656132	638165	1
3	5657252	636125	8
4	5644952	629915	9
5	5656822	635375	17
6	5650452	635085	2
7	5663372	614205	4
8	5662522	635525	5
9	5663112	638605	2
10	5640622	630995	3
11	5656262	649055	1
12	5649322	643665	4
13	5655272	639355	7
14	5668322	650815	0
15	5653902	635165	3
		Average =	4.9

3.4.2 Radiometric Correction

After orthorectification, the image data were converted from raw digital counts (DN) to at-sensor radiance (L) ($W/m^2/sr/\mu m$) using calibration gains and offsets available from SPOT image corporation (SPOT image, 2004):

$$L = (DN/gain) + offset \qquad \text{(Equation 3.3)}$$

Each image band was then further calibrated to top of the atmosphere reflectance, or reflectance negating the influence of atmosphere using the formula:

$$\rho = \frac{L\pi d^2}{E_0 \cos\theta_0} \qquad \text{(Equation 3.4)}$$

Where ρ is reflectance, d is earth-sun distance at time of image acquisition, and E_0 is solar irradiance for a given band at d given by SPOT Image (2004). Earth-sun distance for the Julian day (J) of image acquisition was calculated using a Fourier series representation (Spencer, 1971):

$$d = 1.00011+(0.034221*\cos(\varphi))+(0.00128*\sin(\varphi))+(0.000719*\cos(2*\varphi))+(0.000077*\sin(2*\varphi)) \quad \text{(Equation 3.5)}$$

where

$$\varphi = \frac{2\pi(J-1)}{365} \quad \text{(Equation 3.6)}$$

A further calibration procedure was applied to the SPOT data to account for the potential effects of atmospheric transmission and path radiance (Schott et al., 1988; Moran et al., 1997). Two pseudo-invariant features (PIF), each larger than the spatial resolution of the image were selected for and their spectra were measured using an ASD spectroradiometer near the time of image acquisition. The ASD measured reflectance values were converted to simulated at-sensor reflectance negating atmospheric effects using published spectral response curves for the SPOT sensor. The SPOT data was then linearly transformed using an empirical line procedure. PIF inputs for the empirical line calibration were selected to represent high reflectance and low reflectance for a given band.

The topographic effect, detailed in the literature review (§ 2.4.1), has a substantial effect on recorded reflectance values for forested terrain as a result of altered canopy structure and terrain shadowing. Topographic correction procedures were selected according to results from a previous topographic correction study (Soenen, et al. 2003; 2005). The corrected imagery was used in the subsequent spectral mixture analysis procedures along with the uncorrected imagery to facilitate a comparison of the relationship between the corrected and uncorrected data and biomass density.

3.5 MFM-GOMS Model Parameterization and Operation

3.5.1 Model Input Selection

MFM operation of the Li and Strahler (1992) geometric optical mutual shadowing (GOMS) model assumes no *a priori* knowledge of structural conditions on the ground. A very wide range of input parameters, encompassing any physical structural possibility, may be selected to yield all potential combinations of structural conditions in a forest stand. However, the time required for computation of a large range of conditions can be excessive at fine increment step sizes. For example, a range of conditions encompassing all possible structural variations within a montane forest at a fine increment size (e.g. physical parameters within a half meter, density within 100 stems/ha) can yield upwards of 10^7 model executions per species per band. If on average, five forward mode executions are performed per second the required processing time on an Intel 2GHz processor was nearly 72 hours.

Sorting and linear searching of an output table of this magnitude can be as computationally demanding as the modelling operation. Thus, a two-stage MFM procedure was implemented whereby a wide parameter range MFM model run with a coarse step size was used to first narrow the possible physical-structural conditions in the image. A subsequent set of MFM model runs using the narrower parameter ranges found by examining the field data was used to determine stand structure from a constrained LUT (i.e. using a range of two standard deviations from the mean of observed structure).

Little has been done in the past to examine the effect of increment size and parameter range on the number of multiple matches and accuracy of the structural parameter estimates. The general rule has been to use two standard deviations from the mean of a given model parameter measured in the field data to determine the potential

range of inputs, and the measurement precision to determine the increment size (Pilger, 2003). However, structural parameter distributions are assumed to be Gaussian for this method to properly characterize the majority of potential structural values. However, this is not always the case, for example, sampled height often displays a log-normal distribution (Li and Strahler, 1985).

In this study, four input parameter sets were used for each species to produce LUTs of varying increment and range size to quantify the effects of these parameters on the matching procedure and to evaluate the effectiveness of iteratively constraining the LUT parameters. The MFM input parameter sets fall into four general categories (Tables 3.4 and 3.5): 1) unconstrained, coarse increment, 2) unconstrained, fine increment, 3) constrained, coarse increment, 4) constrained, fine increment. The first two structural categories (MFM run 1, MFM run 2) were set with ranges that would include any possible physical condition (i.e. large ranges). The second two sets (MFM run 3, MFM run 4) were created using two standard deviations from the mean of the structural conditions recorded in the field for both species types to constrain the ranges. The increment size was set by examining the modeled reflectance output. The fine increment size (MFM run 2, MFM run 4) was set so that there would be close agreement between all image reflectance values and model reflectance values.

Table 3.4 – MFM input parameter sets. MFM run 1 was an unconstrained, coarse increment parameterization, MFM run 2 was an unconstrained, fine increment parameterization, MFM run 3 was a constrained, coarse increment parameterization, and MFM run 4 was a constrained, fine increment parameterization. The constraint range applied in MFM run 3 and MFM run 4 was two standard deviations from the mean of observed structural conditions in the field for the two species types.

		MFM run 1			MFM run 2		
	Structural Parameter	*Min*	*Max*	*inc*	*Min*	*Max*	*inc*
Conifer Species	Density - λ (trees/m)	0.05	0.55	0.1	0.05	0.5	0.05
	Horizontal Crown Radius - r (m)	0.5	6.5	2	0.5	6.5	1
	Vertical Crown Radius - b (m)	0.5	6.5	2	0.5	6.5	2
	Height to Centre - h (m)	5	15	5	4	14	2
	Height Distribution - dh (m)	5	25	10	5	25	5
	Slope - α (°)	0	60	20	0	60	10
	Aspect - φ (°)	0	315	45	0	315	45
	LUT Size (Combinations)		31104			829440	
Trembling Aspen	Density - λ (trees/m)	0.05	0.55	0.1	0.05	0.5	0.05
	Horizontal Crown Radius - r (m)	0.5	6.5	2	0.5	6.5	1
	Vertical Crown Radius - b (m)	0.5	6.5	2	0.5	6.5	2
	Height to Centre - h (m)	5	15	5	4	14	2
	Height Distribution - dh (m)	5	25	10	5	25	5
	Slope - α (°)	0	60	20	0	60	10
	Aspect - φ (°)	0	315	45	0	315	45
	LUT Size (Combinations)		31104			829440	

		MFM run 3			MFM run 4		
	Structural Parameter	*Min*	*Max*	*inc*	*Min*	*Max*	*inc*
Conifer Species	Density - λ (trees/m)	0.05	0.25	0.05	0.06	0.26	0.02
	Horizontal Crown Radius - r (m)	0.5	2.5	1	0.5	2.5	0.5
	Vertical Crown Radius - b (m)	1	4	1	1	4	1
	Height to Centre - h (m)	10	14	1	10	14	1
	Height Distribution - dh (m)	5	15	5	6	16	2
	Slope - α (°)	0	40	10	0	40	5
	Aspect - φ (°)	0	315	45	0	315	45
	LUT Size (Combinations)		40500			534600	
Trembling Aspen	Density - λ (trees/m)	0.05	0.2	0.05	0.06	0.2	0.02
	Horizontal Crown Radius - r (m)	1	4	1	1	4	0.5
	Vertical Crown Radius - b (m)	1	3	1	1	3	1
	Height to Centre - h (m)	11	15	1	11	15	1
	Height Distribution - dh (m)	5	20	5	6	20	2
	Slope - α (°)	0	20	10	0	20	5
	Aspect - φ (°)	0	315	45	0	315	45
	LUT Size (Combinations)		25920			302400	

Table 3.5 – Illumination geometry, view geometry, and endmember values

Illumination and View Angle	
Solar Zenith Angle	37°
Solar Azimuth Angle	157°
View Zenith Angle	7°
View Azimuth Angle	15°

Endmembers	ρ_{SWIR}	ρ_{NIR}	ρ_{RED}	ρ_{GREEN}
Sunlit Pine Canopy	0.168	0.487	0.041	0.061
Sunlit Aspen Canopy	0.299	0.585	0.064	0.093
Sunlit Spruce Canopy	0.083	0.411	0.055	0.071
Sunlit Background (Pine, Spruce)	0.333	0.243	0.086	0.061
Sunlit Background (Aspen)	0.327	0.501	0.059	0.104
Shadow	0.013	0.072	0.005	0.012

3.5.2 MFM-GOMS Modelling Procedure

The GOMS model was executed once in forward mode for each combination of structural and spectral parameters for each image band. Multiple executions of the GOMS model were automated within the MFM software (v5.1, Peddle, Johnson and Soenen). The MFM software is separated into four stages. In the first stage the MFM software takes input through ASCII text files and creates structural and illumination geometry input files for the G-O model. The first stage also creates a batch execution file for G-O model execution. The second stage is a batch execution consisting of execution of the G-O model for all possible combinations of illumination and structural inputs. The output from the second stage consists of a number of intermediate ASCII text files including the areal proportions of scene fractions and pixel level reflectance from each combination of structural and illumination inputs. The third stage reads and collates these output files to create a look-up table (LUT) with entries that contain the input and output parameters for each model execution. The fourth stage is the indirect inversion stage where the potential solutions to the inversion problem are extracted from the LUT based

on matches between the GOMS model reflectance and the remote sensing image reflectance (§3.6.4).

3.5.3 Preliminary Model Testing

A set of preliminary GOMS model tests was carried out to determine the level of agreement between the GOMS model output reflectance and image reflectance as well as proper tolerances for the LUT search and match procedure. Reflectance values from IKONOS imagery of the study site were used to validate the GOMS model reflectance values. The test was performed prior to the SPOT image data collection. Structural data from a subset of 15 field plots for both conifer and deciduous species were used in forward mode model runs and compared with spatially co-incident IKONOS image pixels. IKONOS pixel reflectance values were taken from a 5x5 kernel representing an area spatially similar to the field plots and within the acceptable spatial range for the GOMS model.

3.5.4 Indirect LUT Inversion

In the past, the matching stage of indirect inversion has been completed using existing software such as Microsoft Access™. These types of programs are suitable for smaller LUTs (< 100,000 records). However, these programs are unable to load and efficiently manage larger LUTs. These programs are also unable to complete the indirect inversion procedure for image data as a query-based match would require an interface with image processing software that does not currently exist. Thus, new software was created to automate the LUT search procedure and to create a robust, repeatable, and efficient method of linking the G-O model outputs and satellite imagery (Figure 3.11).

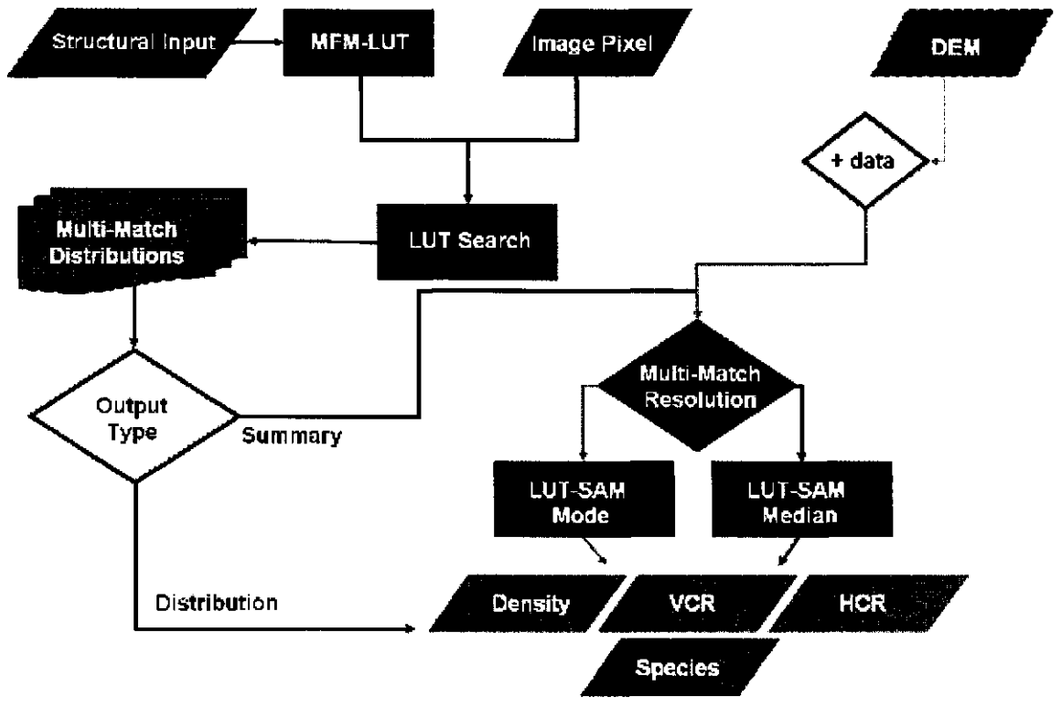

Figure 3.10 – A flowchart describing the LUT inversion algorithm. The LUT search procedure takes LUT and image input and, using one of three search methods, describes the inversion result as either a distribution of potential matches or a summary of the distribution using central tendency. DEM values may be used as an additional constraint.

The LUT search and match procedure software (developed for this thesis) reads LUTs containing the results of the MFM model executions for multiple species and spectral bands (Figure 3.10). The user is presented the option of searching the tables through text file input (plot-level) or image input (pixel-level). In both cases, the program reads in calibrated reflectance values for a predetermined number of bands. The user can choose between three methods to determine potential matches from the LUTs including: 1) selection of exact reflectance matches, 2) closest spectral distance; and 3) selection of all potential matches within a domain of uncertainty defined by a spectral distance function. The algorithm to limit these potential solutions was based on using ancillary

information (i.e. DEM values). The potential matches may then be output as either a full distribution or a value based on the central tendency of the distribution.

3.5.4.1 Limiting the Potential Matches

When developing modelling procedures it is important to always keep the following axiom regarding systems and models in mind: "All models will be inadequate or incorrect to some degree, so that no model can achieve identity with the system it represents. By the same token, the true and complete nature of a system can never be known, but can only be subject to speculation" (Strahler, 1980). The three reflectance matching algorithms within the LUT-SAM software were created following the above maxim.

In the first reflectance matching procedure it was assumed that the true nature of the system is unknown, the model speculation is correct, or at least consistent, and that there is a potential for exact reflectance matches. In this procedure, the software scans the look-up table for cases where modeled reflectance and image reflectance are equal for all input bands. The user may select input precision based on model and structural input precision for potential matches at whole reflectance values (e.g. 30% = 30% and 30.1% = 30.2% but 30% $\neq$ 31%). The radiometric precision selected for the matching process will have a marked effect on the potential for multiple matches. In this study, the radiometric precision is a function of the input values. However, it is possible to match the radiometric resolution within the modeled data to the satellite data using a model sensitivity analysis and resulting functions to select physical parameters based on the spectral characterization needs. For example, 11-bit sensor data will have a larger radiometric range to characterize than 8-bit data.

To account for any discrepancy between the radiometric resolution within the model and that of the satellite imagery, a spectral distance criterion was implemented to select the nearest matching set of structural values within spectral space. The spectral distance criterion was based on the relative RMSE between the image data and modeled reflectance within the LUT (Weiss et al., 2000):

$$RMSE = \sqrt{\frac{1}{n_b}\sum_{i=1}^{nb}\left(\frac{\rho_i - \hat{\rho}_i}{\rho_i}\right)^2} \qquad \text{(Equation 3.7)}$$

where i is the band number and $\hat{\rho}$ is the modeled reflectance from the MFM model runs. This function evaluates the spectral distance for each entry within the LUT set and returns the set of records with the lowest relative RMSE.

The reflectance domain procedure assumes both model inadequacy and error prior to model input. As a result, the LUT-SAM procedure includes a user defined error margin that simulates the domain of uncertainty (§2.5.2) when selecting potential matches between modeled and image reflectance. While considerable efforts were made to reduce the level of inherent error in the input files (i.e. image reflectance data) as a result of atmospheric, topographic and geometric influences, it was likely that some remained. Ideally, the user will first identify the primary source of error in the input values and determine a domain of uncertainty that best suits the type and magnitude of error based on the signal to noise ratio or other measures of uncertainty. For example, consider the case where positional error is greater than the image spatial resolution but less than two times that resolution. In this scenario, a suitable LUT match range could be taken from the level of dispersion from the mean of pixel level reflectance in sampled 3x3 pixel

windows, assuming some level of spatial autocorrelation. The standard deviation from the pixel window is then used to determine the range of values extracted from the LUT for further analysis.

In another situation, the domain of uncertainty may also be thought of as a distance value within n-dimensional spectral space. This distance value is then used along with the relative RMSE calculation to extract all LUT records within the domain of uncertainty. The techniques and constraints within the multiple match handling algorithms described later may then be applied to the potential matches.

3.5.4.2 Reducing Multiple Solutions

The potential solutions can be filtered through the use of ancillary terrain information (DEM). The use of this data source reduces the number of unknown parameters within the inversion procedure and can reduce the number of potential solutions. In a direct inversion context, this would be similar to applying known information to an unknown parameter. In the case of the GOMS model it is possible to limit potential matches using input DEM derivative values since GOMS contains explicit slope and aspect inputs. Within the MFM software, an algorithm can be applied that constrains matches selected from the LUTs using any of the limit methods to those that contain terrain values that match the DEM derived slope and aspect.

3.5.4.3 Describing Multiple Solutions for Structural Parameter Output

Multiple matches (§ 2.5) are described in one of two ways within the software. The first option presents the user with a description of the structural values within the distribution of potential solutions. A frequency distribution and simple descriptive statistics (minimum, maximum, median, mode, and standard deviation) are output. This

information allows the user the option of examining the multiple matches for trends that might reveal the nature of the physical structure on the ground as well as outlying structural values that may be excluded from subsequent MFM model runs.

The second output option is most useful when a single output value is desired. This option involves the use of measures of central tendency only to describe structural values from the multiple matches. The user has the option of selecting either the median or mode of the structural outputs. If the mode is selected, the software examines the distribution of extracted matches and selects the most frequently occurring value for each structural parameter.

$$P_{struc} = \frac{\text{number of occurrences of structural parameter (value = x)}}{\text{total occurrences of structural parameter}} \quad \text{(Equation 3.8)}$$

In cases of a multi-modal distribution, the mode with the greatest number of occurrences clustered within +/- σ is used. The median value may also be selected for output. The median value was selected rather than the mean value to reduce sensitivity to the extreme ends of a distribution (Weiss et al., 2000).

An additional advantage to the indirect inversion procedure is that a simple overstory vegetation species classification is produced based on the spectral inputs within the potential solutions. It is possible to have different species represented within the potential solutions, and thus the species that represents the majority of potential solutions is output as the classification result analogous to the most probable class label. It is also possible to use a measure of elipticity and crown elongation to discriminate species if spectral ranges are used as input rather than field spectral measurements. This provides a more direct structural basis to a classification, which may be more reliable. This more sophisticated classification rule would, however, require a higher level of field

information (i.e. structural measurements), or in the least, known structure characteristics for a basis for this advanced discrimination. While this violates one of the fundamental tenets of MFM, that of requiring no *a priori* information, it does provide another option and higher level of sophistication to the user, where available and appropriate.

The inversion results can be output in two forms. The first output type is an ASCII text file and the second is a band interleaved by pixel image file where each structural parameter is displayed in an information band along with species. Of course, for image output the single value (e.g. median, mode) option must be used. An ENVI header file including geographic position information and band information is also created for the file.

3.5.5 Pixel Level Biomass Calculation

The intent of this research was to calculate per-pixel biomass using previously developed stand-level biomass prediction models (Hall et al., 2006). In these models, biomass is a function of crown closure and height within a forest stand. However, these models can be applied to any area greater than an individual tree crown. Neither CC nor height (h) are explicit model outputs but can easily be calculated using the following equations:

$$h = htc + b \qquad \text{(Equation 3.9)}$$

and

$$CC = \pi r^2 x\lambda \qquad \text{(Equation 3.10)}$$

where *htc* is height to center of the crown, *b* is vertical crown radius, *r* is horizontal crown radius and λ is density (trees/area). The formula above assumes that crown closure is the vertical projection of the canopy elements onto the horizontal plane and that the

canopy elements are non-overlapping. The biomass prediction equations for all species are of the form (Hall et al., 2006):

$$\text{Biomass density} = (b_0 + b_1(\ln(h)) + b_2(CC))^3 \qquad \text{(Equation 3.11)}$$

where b_0, b_1, and b_2 are all empirically derived values that vary by species (Table 3.6). Values for biomass are output in a way similar to basic structural parameters as the algorithm for biomass calculation is called for all potential solutions to the inversion problem. Thus, the model is able to be inverted for biomass, a second order parameter, not found directly in the model, yet still attainable.

Table 3.6 – Coefficients and error for stand level biomass prediction equations[3]

Species	b_0	b_1	b_2	RMSE
Pl	-1.688	2.238	0.009	39.52
SwFir	-1.397	2.028	0.010	49.48
Deciduous	-2.075	2.222	0.011	37.88
Mixed	-2.039	2.246	0.011	38.97

3.6 Satellite Image Analysis

Biophysical structure and biomass density estimates from the MFM modelling technique were compared with biomass estimates using empirical relationships with variables derived from two image analysis techniques (spectral mixture analysis and vegetation indices). These other analysis techniques rely on statistical descriptions (regression) with field data and the remote sensing data or a derivative of the image data.

3.6.1 Vegetation Indices and Reflectance Data

The normalized difference vegetation index (NDVI) was related to biomass density using a linear model and the field biomass density calculations as in previous

[3] Personal communication with R.J. Hall (2004)

studies (Peddle et al., 2001). NDVI is calculated as the fraction of the difference between NIR and red reflectance and their sum (Rouse et al., 1974). The NDVI creates a fixed range of values between -1 and 1. NDVI was chosen due to its ease of computation and pervasiveness in the biophysical parameter estimation literature.

3.6.2 Spectral Mixture Analysis

Sub-pixel abundance of sunlit canopy, shadow and background has also been found to be related to forest structure and biomass (Wu and Strahler, 1994; Hall et al., 1995; Peddle et al., 1999). Linear spectral mixture analysis was used to determine the relative abundances of sub-pixel components for the SPOT imagery. The linear mixture equation was:

$$\rho_{pixel} = \rho_c(f_c) + \rho_b(f_b) + \rho_s(f_s) + \varepsilon \qquad \text{(Equation 3.12)}$$

where ϵ is error, f is fractional abundance, ρ is reflectance and subscripts c, b, and s denote canopy, background and shadow respectively. These scene components were regressed against the plot level biomass density values to create biomass prediction models. Terrain can affect the radiometric signal measured by the sensor and can confound the mixture analysis equation (Johnson, 2000). A series of topographic correction procedures (§ 2.4.2) were employed prior to the mixture analysis in an attempt to improve the biomass prediction models developed using sub-pixel components.

3.7 Biomass Estimates from Satellite Image Analysis and Empirical Models

Past studies have demonstrated that it is possible to relate parameters derived from multispectral data to biomass (§2.6.4, 2.6.5). In this study, the normalized difference vegetation index (NDVI) and endmember fractions derived through spectral

mixture analysis (SMA) were related to biomass through linear regression. Also, the spectral endmember abundances were derived from topographically corrected imagery in an attempt to remove any non-canopy influences on the subpixel components. Separate regression models were created for each species type (conifer, deciduous). In all cases, a cross-validation method was used to estimate prediction error for a field validation plot (Green, 1979).

Cross-validation was used to retain the most information possible (i.e. n-1 data points) within the regression model. The estimates from the linear models were compared based on overall prediction error (absolute RMSE) from the cross-validation analysis and difference between estimated and measured biomass density for individual validation plots.

3.8 Summary

A methodology for obtaining and validating canopy structure estimates was presented in this chapter. First, field data including plot location and canopy structure were collected for 40 plots. The field data were used to derive biomass and biomass density for each plot using published empirical models. These data were compared with estimates of canopy structure and biomass from a LUT-based canopy reflectance model inversion using SPOT-5 image data.

The canopy reflectance model inversion method involved searching of LUTs containing structural data and modeled reflectance. The search procedure, which was developed as software, included new methods for limiting and describing potential solutions in situations where more than one set of structure values produced modeled reflectance values that corresponded to image data. The estimates of canopy structure

produced using this method could also be used to derive average biomass and plot biomass density using empirical relationships between field measured biomass and canopy structure parameters. Two alternative methods (SMA, NDVI) of estimating biomass using empirical relationships with remote sensing derivatives were also used as a comparison to the canopy reflectance model method.

CHAPTER 4

Canopy Structure Estimates from Indirect Canopy Reflectance Model Inversion

4.1 Introduction

In this chapter, the structural parameter estimates from the indirect MFM inversion of the GOMS model are presented. Canopy structure conditions found in the field were used to validate the estimates from the canopy reflectance model inversion approach. The results from the available algorithms (i.e. reflectance equality, closest spectral distance, and spectral range) and input LUTs (i.e. constrained, unconstrained, fine and coarse increments) were compared to determine the most effective methods for obtaining inversion results using the MFM inversion methodology. The comparison was based on overall prediction error (absolute RMSE) for all field plots within each species designation. The methods were also examined at the plot level using error for conifer horizontal and vertical crown radius as an example. This allowed a detailed assessment of predictive capabilities.

4.2 Canopy Structure Description

Field data, as they pertain to the MFM-GOMS inversion procedure, were collected and summarized for deciduous and coniferous species in the study area (Table 4.1). The percentages of total basal area for each species within the field plots were 53.8%, 12.3%, and 33.9% for lodgepole pine (Pl, *Pinus contorta* Loudon), white spruce (Sw, *Picea glauca* (Moench) Voss) and trembling aspen (Aw, *Populus tremuloides* Michx.) respectively.

Table 4.1 – Mean and standard deviation (S.D.) of GOMS structural parameters for lodgepole pine (Pl), Spruce (Sw), and trembling aspen (Aw) within the study area as measured in the field. Parameters include density (λ), horizontal crown radius (r), vertical crown radius (b), and height (h).

Species	n	Parameter	mean	S.D.
Pl	1221	λ (trees/ha)	1500	600
		r (m)	0.99	0.42
		b (m)	2.97	1.2
		h (m)	12.13	2.9
Sw	258	λ	1500	700
		r	1.29	0.48
		b	3.66	1.84
		h	8.94	4.25
Aw	667	λ	1200	400
		r	1.6	0.61
		b	1.62	0.79
		h	12.95	2.71

The measured structural parameters were used to parameterize the GOMS model for LUT generation where the input parameters were constrained. The model run constraints were a function of the distribution of values (Table 4.1). The constraints were within +/- two standard deviations (S.D.) of the mean. Distribution of height (dh) was calculated as four times S.D. or 11.6 m, 17.0 m, and 10.8 m for pine, spruce and aspen respectively as suggested by Wanner (1994).

The observed forest stand conditions used for validation were homogeneous with respect to species composition, and to some extent, structure (Table 4.2 and Table 4.3). As a result, the evaluation of predictive accuracy was likely biased to a smaller range of structural values. Thus, the conclusions regarding applicability of the inversion algorithm improvement only pertain to this montane, sub-alpine forest application. There were, however, some stands with mixed species (e.g. plot 2, plot 5, plot 15). In these stands there was more variation in canopy structure, especially in crown dimensions (horizontal and vertical crown radius).

Table 4.2 – Mean and standard deviation (S.D.) of canopy structure in trembling aspen (Aw) dominant validation plots. Values for density, horizontal (r) and vertical (b) crown radius, height, and basal area shown.

Plot	Dominant Species	Density (trees/ha) *total*	r (m) mean	r (m) S.D.	b (m) mean	b (m) S.D.	h (m) mean	h (m) S.D.	Basal Area (%) Pl / Aw / Sw
3	Aw	1100	1.4	0.3	2.1	2.0	16.3	1.5	19 / 81 / 0
4	Aw	1550	1.1	0.4	1.2	0.4	13.1	1.5	0 / 100 / 0
7	Aw	1100	0.9	0.3	1.2	0.9	9.8	1.3	0 / 89 / 11
9	Aw	950	1.5	0.8	2.7	1.6	14.0	5.0	0 / 69 / 31
10	Aw	1025	1.5	0.4	2.7	0.8	16.1	5.0	0 / 94 / 6
12	Aw	1400	1.1	0.5	2.3	0.8	17.9	3.5	15 / 81 / 4
15	Aw	1675	1.1	0.3	2.5	1.1	15.2	3.5	32 / 61 / 7
18	Aw	775	1.6	0.6	2.8	1.0	18.0	1.8	8 / 92 / 0
25	Aw	1025	1.9	0.5	1.5	0.7	15.8	1.5	0 / 100 / 0
26	Aw	1850	1.6	0.5	1.6	1.3	13.3	2.2	0 / 88 / 12
36	Aw	725	2.6	0.4	1.1	0.4	13.4	1.0	0 / 100 / 0
37	Aw	775	2.2	0.4	1.1	0.5	10.8	2.3	0 / 100 / 0
38	Aw	1725	1.8	0.4	1.4	0.5	15.3	1.6	0 / 100 / 0
39	Aw	1200	2.2	0.4	1.9	1.5	14.7	2.6	8 / 87 / 5
40	Aw	1650	1.9	0.5	1.3	0.6	13.4	2.0	0 / 100 / 0

Table 4.3 – Mean and standard deviation (S.D.) of canopy structure in lodgepole pine (Pl) and white spruce (Sw) dominant validation plots. Values for density, horizontal (r) and vertical (b) crown radius, height, and basal area shown.

Plot	Dominant Species	Density (trees/ha) *total*	r (m) mean	r (m) S.D.	b (m) mean	b (m) S.D.	h (m) mean	h (m) S.D.	Basal Area (%) Pl / Aw / Sw
2	Sw	1375	1.5	0.4	3.1	1.5	15.6	4.6	47 / 3 / 50
6	Sw	750	1.5	0.4	4.6	1.1	14.5	2.0	15 / 0 / 85
5	Sw	1700	1.1	0.3	3.7	1.8	15.9	4.8	27 / 0 / 73
8	Sw	950	1.1	0.4	4.5	2.0	14.8	6.6	0 / 0 / 100
1	Pl	2800	1.1	0.4	2.6	1.2	12.7	4.2	88 / 0 / 12
11	Pl	1425	0.7	0.3	2.6	0.7	14.8	2.5	100 / 0 / 0
13	Pl	1550	0.8	0.3	3.0	1.2	16.5	2.4	100 / 0 / 0
14	Pl	1200	0.9	0.2	3.1	1.3	16.8	3.0	99 / 0 / 1
16	Pl	3025	0.8	0.2	2.2	0.8	14.0	2.4	100 / 0 / 0
17	Pl	1725	0.6	0.3	2.9	1.2	16.7	2.5	100 / 0 / 0
19	Pl	1650	0.8	0.3	3.4	1.0	15.9	2.3	100 / 0 / 0
20	Pl	1350	0.9	0.3	3.2	1.1	10.7	2.1	91 / 0 / 9
21	Pl	2025	0.9	0.3	2.9	1.0	15.4	3.2	98 / 0 / 2
22	Pl	1625	1.0	0.4	3.1	0.9	15.9	1.9	100 / 0 / 0
23	Pl	1950	0.9	0.4	3.4	1.4	15.2	3.4	81 / 3 / 16
24	Pl	1450	0.9	0.3	2.8	1.1	15.0	3.0	100 / 0 / 0
27	Pl	825	1.8	0.7	3.4	1.6	15.3	3.0	69 / 20 / 11
28	Pl	1325	1.4	0.5	3.1	1.2	17.3	4.2	64 / 0 / 36
29	Pl	825	1.6	0.6	3.6	1.4	13.0	3.7	58 / 0 / 42
30	Pl	1900	1.1	0.4	2.4	0.8	15.8	2.5	100 / 0 / 0
31	Pl	650	1.8	0.6	5.0	1.7	19.0	4.2	94 / 0 / 6
32	Pl	1900	0.9	0.2	2.3	0.6	10.6	1.5	100 / 0 / 0
33	Pl	775	1.3	0.4	3.8	1.2	14.3	3.9	94 / 0 / 6
34	Pl	1250	1.5	0.6	3.0	1.0	11.7	2.3	100 / 0 / 0
35	Pl	1275	1.2	0.3	3.3	1.4	12.2	2.5	100 / 0 / 0

The forest structure prediction results for these validation plots may give some indication as to how effective the canopy reflectance model inversion algorithm is when mixed canopy is not explicitly accounted for in the MFM parameterization.

4.3 Indirect Inversion Validation Method

Results were divided into three sets based on the limiting method used for selection of potential matches. These limiting methods were: a) matching based on closest spectral distance, b) matching using exact values, and c) matching based on a range of spectral distance or domains of uncertainty. In the following sections, the benefits of using other constraint methods (multiple bands, DEM) are discussed along with the measures of central tendency used to select an inversion result from the distribution (median, mode). The efficacy of the inversion methods were evaluated based on agreement between measured canopy element dimensions and values extracted from solution distributions from the LUT inversion procedure. This was done for the entire set of validation sites for each species type and evaluated based on absolute RMSE:

$$RMSE_{absolute} = \sqrt{\frac{1}{n}\sum_{i=1}^{n}\left(x - x_m\right)^2} \qquad \text{(Equation 4.1)}$$

where x is the model predicted structural value, x_m is the measured structural value and n is the number of validation plots. It is important to note that while the value being extracted via central tendency was used for validation purposes, the actual "true value" may have been located anywhere within the distribution of potential solutions. Also, the validation data were averaged for an area corresponding to the same physical dimensions as a SPOT image pixel (20 m).

4.3.1 Estimates of Structure Using Reflectance Equality as a Match Criteria

The use of reflectance equality as match criteria in indirect inversion has been used most extensively in past MFM inversion studies (Peddle et al., 2003a; 2004). This method assumes little or no error in imaging and calibration processes as well as a high level of agreement between model and measured reflectance unless a tolerance is used, as in Peddle et al. (2004). The assumptions within this technique are similar to those of the closest spectral distance method but with two primary differences. By using reflectance equality at proper precision it is possible to find more than one potential inversion solution within the LUT set. Thus, if a single output value is desired, it is necessary to summarize these solutions using a measure of central tendency or some other summary statistic. It is also possible to find no solutions to the inversion problem, or no reflectance values in the LUT set that correspond to the measured reflectance. A "no solution" mask was assigned to the image pixel if there was no solution. These pixels are typically non-forest, or contain a forest type not included in the LUT.

With a smaller number of input matching criteria (i.e. two band input or two band input with DEM derivatives) the inversion procedure yielded a near-complete set of inversion solutions with the exception of three validation sites (Tables 4.4 and 4.5). With more input matching criteria, the number of sites with no solution increased to include the majority of the field plots.

This suggested one, or a combination of the following issues. The first potential issue was that the amount of modeled reflectance coverage within the spectral space co-occupied by the measured reflectance was inadequate (i.e. areas with no modeled data due to input parameter limiting). Another potential problem was that the canopy

reflectance model was not appropriate for some wavelengths (e.g. SPOT band 4) and was incapable of producing a proper set of modeled reflectance for an expanded set of inversion spectral inputs. Finally, it was possible that there was no match due to endmember measurement or calibration error and image calibration error, or pixels containing elements not represented by the endmember model.

To properly compare the error results from this inversion method to the results from the methods based on a spectral distance function, situations where more than 20% of the validation plots result in no matches were excluded. If these situations were utilized within a mapping context, there would be a considerable lack of spatial coverage that would be undesirable in evaluating forest structure over large areas. However, in these situations it appeared that the model inversion was reasonably effective in predicting canopy structure for the few plots where a match occurred as evidenced by the relatively low prediction error values.

Within this method, estimates were improved for all conifer structural parameters through limiting the LUTs using extents from the *in situ* parameter distributions (MFM run 3 and 4). The choice of central tendency measure also had an effect on estimate accuracy. The mode-based estimate was most accurate for the unconstrained LUTs (MFM run 1 and 2) while the median method was most accurate for the constrained LUTs. Within this method the use of more complex LUTs (MFM run 2 and 4) improved accuracy for the unconstrained LUTs but not for constrained LUTs. The minimum error using the reflectance equality method was: 707 stems/ha density, 2 m h, 0.8 m r, 0.7 m b, and 3.9 m dh for conifer stands. For deciduous stands the minimum error was: 356

stems/ha density, 2.5 m *h*, 0.7 m *r*, 0.9 m *b*, and 5.5 m dh. These observations were consistent with the results for deciduous stands (Tables 4.6 and 4.7).

The number of input bands and ancillary information also had an effect on the predictive ability. Ancillary information, in the form of terrain slope and aspect, was included so that a reflectance match must also include a match between DEM data and model inputs for terrain. The inclusion of terrain data as a constant within the inversion procedure did not improve prediction error when compared to cases where terrain data was not included, with the exception of conifer stem density in MFM run 1 and MFM run 2, deciduous stem density in MFM run 1, and deciduous vertical crown radius in MFM run 1. As mentioned earlier, the inclusion of additional spectral input bands resulted in an increase in cases where no matching value was found between model and measured reflectance resulting in an incomplete inversion.

Table 4.4 – Absolute RMSE in prediction of density and height (h) for 25 conifer validation plots using the reflectance equality match criterion.

		Absolute RMSE				
		density (trees/ha)		h (m)		
	Input Bands	median	mode	median	mode	no matches
MFM Run 1	2,3	1544	2811	2.0	2.0	3
	2,3, slope, aspect	2046	1656	2.0	2.0	3
	1,2,3,4	578	578	2.0	2.0	23
	1,2,3,4, slope, aspect	-	-	-	-	25
MFM Run 2	2,3	1174	2253	2.0	2.0	3
	2,3, slope, aspect	1715	1602	2.0	2.0	3
	1,2,3,4	980	987	2.0	2.0	14
	1,2,3,4, slope, aspect	260	260	2.0	2.0	24
MFM Run 3	2,3	707	822	2.0	2.0	0
	2,3, slope, aspect	808	956	2.0	2.0	2
	1,2,3,4	615	615	2.0	2.0	14
	1,2,3,4, slope, aspect	394	394	2.0	2.0	23
MFM Run 4	2,3	723	801	2.0	2.0	0
	2,3, slope, aspect	758	1038	2.0	2.0	1
	1,2,3,4	564	821	2.0	2.0	12
	1,2,3,4, slope, aspect	405	405	2.0	2.0	18

Table 4.5 – Absolute RMSE in prediction of vertical crown radius (r), vertical crown radius (h), and height distribution (dh) for 25 conifer validation plots using the reflectance equality match criterion.

		Absolute RMSE					
		r (m)		b (m)		dh (m)	
	Input Bands	median	mode	median	mode	median	mode
MFM Run 1	2,3	3.0	1.6	1.4	1.3	5.0	8.8
	2,3, slope, aspect	3.2	2.8	1.5	1.4	8.4	8.2
	1,2,3,4	0.2	0.2	0.3	0.3	0.4	3.1
	1,2,3,4, slope, aspect	-	-	-	-	-	-
MFM Run 2	2,3	2.3	1.9	0.9	1.0	5.8	5.4
	2,3, slope, aspect	2.2	1.8	0.9	1.0	6.1	7.2
	1,2,3,4	2.9	2.7	0.9	0.9	2.6	6.1
	1,2,3,4, slope, aspect	0.1	0.1	0.2	0.2	0.6	2.4
MFM Run 3	2,3	0.8	0.8	0.9	0.9	4.3	6.0
	2,3, slope, aspect	0.9	0.9	0.7	0.8	3.9	6.1
	1,2,3,4	0.3	0.3	0.5	0.5	4.0	4.5
	1,2,3,4, slope, aspect	0.2	0.2	0.2	0.2	0.8	2.7
MFM Run 4	2,3	0.9	1.0	1.0	1.1	4.1	5.7
	2,3, slope, aspect	0.9	0.9	1.0	1.3	4.0	5.8
	1,2,3,4	0.3	0.3	0.9	0.9	3.1	5.1
	1,2,3,4, slope, aspect	0.3	0.2	0.8	0.8	3.6	4.2

Table 4.6 - Absolute RMSE in prediction of density and height (h) for 15 deciduous validation plots using the reflectance equality match criterion.

		Absolute RMSE				
		density (trees/ha)		h (m)		
	Input Bands	median	mode	median	mode	no matches
MFM Run 1	2,3	1650	2241	2.5	2.5	0
	2,3, slope, aspect	1123	856	2.5	2.5	2
	1,2,3,4	-	-	-	-	15
	1,2,3,4, slope, aspect	-	-	-	-	15
MFM Run 2	2,3	755	908	2.5	2.5	0
	2,3, slope, aspect	998	1016	2.5	2.5	1
	1,2,3,4	-	-	-	-	15
	1,2,3,4, slope, aspect	-	-	-	-	15
MFM Run 3	2,3	356	398	2.5	2.5	0
	2,3, slope, aspect	604	675	2.5	2.5	0
	1,2,3,4	-	-	-	-	15
	1,2,3,4, slope, aspect	-	-	-	-	15
MFM Run 4	2,3	482	807	2.5	2.5	0
	2,3, slope, aspect	868	1046	2.5	2.5	0
	1,2,3,4	-	-	-	-	15
	1,2,3,4, slope, aspect	-	-	-	-	15

Table 4.7 – Absolute RMSE in prediction of vertical crown radius (r), vertical crown radius (h), and height distribution (dh) for 15 deciduous validation plots using the reflectance equality match criterion.

		Absolute RMSE					
		r (m)		b (m)		dh (m)	
	Input Bands	median	mode	median	mode	median	mode
MFM Run 1	2,3	1.2	1.2	2.9	2.7	7.6	9.4
	2,3, slope, aspect	3.2	3.1	1.8	1.3	9.0	8.9
	1,2,3,4	-	-	-	-	-	-
	1,2,3,4, slope, aspect	-	-	-	-	-	-
MFM Run 2	2,3	2.6	2.7	1.0	0.9	7.6	10.5
	2,3, slope, aspect	2.6	2.5	1.4	0.9	8.1	6.7
	1,2,3,4	-	-	-	-	-	-
	1,2,3,4, slope, aspect	-	-	-	-	-	-
MFM Run 3	2,3	1.2	0.9	1.1	1.1	5.5	6.3
	2,3, slope, aspect	1.4	1.0	1.2	1.1	7.5	6.9
	1,2,3,4	-	-	-	-	-	-
	1,2,3,4, slope, aspect	-	-	-	-	-	-
MFM Run 4	2,3	0.9	0.7	1.0	1.0	6.5	9.0
	2,3, slope, aspect	1.5	1.1	1.3	1.3	5.8	8.1
	1,2,3,4	-	-	-	-	-	-
	1,2,3,4, slope, aspect	-	-	-	-	-	-

One interesting phenomenon to note within the first set of results was that estimation error for height did not vary between LUTs, input bands, or the measure of central tendency. This was also observed in the results of the other inversion methods. This may suggest that there was little sensitivity to height within the canopy reflectance model or inversion process. Accordingly, a model sensitivity test was carried out to determine the effect of the height parameter on modeled reflectance. The results showed that the GOMS modelled reflectance was not sensitive to the height to crown center input parameter (Appendix A).

4.3.2 Estimates of Structure Using Closest Spectral Distance

Under optimal conditions, choosing a single potential inversion solution based on the closest spectral distance calculated using equation 1 should be as effective for predicting canopy structural parameters as reflectance equality. If the canopy reflectance

is accurately modeled and there is little error in calibrated satellite data then the extracted model input structural parameters should closely correspond to conditions observed *in situ*. Here, the closest spectral values within the LUT were selected according to the spectral distance equation (§ 3.6.4.1) to select individual solutions from the MFM LUTs.

The results for the structural parameter estimates were within an error margin that closely corresponded to the increment size for the vertical and horizontal crown radius (Tables 4.8 and 4.9). Error for conifer horizontal crown radius (r) estimates was between 1.2 m and 1.7 m for MFM run 1 (increment: 2 m), between 0.6 m and 1.1 m for MFM run 2 (increment 1 m), 0.6 m and 0.8 m for MFM run 3 (increment 1 m) and 0.4 m and 0.7 m for MFM run 4 (increment 0.5 m). This may suggest that the average error of this inversion procedure was dependant on the sampling increment of *P*.

As a result, the sampling schemes with the finer increment precision (MFM run 4) yield inversion results with higher levels of agreement with field data. However, as the increment size decreases the mean error values become closer to the increment size and it is likely that a threshold value exists where error will cease to decrease with increasing increment precision. This observation also applied to the vertical crown radius estimates where estimate error was within 2 m for MFM run1 and MFM run 2, and close to 1 m for MFM run 3 and MFM run 4. However, this observation does not hold for deciduous r and b. While the error does decrease with increasing precision it does not follow the increment step size used to generate the LUT as closely as the conifer estimate error. Error for deciduous horizontal crown radius (r) estimates was between 1.2 m and 4.2 m for MFM run 1 (increment: 2 m), between 1.2 m and 2.3 m for MFM run 2 (increment 1

m), 0.8 m and 1.3 m for MFM run 3 (increment 1 m) and 0.8 m and 0.9 m for MFM run 4 (increment 0.5 m).

Error for deciduous crown radius was also related to increment step size. Larger increment size corresponded to larger estimate errors. For example, RMSE for horizontal crown radius estimates was between 1.5m and 4.1 m for MFM run 1 (increment: 2 m), 0.9 m and 4.3 m for MFM run 2 (increment: 2 m), 1.0 m and 1.2 m for MFM run 3 (increment: 1 m), and 1.0 m and 1.3 m for MFM run 4 (increment: 1 m).

Table 4.8 – Absolute RMSE in prediction of conifer canopy structure using the closest spectral distance method for 25 validation plots.

		Absolute RMSE				
	Input Bands	**r (m)**	**b (m)**	**dh (m)**	**density (trees/ha)**	**h (m)**
MFM Run 1	2,3	1.7	1.7	9.1	1596	2.0
	2,3, slope, aspect	1.3	1.7	8.8	1635	2.0
	1,2,3,4	1.3	1.6	10.0	1434	2.0
	1,2,3,4, slope, aspect	1.2	1.2	9.5	1501	2.0
MFM Run 2	2,3	0.9	1.3	8.6	977	2.0
	2,3, slope, aspect	1.1	1.6	11.3	1098	2.0
	1,2,3,4	0.6	0.9	11.3	818	2.0
	1,2,3,4, slope, aspect	0.8	1.1	11.4	992	2.0
MFM Run 3	2,3	0.7	0.8	5.1	868	2.0
	2,3, slope, aspect	0.6	0.9	6.8	825	2.0
	1,2,3,4	0.6	1.0	5.9	954	2.0
	1,2,3,4, slope, aspect	0.8	1.0	5.3	934	2.0
MFM Run 4	2,3	0.5	1.1	5.3	932	2.0
	2,3, slope, aspect	0.6	1.1	6.2	885	2.0
	1,2,3,4	0.4	1.3	6.1	960	2.0
	1,2,3,4, slope, aspect	0.7	1.1	5.5	963	2.0

Table 4.9 – Absolute RMSE in prediction of deciduous canopy structure using the closest spectral distance method for 15 validation plots.

		Absolute RMSE				
	Input Bands	r (m)	b (m)	dh (m)	density (trees/ha)	h (m)
MFM Run 1	2,3	4.2	2.7	7.3	3133	2.5
	2,3, slope, aspect	2.0	1.5	13.3	878	2.5
	1,2,3,4	1.2	4.1	16.5	572	2.5
	1,2,3,4, slope, aspect	1.2	2.3	11.9	931	2.5
MFM Run 2	2,3	2.3	2.8	12.0	1105	2.5
	2,3, slope, aspect	1.3	0.9	12.2	562	2.5
	1,2,3,4	1.2	4.3	16.1	822	2.5
	1,2,3,4, slope, aspect	1.2	2.7	15.8	793	2.5
MFM Run 3	2,3	1.3	1.2	9.3	611	2.5
	2,3, slope, aspect	1.3	1.0	9.7	681	2.5
	1,2,3,4	0.8	1.1	10.9	400	2.5
	1,2,3,4, slope, aspect	0.8	1.1	7.8	407	2.5
MFM Run 4	2,3	0.9	1.0	8.5	520	2.5
	2,3, slope, aspect	0.8	1.0	9.2	488	2.5
	1,2,3,4	0.8	1.3	11.8	470	2.5
	1,2,3,4, slope, aspect	0.8	1.2	9.8	485	2.5

The height distribution estimate error was higher for deciduous species than conifer species, while the error in density estimates was lower for deciduous species. The height distribution and density estimate error was reduced by using the constrained LUT set (MFM run 3, MFM run 4). However, the error did not correspond to increment step size set during LUT generation.

The number of input spectral bands used in the inversion procedure had an effect on the inversion results using the closest spectral distance method. A decrease in mean estimate error for r was observed for all MFM scenarios when all SPOT bands were used in the inversion procedure. The decrease in absolute RMSE was most substantial for the MFM LUTs with larger input parameter increments and ranges.

This suggested that there was a maximum level of accuracy that may be achieved through using smaller input parameter increments after which improvements by using additional techniques are minimal or negligible. For vertical crown radius, the use of

additional input channels only improved the structural estimates for the first two LUT sets (MFM run 1, MFM run 2). For density, a similar observation was made when terrain data were not used in the inversion. The error levels remained similar in the LUT sets where *in situ* data were used to limit the inputs (MFM run 3, MFM run 4). The use of terrain input channels did not consistently improve the structural estimates. There are a number of potential reasons for this including terrain input generalization, and oversimplification of the effect of terrain on modeled reflectance.

4.3.3 Estimates of Structure Using Spectral Domain as a Match Criteria

In cases where there was a level of inherent uncertainty in measured and modeled reflectance, the inversion algorithm was affected and may not have yielded structural values that correspond to parameters measured in the field. To account for discrepancies in the spectral domain resulting from imaging and modelling error, a range of potential solutions were extracted from the LUT using a predefined spectral error domain size based on the relative RMSE between measured and modeled reflectance dictated by the spectral distance function. The number of potential solutions returned was related to the error domain selected. In this study, the domain size was systematically varied to examine the effect of domain size on the inversion results. In some cases, the distribution of potential solutions narrowed and the median or mode value shifted with decreasing domain size (Figure 4.1). As the distribution narrowed, the difference between the measured structure and estimated structure decreased until a minimum point. At this point, the domain of uncertainty may closely approximate that found in the measured and modeled reflectance data set. This was confirmed by minimum absolute RMSE for

structural values occurring at similar error domain sizes when comparing the two band and four band input results across the two LUT sets.

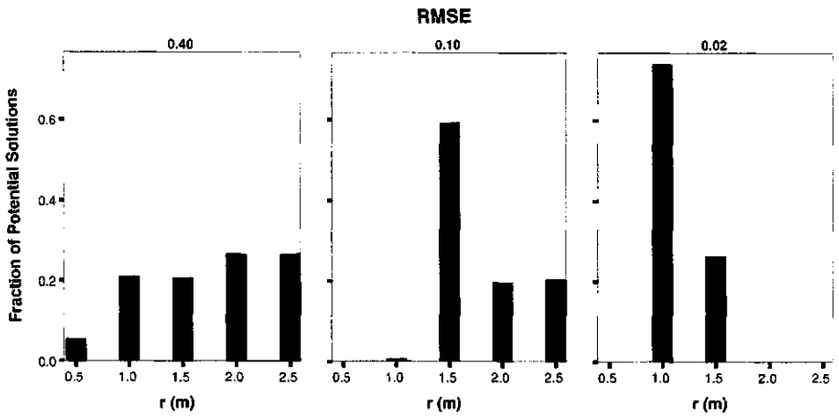

a)

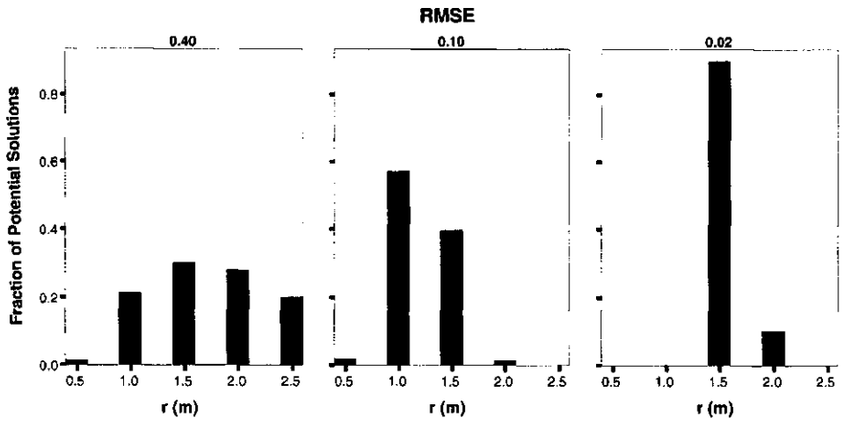

b)

Figure 4.1 – Distribution of potential solutions of horizontal crown radius for two conifer plots with varying spectral distance ranges (relative RMSE 0.4 – 0.02). Average field measured values of horizontal crown radius: a) 1.2m (min: 0.6, max 2.0); b) 1.3 (min: 0.9, max: 2.3).

Table 4.10 – Lowest absolute RMSE for prediction of conifer density and height (h) using the spectral domain method for 25 field validation plots. Values represent lowest RMSE using variable spectral domains. Spectral domain size (relative RMSE) is in brackets. The (-) symbol denotes constant returns over variable spectral domain size.

		Absolute RMSE			
		density (trees/ha)		h (m)	
	Input Bands	median	mode	median	mode
MFM Run 1	2,3	2110 (0.05)	1210 (0.10)	2.0 (-)	2.0 (-)
	2,3, slope, aspect	2860 (0.05)	1220 (0.30)	2.0 (-)	2.0 (-)
	1,2,3,4	2300 (0.34)	940 (0.38)	2.0 (-)	2.0 (-)
	1,2,3,4, slope, aspect	1860 (0.34)	1010 (0.38)	2.0 (-)	2.0 (-)
MFM Run 2	2,3	1030 (0.05)	900 (0.30)	2.0 (-)	2.0 (-)
	2,3, slope, aspect	1060 (0.10)	1040 (0.30)	2.0 (-)	2.0 (-)
	1,2,3,4	880 (0.20)	790 (0.50)	2.0 (-)	2.0 (-)
	1,2,3,4, slope, aspect	1050 (0.40)	1030 (0.40)	2.0 (-)	2.0 (-)
MFM Run 3	2,3	680 (0.40)	820 (0.10)	2.0 (-)	2.0 (-)
	2,3, slope, aspect	700 (0.30)	840 (0.10)	2.0 (-)	2.0 (-)
	1,2,3,4	610 (0.50)	930 (0.40)	2.0 (-)	2.0 (-)
	1,2,3,4, slope, aspect	620 (0.50)	940 (0.50)	2.0 (-)	2.0 (-)
MFM Run 4	2,3	690 (0.20)	950 (0.05)	2.0 (-)	2.0 (-)
	2,3, slope, aspect	660 (0.10)	810 (0.05)	2.0 (-)	2.0 (-)
	1,2,3,4	590 (0.40)	820 (0.40)	2.0 (-)	2.0 (-)
	1,2,3,4, slope, aspect	590 (0.40)	860 (0.40)	2.0 (-)	2.0 (-)

Table 4.11 – Lowest absolute RMSE for prediction of conifer horizontal crown radius (r), vertical crown radius (b), and height distribution (dh) using the spectral domain method for 25 field validation plots. Values represent lowest RMSE using variable spectral domains. Spectral domain size (relative RMSE) is in brackets.

		Absolute RMSE					
		r (m)		b (m)		dh (m)	
	Input Bands	median	mode	median	mode	median	mode
MFM Run 1	2,3	2.2 (0.05)	1.4 (0.50)	1.9 (0.05)	0.8 (0.30)	13.4 (0.05)	8.5 (0.10)
	2,3, slope, aspect	3.5 (0.05)	1.7(0.50)	2.3 (0.05)	0.9 (0.30)	14.6 (0.05)	7.0 (0.05)
	1,2,3,4	2.2 (0.05)	1.6 (0.36)	1.8 (0.34)	0.7 (0.40)	11.8 (0.05)	6.9 (0.50)
	1,2,3,4, slope, aspect	2.6 (0.05)	1.3 (0.35)	1.9 (0.34)	0.9 (0.50)	13.9 (0.05)	7.0 (0.35)
MFM Run 2	2,3	1.0 (0.05)	1.0 (0.05)	1.0 (0.20)	1.0 (0.05)	5.3 (0.20)	6.2 (0.30)
	2,3, slope, aspect	1.3 (0.05)	1.1 (0.50)	1.0 (0.30)	1.1(0.50)	5.6 (0.20)	6.8 (0.20)
	1,2,3,4	1.3 (0.15)	1.3 (0.50)	0.9 (0.30)	1.3 (0.50)	5.5 (0.10)	6.0 (0.20)
	1,2,3,4, slope, aspect	1.3 (0.15)	1.3 (0.50)	0.9 (0.30)	1.4 (0.15)	5.6 (0.20)	5.6 (0.40)
MFM Run 3	2,3	0.5 (0.50)	0.6 (0.05)	0.6 (0.40)	0.9 (0.05)	3.9 (0.50)	4.0 (0.40)
	2,3, slope, aspect	0.6 (0.50)	0.6 (0.05)	0.6 (0.40)	0.9 (0.10)	3.9 (0.50)	3.5 (0.40)
	1,2,3,4	0.6 (0.38)	0.6 (0.38)	0.8 (0.50)	0.8 (0.50)	3.8 (0.40)	4.7 (0.50)
	1,2,3,4, slope, aspect	0.7 (0.38)	0.6 (0.36)	0.8 (0.50)	0.9 (0.50)	3.5 (0.40)	4.7 (0.40)
MFM Run 4	2,3	0.5 (0.05)	0.4 (0.10)	0.7 (0.50)	0.8 (0.20)	3.4 (0.20)	3.7 (0.20)
	2,3, slope, aspect	0.5 (0.10)	0.5 (0.10)	0.7 (0.50)	0.8 (0.30)	3.4 (0.20)	3.9 (0.40)
	1,2,3,4	0.4 (0.34)	0.4 (0.36)	0.9 (0.50)	0.9 (0.50)	3.7 (0.50)	4.1 (0.35)
	1,2,3,4, slope, aspect	0.4 (0.38)	0.5 (0.38)	0.9 (0.50)	0.9 (0.50)	3.4 (0.50)	3.6 (0.50)

Table 4.12 – Lowest absolute RMSE for prediction of deciduous density and height (h) using the spectral domain method for 15 field validation plots. Values represent lowest RMSE using variable spectral domains. Spectral domain size (relative RMSE) is in brackets. The (-) symbol denotes constant returns over variable spectral domain size.

		Absolute RMSE			
		density (trees/ha)		h (m)	
	Input Bands	median	mode	median	mode
MFM Run 1	2,3	830 (0.10)	420 (0.30)	2.5 (-)	2.5 (-)
	2,3, slope, aspect	590 (0.30)	460 (0.40)	2.5 (-)	2.5 (-)
	1,2,3,4	790 (0.18)	450 (0.30)	2.5 (-)	2.5 (-)
	1,2,3,4, slope, aspect	570 (0.40)	480 (0.30)	2.5 (-)	2.5 (-)
MFM Run 2	2,3	820 (0.50)	510 (0.50)	2.5 (-)	2.5 (-)
	2,3, slope, aspect	830 (0.30)	390 (0.50)	2.5 (-)	2.5 (-)
	1,2,3,4	300 (0.18)	460 (0.18)	2.5 (-)	2.5 (-)
	1,2,3,4, slope, aspect	530 (0.30)	570 (0.30)	2.5 (-)	2.5 (-)
MFM Run 3	2,3	420 (0.05)	430 (0.10)	2.5 (-)	2.5 (-)
	2,3, slope, aspect	420 (0.10)	400 (0.10)	2.5 (-)	2.5 (-)
	1,2,3,4	330 (0.20)	310 (0.30)	2.5 (-)	2.5 (-)
	1,2,3,4, slope, aspect	360 (0.20)	360 (0.18)	2.5 (-)	2.5 (-)
MFM Run 4	2,3	350 (0.05)	440 (0.20)	2.5 (-)	2.5 (-)
	2,3, slope, aspect	380 (0.20)	470 (0.10)	2.5 (-)	2.5 (-)
	1,2,3,4	320 (0.20)	400 (0.18)	2.5 (-)	2.5 (-)
	1,2,3,4, slope, aspect	340 (0.20)	360 (0.18)	2.5 (-)	2.5 (-)

Table 4.13 – Lowest absolute RMSE for prediction of deciduous horizontal crown radius (r), vertical crown radius (b), and height distribution (dh) using the spectral domain method for 15 field validation plots. Values represent lowest RMSE using variable spectral domains. Spectral domain size (relative RMSE) is in brackets.

		Absolute RMSE					
		r (m)		b (m)		dh (m)	
	Input Bands	median	mode	median	mode	median	mode
MFM Run 1	2,3	1.2 (0.50)	1.0 (0.50)	0.9 (0.05)	0.9 (0.10)	7.6 (0.50)	6.9 (0.50)
	2,3, slope, aspect	1.6 (0.50)	0.9 (0.50)	0.9 (0.20)	0.9 (0.50)	7.6 (0.50)	5.7 (0.50)
	1,2,3,4	1.0 (0.50)	1.2 (0.40)	1.0 (0.50)	0.9 (0.50)	7.6 (0.50)	5.6 (0.40)
	1,2,3,4, slope, aspect	1.2 (0.30)	1.2 (0.30)	0.9 (0.40)	0.9 (0.50)	7.6 (0.50)	6.6 (0.40)
MFM Run 2	2,3	1.9 (0.50)	1.1 (0.50)	1.0 (0.30)	0.9 (0.10)	7.6 (0.50)	6.4 (0.10)
	2,3, slope, aspect	1.9 (0.50)	1.4 (0.40)	0.9 (0.20)	0.9 (0.30)	7.6 (0.50)	6.1 (0.40)
	1,2,3,4	1.1 (0.18)	1.1 (0.18)	1.0 (0.40)	0.9 (0.50)	7.6 (0.50)	6.0 (0.30)
	1,2,3,4, slope, aspect	0.9 (0.18)	0.9 (0.18)	0.9 (0.40)	0.9 (0.50)	7.6 (0.50)	5.1 (0.20)
MFM Run 3	2,3	0.6 (0.50)	0.4 (0.40)	1.1 (0.30)	1.1 (0.20)	4.4 (0.05)	8.6 (0.30)
	2,3, slope, aspect	0.6 (0.50)	0.4 (0.30)	1.1 (0.30)	1.1 (0.05)	6.7 (0.30)	7.8 (0.20)
	1,2,3,4	0.5 (0.30)	0.5 (0.30)	0.7 (0.30)	1.0 (0.30)	5.5 (0.40)	5.9 (0.40)
	1,2,3,4, slope, aspect	0.5 (0.30)	0.5 (0.30)	0.8 (0.30)	0.8 (0.30)	6.0 (0.40)	6.2 (0.40)
MFM Run 4	2,3	0.6 (0.50)	0.4 (0.30)	1.0 (0.10)	1.0 (0.20)	4.6 (0.05)	7.6 (0.10)
	2,3, slope, aspect	0.7 (0.50)	0.4 (0.30)	1.1 (0.50)	1.1 (0.10)	6.3 (0.20)	7.2 (0.20)
	1,2,3,4	0.9 (0.20)	0.8 (0.30)	0.7 (0.30)	1.0 (0.40)	5.7 (0.30)	5.7 (0.30)
	1,2,3,4, slope, aspect	0.8 (0.20)	0.5 (0.30)	0.7 (0.50)	0.8 (0.30)	5.9 (0.30)	6.2 (0.40)

Comparing the structural estimate error using error domains to those using closest spectral distance showed that in general the absolute structural estimate error using this technique reached levels equivalent to, or lower than closest spectral distance (Tables 4.10 – 4.13). For example, the minimum absolute structural RMSE for MFM run 4 conifer horizontal crown radius estimates for the error domain method were all less than or equal to 0.5 m while the closest spectral distance values were within 0.7 m.

The results are similar for the conifer vertical crown radius with overall estimate error within 1m for minimum values within the error domain method and within 1.3 m for the closest spectral distance method. The estimate error for conifer density using the spectral domain technique was also lower than the closest spectral distance method. However in some cases (e.g. MFM run 2), the horizontal crown radius estimate error using four input bands was considerably higher for the spectral domain method with the closest spectral distance method showing an RMSE improvement greater than 1m.

Similar observations can be made regarding the RMSE for the deciduous validation stands. For example, the lowest density RMSE was 310 stems/ha compared to 398 stems/ha and 400 stems/ha for reflectance equality and spectral distance respectively. Horizontal crown radius reached a minimum prediction error of 0.4 m, vertical crown radius prediction error reached a minimum of 0.7 m, and height distribution prediction error reached a minimum of 4.4 m. There were no values lower than these found within the spectral distance and reflectance equality results.

There was a substantial difference in structural RMSE between mode and median methods. Selection of the mode values appears to be more effective for selecting structural values in the LUTs with an unconstrained parameter range (MFM run 1, MFM

run 2). Conversely, the median was more appropriate for selecting values from the constrained range LUTs. The distribution of potential solutions selected from LUTs with unconstrained ranges may contain potential solutions located at the extremes of the distribution. The potential for extreme values increases with domain size. The median method is affected by the inclusion of these values within the distribution, while the mode method is not. The median method would be least effective in situations where a large skewed distribution of potential solutions was present or in multimodal distributions. There is potential for both of these situations when selecting a large range of potential solutions from the unconstrained range LUT sets.

In most cases, the use of four spectral information bands improved the estimates of structure. While this observation did not hold for all cases, it should be noted that there were no instances of a considerable error increase resulting from the use of four information bands. Any increases in error were generally less than 0.3 m for crown dimensions and less than 300 stems/ha density. The use of terrain data bands did not consistently improve the structural RMSE.

4.4 Canopy Structure Estimates: Individual Plots

It is possible to gain additional perspective by examining the structural estimates in detail. As an example, a detailed plot level vertical and horizontal canopy radius results were examined and discussed for conifer validation plots. The difference between estimated and actual structural values reveals that, for this example, there is no general trend to the prediction error with the exception of the reflectance equality-based estimates of horizontal crown radius where the structural values were consistently over-predicted

(Figure 4.2). There were also consistently high levels of difference for some test plots. For instance, structural estimates for validation plot 4 showed consistently high error regardless of estimation method (Figures 4.2 and 4.3).

A wide range of canopy conditions were found within the distributed validation plots. As a result some conditions within these validation plots were outside of the bounds of the distributions used to generate the restricted (2 S.D. of structure) LUT sets. In validation plot 4, while the horizontal and vertical crown radii were within the distribution of values present in the LUT, the stem density falls outside the range of LUT inputs. Therefore, the structural estimates from this inversion procedure were in error as the true structural conditions were not represented within the potential solutions based on the inputs and ranges specified. The inversion procedure will still select a set of potential solutions, however the matching reflectance will have been generated by a set of structural conditions that, in effect, are overcompensating for the single structural parameter not found within the distribution of values.

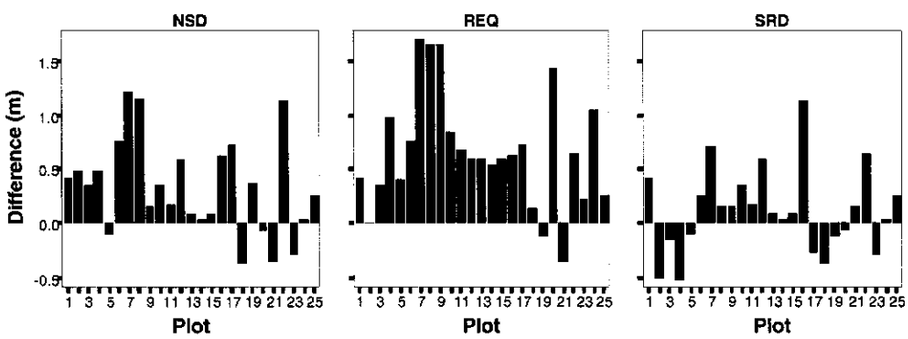

Figure 4.2 – Difference between predicted and measured horizontal crown radius for 25 plots. Figures are for nearest spectral distance (NSD), reflectance equality (REQ), and spectral range (SRD), respectively. Figures show lowest overall absolute RMSE.

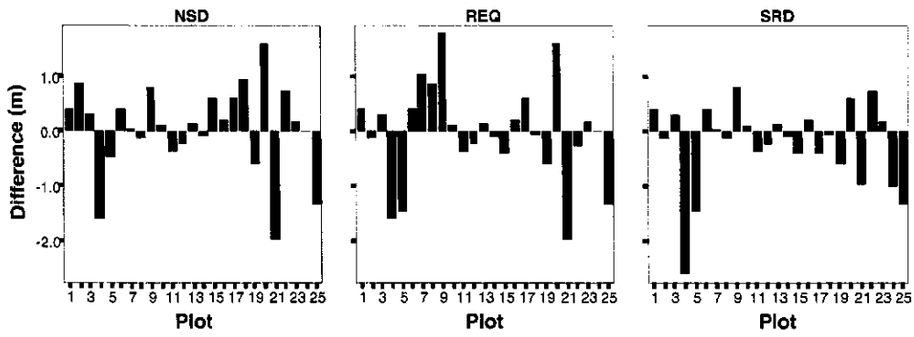

Figure 4.3 - Difference between predicted and measured vertical crown radius for 25 plots. Figures are for nearest spectral distance (NSD), reflectance equality (REQ), and spectral range (SRD), respectively. Figures show lowest overall absolute RMSE.

While there were cases of high estimation error, the majority of the estimates were within 0.5 m of the averaged crown dimensions measured on the ground, with the exception of the estimates of horizontal crown radius using the reflectance equality inversion method. This was viewed as a very positive result, given that this information has been extracted from information recorded on an orbital platform hundreds of kilometres above the earth. For horizontal crown radius, the percentage of estimates falling within 0.5 m difference of the averaged measured value was 72% of the estimates for the nearest spectral distance method, 36% of the estimates for the reflectance equality method, and 80% of the estimates for the method using spectral domains. For vertical crown radius, the percentage of estimates falling within 0.5 m difference was 56% for the nearest spectral distance method, 72% for the reflectance equality method, and 60% for the spectral domain method. The maximum error was 1.7 m for horizontal crown radius and 3.6 m for vertical crown radius, both occurring within the reflectance equality method.

4.5 Sample Image Output

It is possible to use the canopy reflectance model inversion software to map stand structure parameters over large areas using satellite image input. The following example is for a 400x400 pixel (6400 ha) area centered on Barrier Lake (Figure 4.4). The results for density show relatively homogeneous densities for the majority of the area with some expected low density areas near paths, roads and at higher elevations (Figure 4.5). Horizontal and vertical crown radius show some expected patterns as well, including lower horizontal crown radius at higher elevations (Figure 4.6), lower vertical crown radius values in the cut-blocks on the right side of the image (Figure 4.7), and higher horizontal crown radius with lower vertical crown radius for aspen stands on the north end of Barrier Lake.

Some areas showed a potential topographic influence on the estimates of forest stand structure. For example, north-northwest facing slopes typically had lower predicted values of horizontal crown radius and higher predicted values of vertical crown radius than south facing slopes. It was possible to examine this by comparing structural validation values in plots located on north-northwest facing slopes against those on more south facing slopes (Figure 3.4, Table 4.3). The field data for north facing plots (e.g. plots 11, 28, and 32) showed lower mean horizontal crown radius and lower mean vertical crown radius than south facing validation plots (e.g. plots 6, 34, 35). This was not fully consistent with the mapped output for vertical crown radius (Figure 4.7). This might be explained as a result of the topographic effect (§ 2.4.1) in the input satellite imagery. It is possible that the canopy reflectance model was not able to fully characterize terrain effects, and some structural estimates may have been affected as a result.

Figure 4.4 – 400x400 pixel SPOT test image (acquisition: Aug 12th, 2004) centered on Barrier Lake. This image was used as input to create the structural estimates

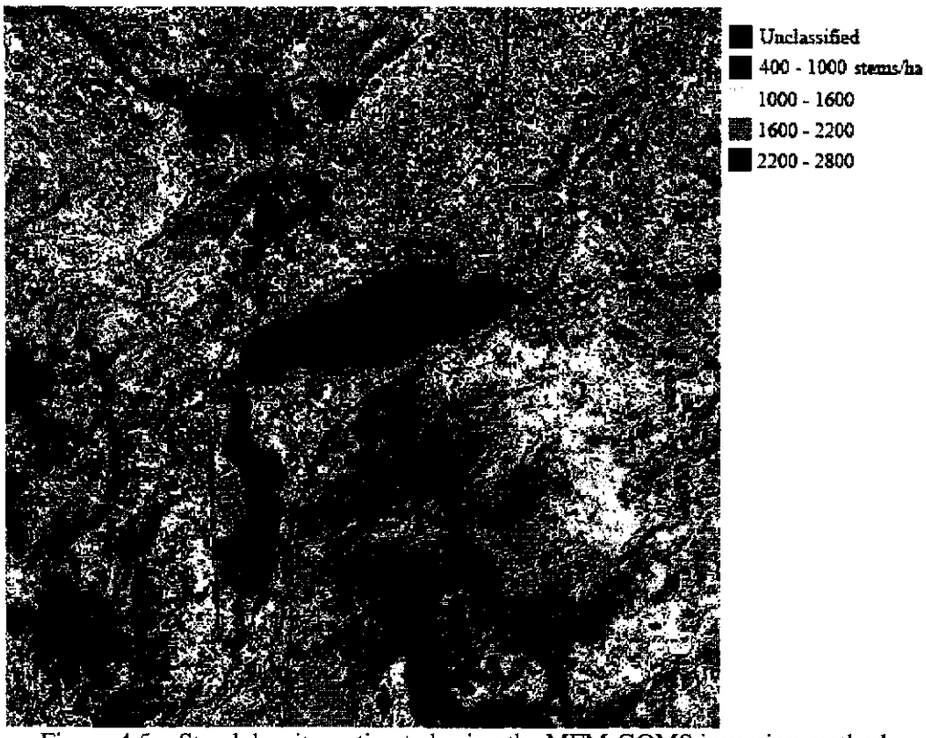

Figure 4.5 – Stand density, estimated using the MFM-GOMS inversion method.

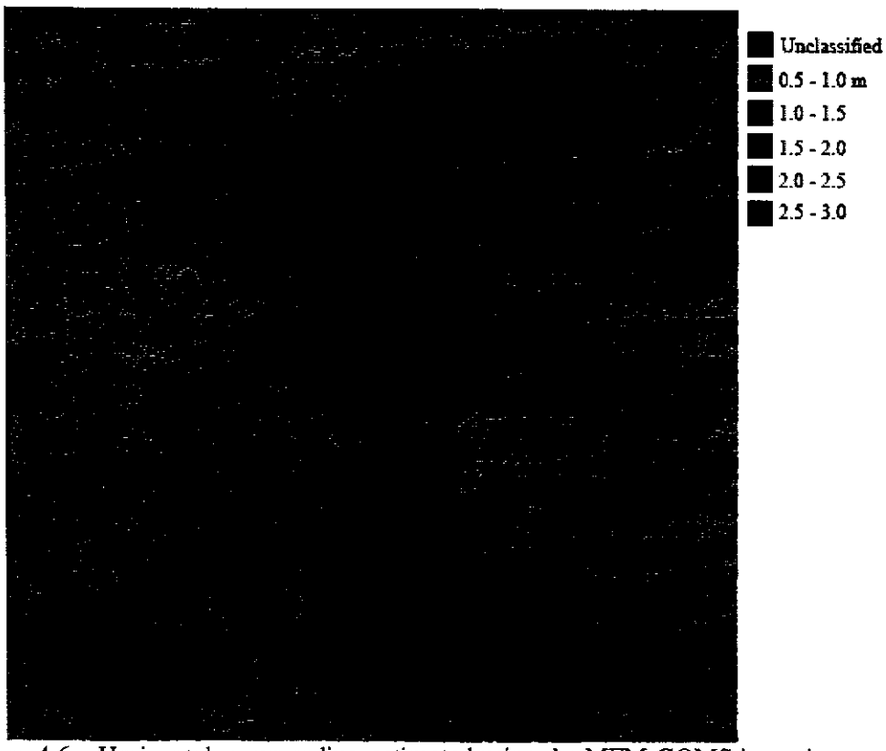

Figure 4.6 – Horizontal crown radius, estimated using the MFM-GOMS inversion method.

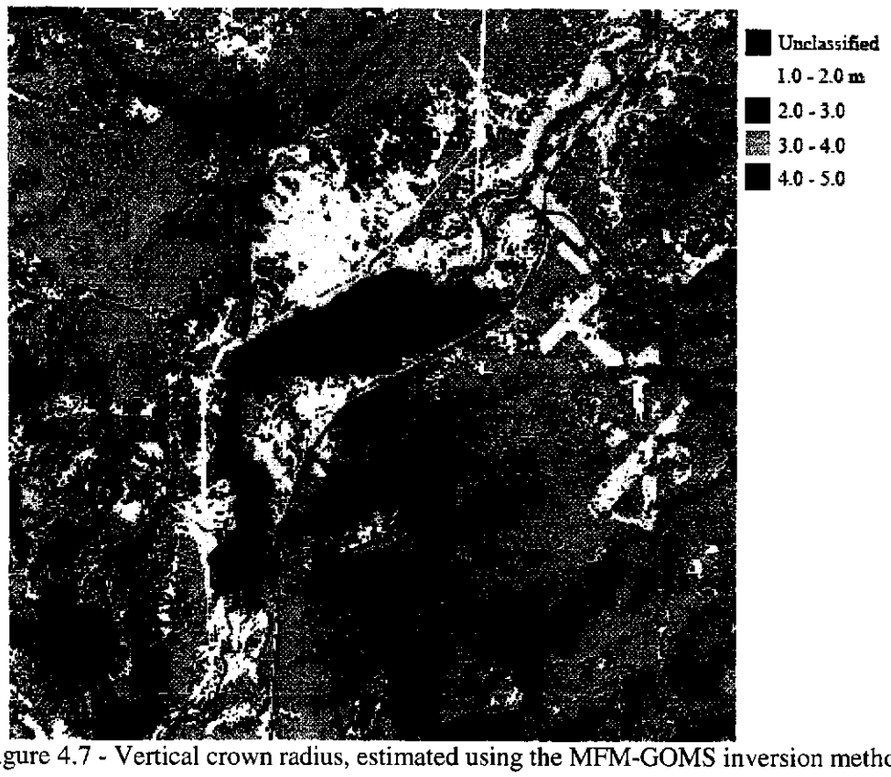

Figure 4.7 - Vertical crown radius, estimated using the MFM-GOMS inversion method.

4.6 Discussion and Summary

Three variations of an indirect inversion method (i.e. direct reflectance match, closest spectral distance, and spectral domain) for a geometric optical canopy reflectance model were tested and evaluated for estimating canopy structure and stand density in a montane sub-alpine forest. The ability to estimate these parameters was highly dependant on the information content of the LUT sets used in the indirect inversion procedure. The mean estimate error for the field plots showed some dependency on the MFM input increment size, with error decreasing with smaller increment sizes. Estimates taken from constrained LUTs generated using *in situ* knowledge were also slightly more accurate than those from LUTs using generalized ranges not based on field data.

Parameter range and increment define the spectral location of the information content within the LUTs. When coarser increments and ranges were used the content was less focused within the image domain where there was a high density of *d*. When fine increments were used, the estimate accuracy was improved. This statement may be generally applicable to LUT inversion. It is expected that while higher information content with respect to increment size may lead to increased potential for multiple solutions, it also provides a more accurate characterization of all potential forest conditions.

Use of additional spectral information bands improved estimates based on closest spectral distance. When additional information bands were used in the reflectance equality method, there was an increase in "no match" cases (i.e. cases where there was no matching reflectance between modeled and measured data). For the range match method, using additional spectral inputs did not consistently improve estimates. Also, use of terrain data to constrain potential matches did not consistently improve estimates. This

was likely due to the generalized input structure created by compromising LUT detail for computational efficiency. However, it should be noted that the use of DEM input did not significantly increase the level of error found in the estimates.

The results also suggested that a spectral distance function approach to indirect inversion was preferable to a strict reflectance equality approach (Figure 4.8). This was because the estimates maintain a similar or improved level of accuracy when comparing the spectral distance method in situations where a full set of estimates was returned within the reflectance equality method. Using the spectral distance method the lowest average prediction errors (absolute RMSE) were 590 stems/ha for density, 0.4 m for horizontal crown radius, 0.7 m for vertical crown radius and 3.5 m for height distribution for conifer validation plots. For deciduous validation plots, the minimum prediction errors were 310 stems/ha for density estimates, 0.4 m for horizontal crown radius, 0.9m for vertical crown radius, and 4.2 m for height distribution. The horizontal crown radius predictions were more accurate than results reported by Wu and Strahler (1994) where difference between validation data and estimates averaged 1.0m.

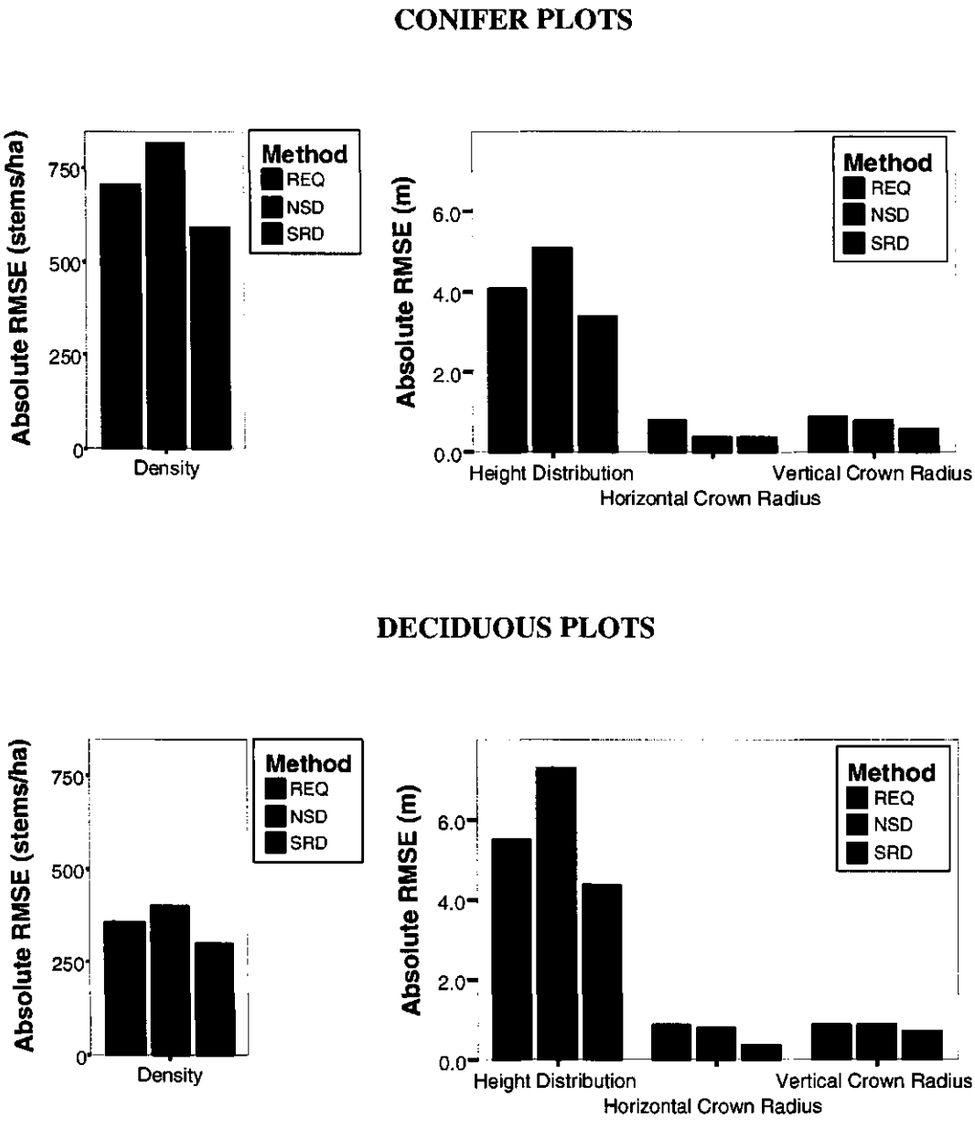

Figure 4.8 – Absolute RMSE between predicted and validation data summarized by structural parameter for each of the three matching methods: 1) reflectance equality (REQ), 2) nearest spectral distance (NSD), and 3) spectral domain (SRD).

The spectral distance function has two primary advantages: 1) the ability to indirectly account for domains of uncertainty; and 2) the ability to provide potential

solution information focused within a user defined spectral range. Using the spectral distance function, it is also possible to explore distributions of potential solutions which may yield more information regarding surface conditions than summaries of the solution sets achieved through indirect inversion. For these reasons, the most appropriate method for forest structure estimation in this study area was a spectral domain based method using constrained range LUTs.

CHAPTER 5

Biomass Estimates Using Indirect Inversion Methods, Empirical Methods and Allometry

5.1 Introduction

This chapter presents a new application of the MFM inversion method for estimating biomass density from empirical models using parameters from the canopy reflectance model inversion. The canopy reflectance model based estimates were compared to other estimates derived using linear regression with vegetation indices and endmember fractions obtained through spectral mixture analysis. This application of canopy reflectance modelling in a biomass context demonstrated the flexibility of the MFM procedure for predicting forest stand structural parameters that were not directly included within the canopy reflectance model parameter set. The results from the canopy reflectance model inversion for biomass density are presented and compared with results from empirical relationships with SMA endmember fractions and NDVI.

5.2 Above Ground Total Biomass and Biomass Density for Field Validation Plots

Above ground total biomass values range from 2686 kg to 9702 kg in deciduous validation plots and 2927 kg to 10624 kg in conifer plots (Table 5.1, Table 5.2). Biomass density ranged from 67 t/ha to 243 t/ha in deciduous plots and 73 t/ha to 266 t/ha in conifer plots. Average biomass density for conifer plots was 153 t/ha with a standard deviation of 43 t/ha. For deciduous validation plots the average biomass density was 155 t/ha with a standard deviation of 46 t/ha.

Table 5.1 – Aboveground total biomass and biomass density calculated for deciduous validation plots.

Plot	Dominant Species	Biomass Total (kg)	Biomass Density (t/ha)
3	Aw	6156	154
4	Aw	4371	109
7	Aw	4209	105
9	Aw	7922	198
10	Aw	9702	243
12	Aw	8814	220
15	Aw	6074	152
18	Aw	6476	162
25	Aw	4744	119
26	Aw	7708	193
36	Aw	5360	134
37	Aw	2686	67
38	Aw	5881	147
39	Aw	7212	180
40	Aw	5955	149

Table 5.2 – Aboveground total biomass and biomass density calculated for conifer validation plots.

Plot	Dominant Species	Biomass Total (kg)	Biomass Density (t/ha)
1	Pl	7188	180
2	Sw	7849	196
5	Sw	7537	188
6	Sw	10624	266
8	Sw	8052	201
11	Pl	4819	120
13	Pl	5736	143
14	Pl	5154	129
16	Pl	8526	213
17	Pl	7143	179
19	Pl	6338	158
20	Pl	2927	73
21	Pl	5464	137
22	Pl	5158	129
23	Pl	5815	145
24	Pl	4885	122
27	Pl	5648	141
28	Pl	7594	190
29	Pl	5465	137
30	Pl	5752	144
31	Pl	6610	165
32	Pl	4038	101
33	Pl	3072	77
34	Pl	6344	159
35	Pl	5025	126

5.3 A Method for Estimating Biomass Using Crown Surface Area

An alternative to the canopy height based empirical model (§ 3.5.5) for predicting biomass was developed for even aged stands using crown spheroidal surface area derived from field measurements of vertical and horizontal crown radius. This model did not use tree height due to the inability to accurately estimate height using the inversion method. This model represents a first-level approximation of the relationship between the area of the organism responsible for photosynthesis and respiration, and the mass of the organism. Crown surface area in this model, as represented by a spheroid, is an abstraction of the true crown surface area, which was much more structurally complex than estimates from the GOMS canopy reflectance model were able to represent. These estimates of biomass, therefore, are averaged at the pixel level and at the level of abstraction or generalization of the GOMS model. However, this method was meant only to demonstrate the ability to expand the functionality of the MFM-GOMS method past the inherent parameter set, and to generate estimates of biomass.

Tree-level parameters were plotted against biomass to determine potential relationships. Crown surface area, a combination of horizontal crown radius and vertical crown radius measured in the field, was related to individual tree biomass. The relationship was based on the physical explanation that crown area is related to photosynthetic capacity for the tree. Thus, the larger the tree the more crown needed to support these physiological processes. Crown surface area was calculated using maximum horizontal and vertical crown radial extent within spheroid area equations. Equations used for prolate spheroid area (SA_p, vertical semiaxis > horizontal semiaxis) and oblate spheroids (SA_o, horizontal semiaxis > vertical semiaxis) were:

$$SA_p = \pi\left(2a^2 + \frac{b^2}{e}\ln\left(\frac{1+e}{1-e}\right)\right) \qquad \text{(Equation 5.1)}$$

and

$$SA_o = 2\pi b\left(b + a\frac{e^{\frac{1}{\sin}}}{e}\right) \qquad \text{(Equation 5.2)}$$

where a and b are the horizontal and vertical axes respectively and e is the elipticity or eccentricity defined as:

$$e = \sqrt{1 - \frac{b^2}{a^2}} \qquad \text{(Equation 5.3)}$$

There was an observed relationship between crown surface area as computed from field measurements and individual tree biomass computed by primary species found within the field validation plots including: lodgepole pine (Table 5.3, Figure 5.1), trembling aspen (Table 5.4, Figure 5.2), and white spruce (Table 5.5, Figure 5.3). The strongest relationship was found for lodgepole pine stands ($r^2 = 0.63$) followed by trembling aspen ($r^2 = 0.52$) and spruce ($r^2 = 0.48$).

Table 5.3 – Regression parameters, predictive strength and standard error for crown surface area vs. calculated individual tree biomass for lodgepole pine. p-value < 0.05.

n = 350	b_0	b_1	r	r^2	S.E.
Crown Surface Area f(hcr,vcr)	21.000	2.337	0.79	0.63	32.7

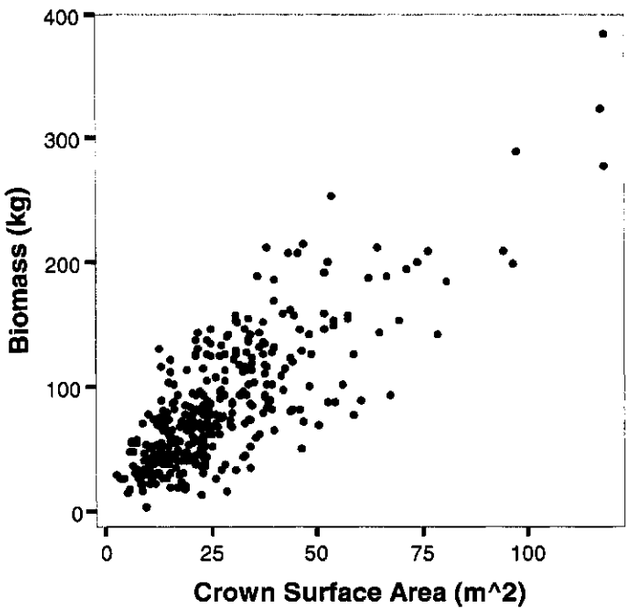

Figure 5.1 – Scatterplot of crown surface area vs. calculated individual tree biomass for lodgepole pine.

Table 5.4 – Regression parameters, predictive strength and standard error for crown surface area vs. calculated individual tree biomass for trembling aspen. *P*-value < 0.05.

n = 350	b_0	b_1	r	r^2	S.E.
Crown Surface Area f(hcr,vcr)	17.121	4.388	0.72	0.52	69.8

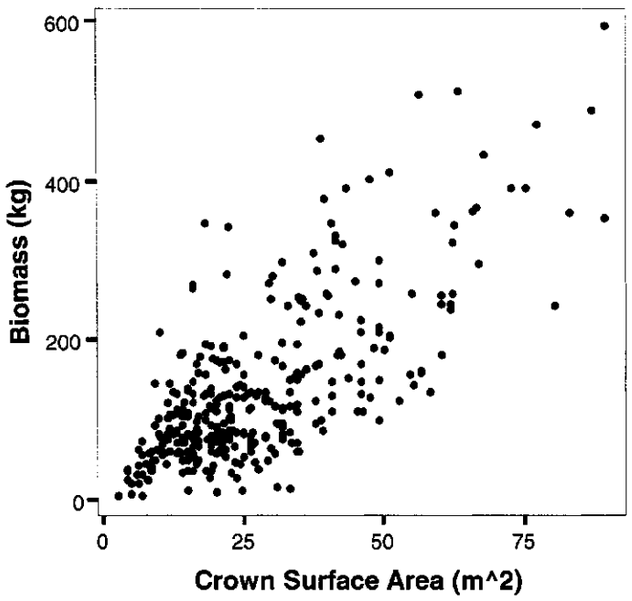

Figure 5.2 – Scatterplot of crown surface area vs. calculated individual tree biomass for trembling aspen.

Table 5.5 – Regression parameters, predictive strength and standard error for crown surface area vs. calculated individual tree biomass for white spruce. *P*-value < 0.05.

n = 112	b_0	b_1	r	r^2	S.E.
Crown Surface Area f(hcr,vcr)	-40.524	3.432	0.69	0.48	105.3

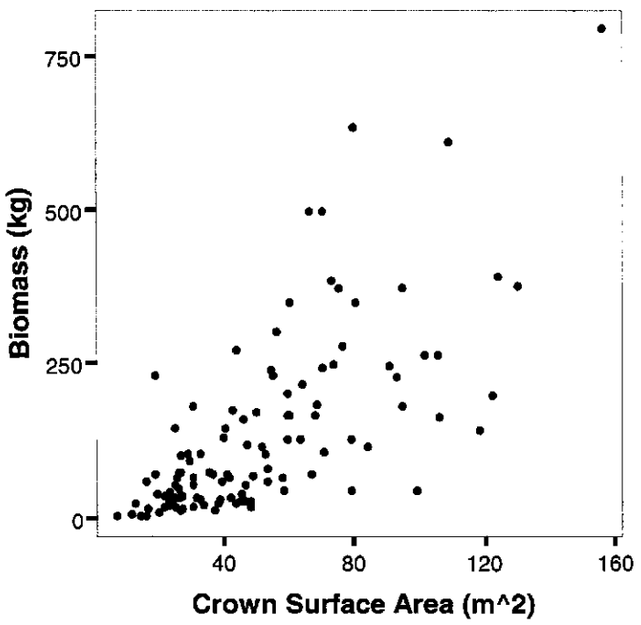

Figure 5.3 – Scatterplot of crown surface area vs. calculated individual tree biomass for white spruce.

Within the model inversion procedure, horizontal and vertical crown radius returns were used to calculate average crown surface area for a given image pixel. The crown surface area was then related to average tree level biomass using a linear regression model with the parameters above. The linear regression model and parameters were:

$$B = b_0 + b_1(SA) \qquad \text{(Equation 5.4)}$$

Average tree-level biomass (B) was then aggregated to the plot level by using the density measure (λ) in the GOMS model, which was given in units of trees per unit area. The following equation was used to convert biomass density to units of tonnes per hectare.

$$\text{Biomass Density} = B \cdot \lambda \cdot 10 \qquad \text{(Equation 5.5)}$$

In this way, biomass density becomes a second-order canopy reflectance model parameter for which the GOMS model is invertible. Of course, any error in predicting canopy structure will translate through to the biomass predictions. Thus, inversion for biomass density can lead to a situation where a number of potential solutions are present for a given pixel-level reflectance value if spectral domain or reflectance equality match criteria are implemented. It is possible to employ the techniques used to derive solution distributions of structural parameters (§3.6.4) to detail biomass solutions distributions.

5.4 Biomass Estimates from Canopy Reflectance Model Inversion

5.4.1 Biomass Estimates using Estimated Height

It was not possible to estimate height reliably using the canopy reflectance model inversion method in this study. The results from a sensitivity analysis demonstrate that estimated height was constant regardless of spectral input (Appendix A). If estimated height is constant, the model is dependant on crown closure variation within a constant height domain. As a result, that approach was deemed inappropriate for use within the canopy reflectance model inversion procedure and abandoned in favour of the crown surface area (SA) method.

5.4.2 Biomass Estimates from a Crown SA Model – Closest Spectral Distance

Conifer biomass estimates taken from MFM run 2 using the closest spectral distance method had a maximum error of 232 t/ha and a minimum error of 3 t/ha with an

absolute RMSE for all plots of 78 t/ha using 2 spectral bands for input, and 75 t/ha using 4 spectral bands. When the MFM run 4 LUT was used, the maximum error was 225 t/ha and minimum was 2 t/ha (Figure 5.4). The absolute RMSE for MFM run 4 estimates was 74 t/ha using 2 band inputs and 81 t/ha using 4 band inputs. Individual plot error was, for the most part, lower than the RMSE with a few plots increasing overall error due to large differences between predicted and measured biomass (Figure 5.4). In fact, 10 of the 25 estimated values for the validation plots were within 20 t/ha of the actual value when using 2 band input for the MFM run 4 LUT and 8 of the 25 estimated values fell within 20 t/ha of the actual value when using the MFM run 2 LUT. The 20 t/ha error threshold was based on error levels reported by Hall et al. (1995) in another boreal application and in an atlantic forest application reported by Peddle et al. (2003).

MFM RUN 2 RESULTS

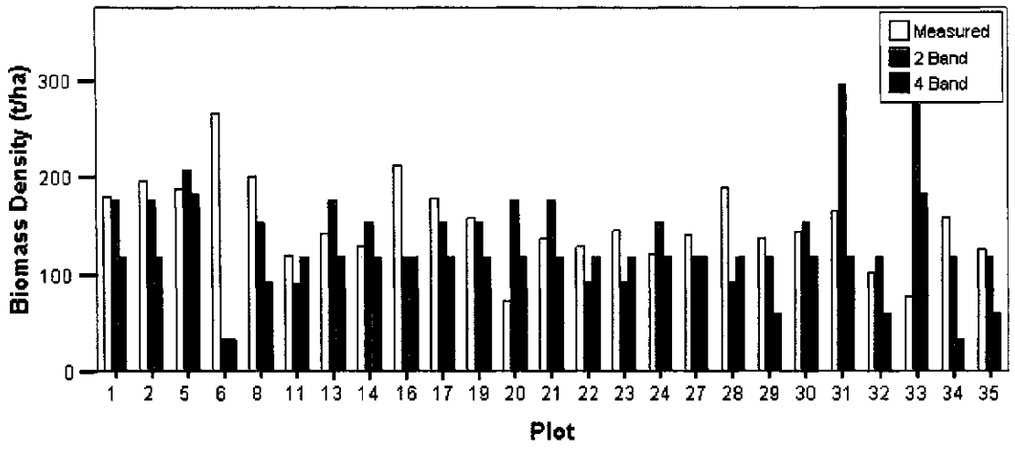

MFM RUN 4 RESULTS

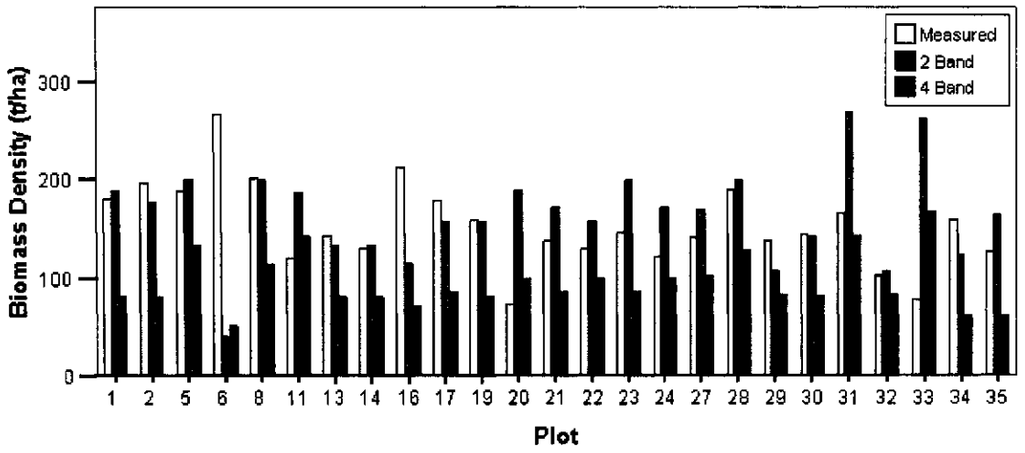

Figure 5.4 – Field measured and model estimated conifer biomass density using the closest spectral distance method, from MFM run 2 and MFM run 4.

Deciduous biomass estimates taken from MFM run 2 using the closest spectral distance method had a maximum error of 840 t/ha and a minimum of 10 t/ha. The absolute RMSE was 375 t/ha using 2 band input and 94 t/ha using 4 band input. Estimates using the MFM run 4 LUT had a maximum error of 631 t/ha and a minimum of 3 t/ha. The RMSE was 191 t/ha and 85 t/ha for two and four band input respectively.

Overall error for deciduous plots was also increased significantly due to a few plots with estimate error in excess of 400t/ha (Figure 5.5). These extreme errors were likely a result of the method used, as they did not appear in this magnitude using the spectral domain method.

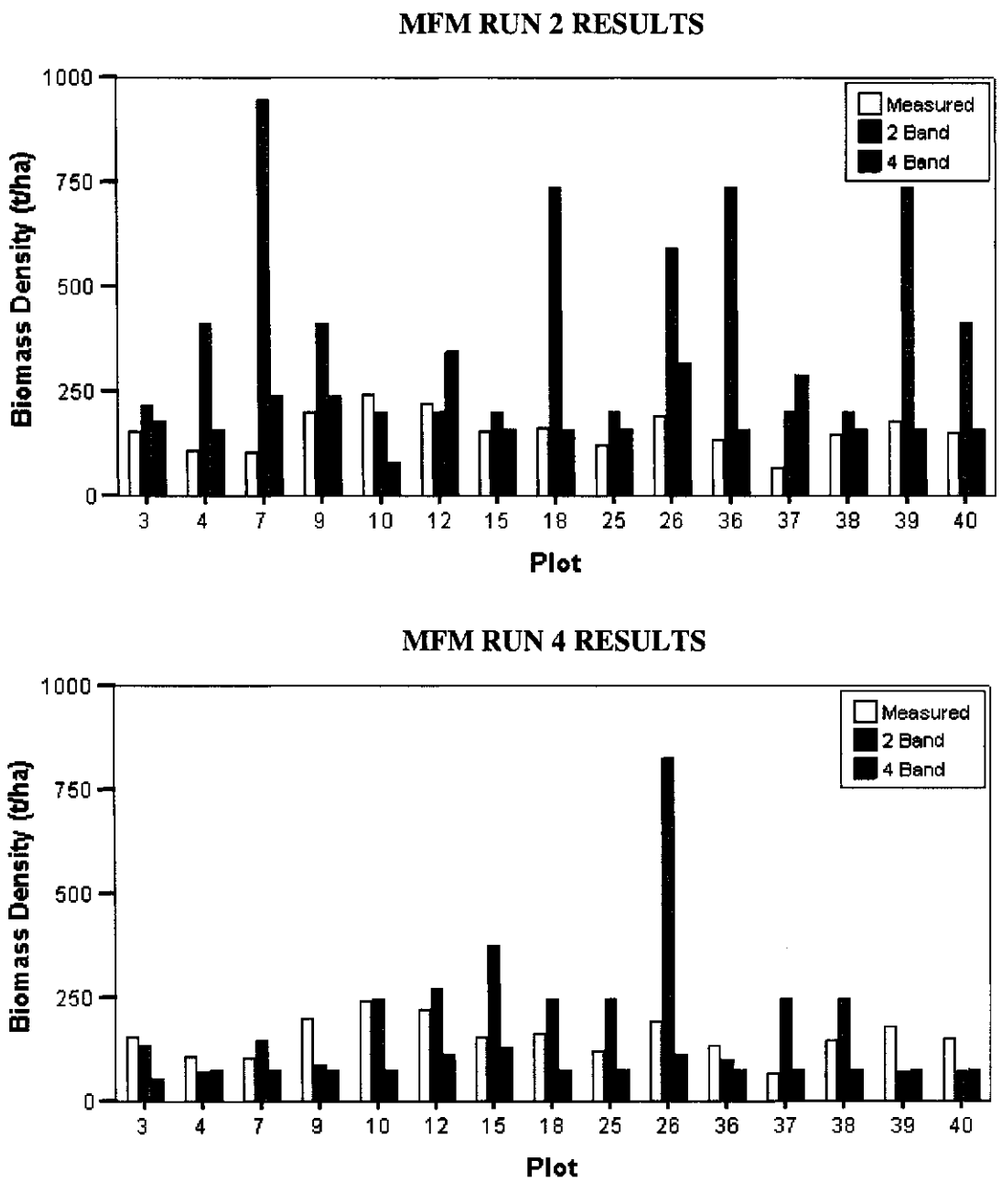

Figure 5.5 –Field measured and model estimated deciduous biomass density using the closest spectral distance method, from MFM run 2 and MFM run 4.

5.4.3 Biomass Estimates from a Crown SA Model – Spectral Domain

As discussed in chapter 4, model estimates using spectral domains are typically more accurate than estimates based on closest spectral distance. Using spectral domains the lowest overall error (RMSE = 51 t/ha) for conifer plots occurred at a spectral domain size of 0.38 when using the median return from MFM run 4 LUTs (Figure 5.6). MFM run 2 LUTs yielded the least accurate biomass estimates. The mode return was more accurate when using MFM run 2 LUTs, yet was less accurate and more variable when using MFM run 4 LUTs.

Within the spectral domain method, the use of four input bands resulted in slightly lower error when extracting returns from the MFM run 4 LUTs but did not decrease the overall error when LUTs from MFM run 2 were used. With the MFM run 4 LUT, there is a higher potential for multiple matches due to the increased coverage of the reflectance space through smaller increment size. Inclusion of additional bands assisted in reducing some erroneous potential matches where reflectance in the short-wave infrared (SWIR) or green bands was not similar between model and measured reflectance. In MFM run 2 the LUT contained less coverage in the reflectance space and likely did not contain as many potential solutions within the reflectance domain. Thus, the inclusion of additional spectral bands did not reduce error in MFM run 2.

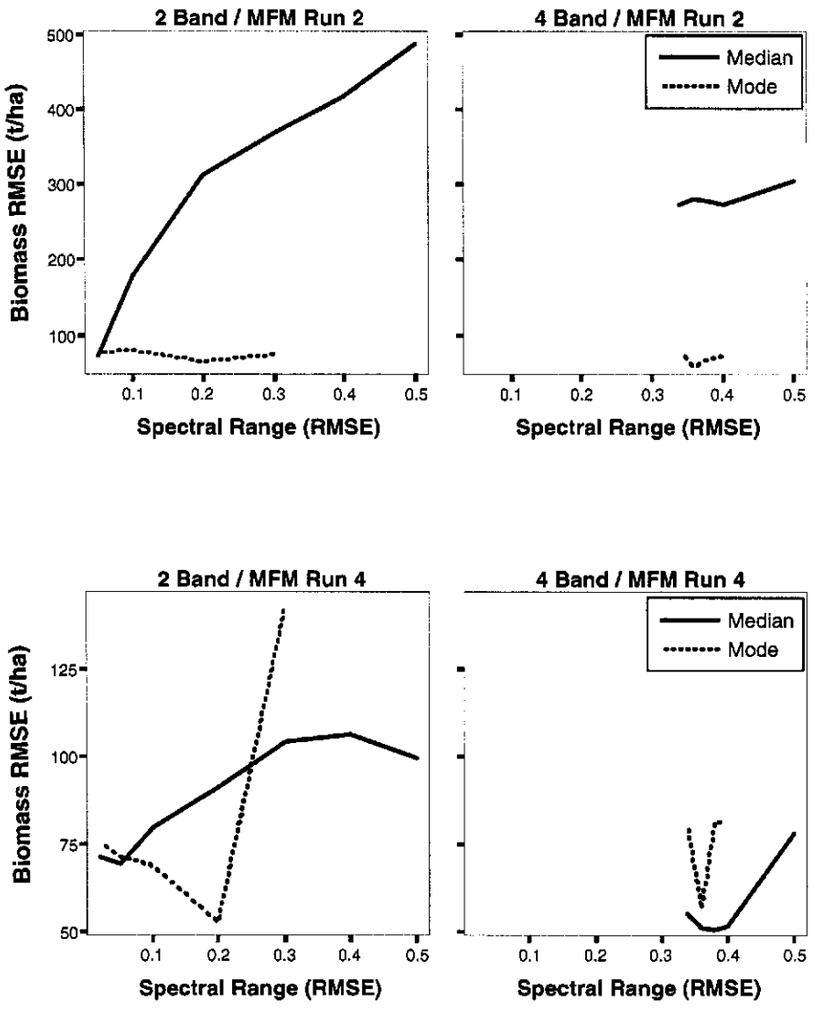

Figure 5.6 – Absolute biomass density RMSE for all conifer validation plots with varying spectral domain size (measured as relative RMSE, x-axis). Median (solid) and mode (dotted) values extracted from potential solution distributions and used as summary biomass density value.

The deciduous prediction error level was related to the spectral domain size in a way similar to the conifer prediction error relationship, however, the magnitude of error was greater (Figure 5.7). The lowest overall error (absolute RMSE = 52 t/ha) occurred when using the median returns from MFM run 4. The range of RMSE in deciduous

validation was considerably higher than that in conifer results. For example, RMSE for deciduous plots reached as high as 740 t/ha compared to the upper limit of 487 t/ha found in the conifer validation. The mode was most accurate for MFM run 2 returns, while the median was more consistently accurate for MFM run 4 returns (Figure 5.8). This is due to the difference in potential solution ranges. The median value is affected by erroneous potential solutions at the extremes of the distribution, while the mode is not. Thus, in the case of MFM run 2 (large ranges) the median value may be affected by these erroneous potential solutions at the extremes of a distribution. In MFM run 4, the error using the mode is only slightly higher than when the mean is used. Also, using four input bands consistently yielded more accurate estimates.

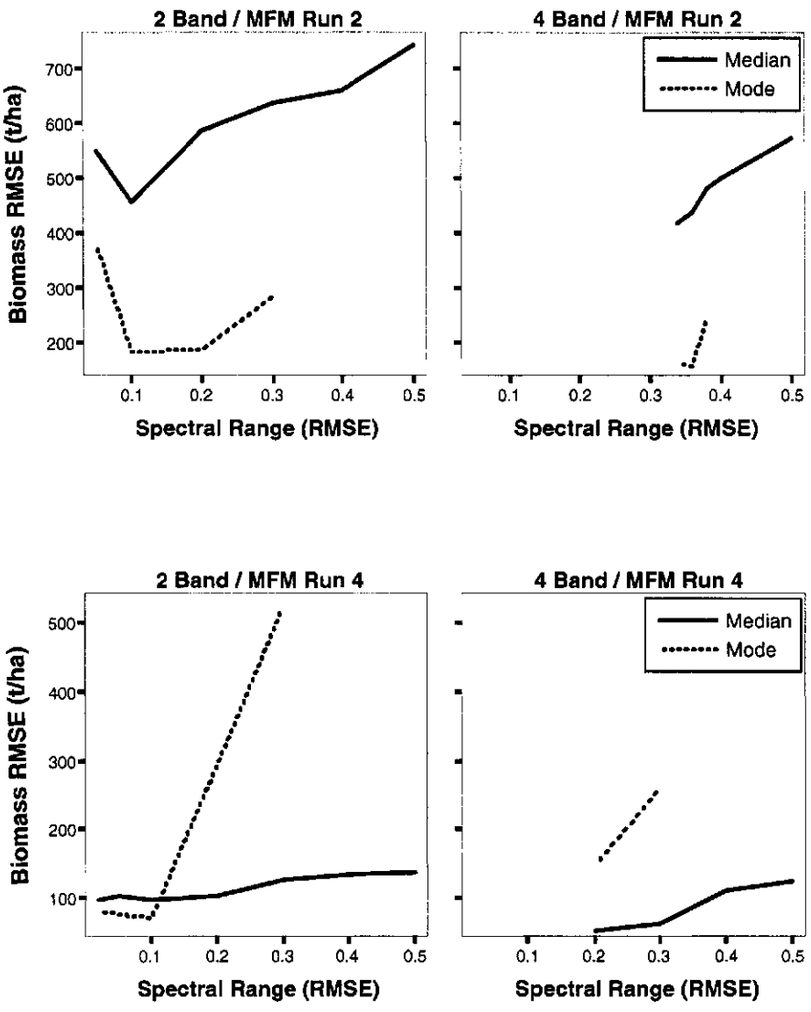

Figure 5.7 – Absolute biomass density RMSE for deciduous validation plots with varying spectral domain size (measured as relative RMSE, x-axis). Median (solid) and mode (dotted) values extracted from potential solution distributions and used as summary biomass density value.

Due to the low absolute RMSE observed for both conifer and deciduous validation sets, individual estimates for the validation plots were selected using 0.2 relative RMSE as the spectral domain size with results taken from MFM run 4 LUT. While in some cases (e.g. spectral domain size > 0.3) the spectral domain method yielded

results with considerably higher error, it was expected that a "best" set of results is achievable by strictly following the error domain formula detailed by Kimes et al. (2000).

The maximum difference between estimated and measured biomass using the spectral domain method was 164 t/ha while the minimum was 0 t/ha. As with the closest spectral distance method, the overall error was affected by a few plots with error levels considerably larger than the majority (plot 6, plot 20). Of the 25 validation plots, 13 fell within a difference of 20t/ha, and 18 fell within a difference of 40t/ha.

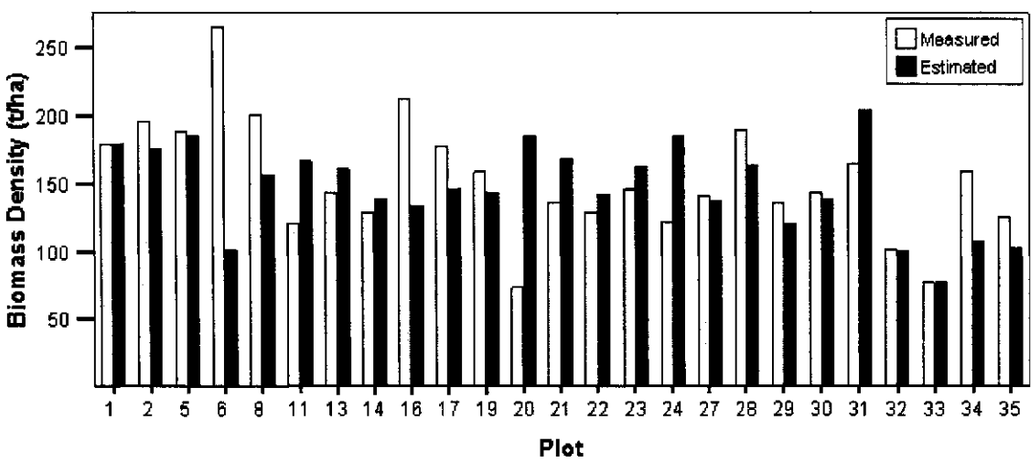

Figure 5.8 – Measured and estimated conifer biomass density using the spectral range method. Results taken from MFM run 4 with a spectral domain size equivalent to 0.2 relative RMSE.

Individual biomass returns for deciduous validation plots were taken from MFM run 4 LUTs using 0.2 as the spectral domain size (Figure 5.9). There were plots within the deciduous validation set where the difference between measured and estimated values was considerably higher than the average (plot 9, plot 37). The maximum difference was 96t/ha while the lowest was 4t/ha. There were 3 validation plots of the 15 within 20t/ha while 8 were within 40t/ha. There was no observed trend in error (e.g. overestimation, underestimation) in either the conifer or deciduous results.

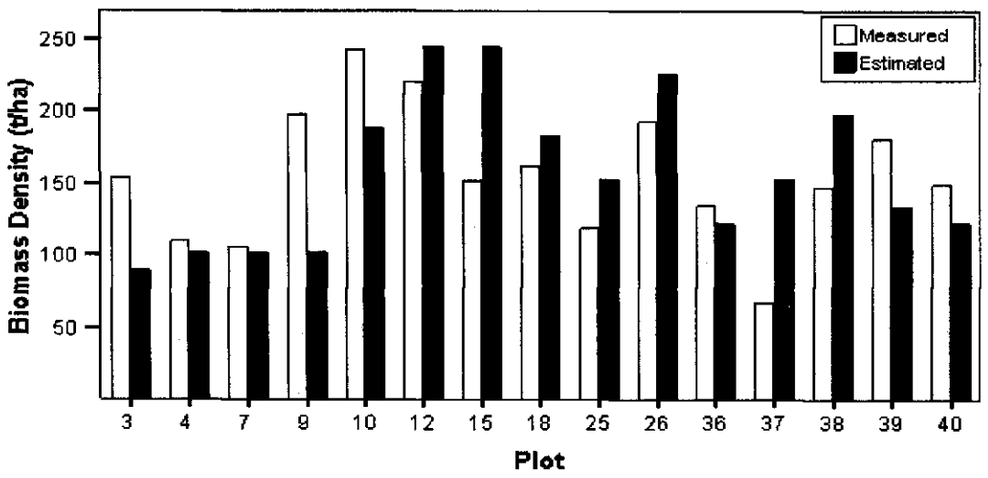

Figure 5.9 – Measured and estimated deciduous biomass density using the spectral range method. Results taken from MFM run 4 with a spectral domain size equivalent to 0.2 relative RMSE.

5.4.4 Sample MFM Inversion Biomass Density Image Output

Biomass density was mapped using the canopy reflectance model inversion method (Figure 5.10). Biomass spatial patterns were as expected, with low values found near roads, trails, and cut-blocks. The influence of topography was visible within the map output with higher biomass estimates occurring over north-northwest facing terrain. This may, however, be a result of the potential over-estimation of vertical crown radius for these slopes (§ 4.5).

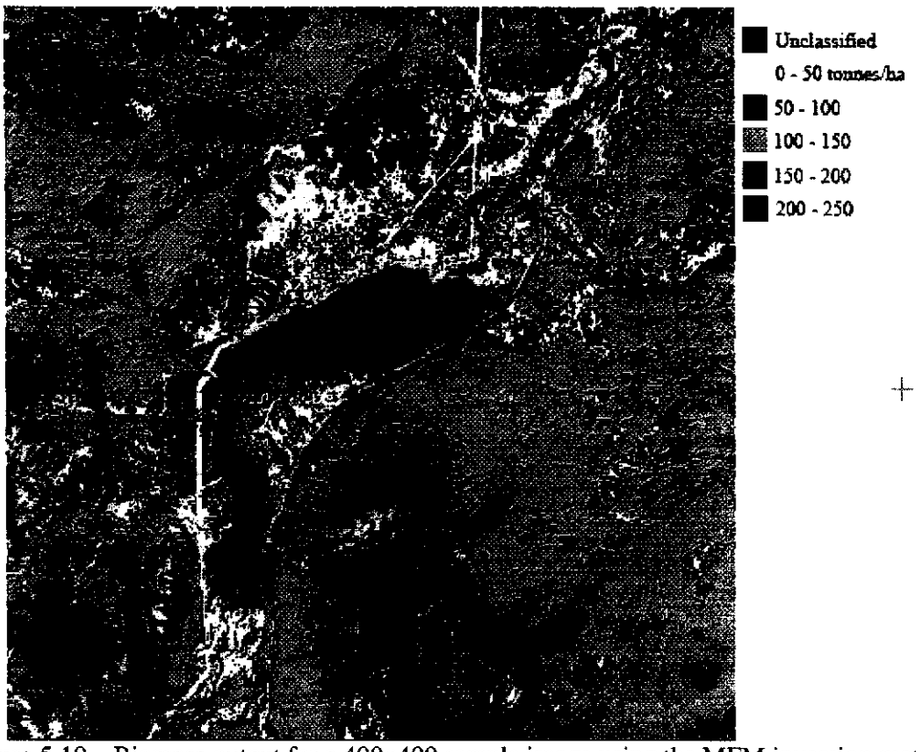

Figure 5.10 – Biomass output for a 400x400 sample image using the MFM inversion method (Spectral Domain method, domain size =0.2 RMSE).

5.5 NDVI Linear Model

There was a weak relationship between NDVI and biomass density calculated for individual field validation plots for both primary species types (Table 5.6). The strongest relationship observed for conifer and deciduous within the cross-validation analysis had an r^2 of 0.054 and 0.046 respectively. The relationship strength for the NDVI model was lower than a similar study (r^2 = 0.39) in a Boreal environment (Peddle et al., 2001). The overall absolute prediction error (RMSE) for biomass using the NDVI linear model was 48 t/ha for conifer validation plots and 53 t/ha for deciduous validation plots. Maximum error (132 t/ha conifer, 106 t/ha deciduous) was found for validation plots with biomass values at the extremes of the distribution of biomass values (e.g. conifer: plot 6, plot 20; deciduous: plot 10, plot 37).

Table 5.6 – NDVI estimates of biomass and their difference from field validation values including regression parameters (b), coefficient of determination (r^2), and standard error (S.E.) from a cross-validation analysis for lodgepole pine (Pl), trembling aspen (Aw), and white spruce (Sw) validation plots.

Plot	Species	b_0	b_1	r^2	S.E.	Estimate (t/ha)	Measured (t/ha)	Difference (t/ha)
3	Aw	144.840	22.069	0.000	50.0	155	154	1
4	Aw	135.684	47.747	0.002	48.1	159	109	50
7	Aw	158.515	1.079	0.000	47.7	159	105	54
9	Aw	156.971	-9.456	0.000	48.4	152	198	46
10	Aw	249.693	-209.373	0.046	41.8	136	243	106
12	Aw	48.661	209.219	0.039	45.2	137	220	83
15	Aw	147.144	17.561	0.000	50.0	155	152	3
18	Aw	149.793	10.820	0.000	50.0	156	162	6
25	Aw	142.451	32.327	0.001	48.8	158	119	40
26	Aw	28.063	254.180	0.039	47.8	127	193	65
36	Aw	128.968	58.199	0.003	49.6	159	134	25
37	Aw	187.016	-52.029	0.003	42.5	163	67	96
38	Aw	143.295	26.395	0.001	50.0	156	147	9
39	Aw	163.459	-20.340	0.000	49.5	153	180	28
40	Aw	141.260	30.403	0.001	50.0	157	149	8
2	Sw	95.192	178.078	0.032	43.2	147	196	49
5	Sw	84.827	211.384	0.041	43.3	140	188	48
6	Sw	194.439	-150.495	0.024	37.2	133	266	133
8	Sw	74.901	241.043	0.054	42.5	136	201	65
1	Pl	103.475	154.253	0.023	44.0	152	180	28
11	Pl	112.132	133.899	0.017	44.0	150	120	30
13	Pl	102.180	163.844	0.025	44.3	158	143	14
14	Pl	107.382	148.299	0.021	44.1	152	129	23
16	Pl	93.644	180.856	0.034	42.2	147	213	66
17	Pl	100.786	162.742	0.026	44.0	150	179	29
19	Pl	103.519	156.689	0.024	44.4	151	158	8
20	Pl	108.132	153.538	0.027	40.9	156	73	83
21	Pl	106.570	149.823	0.022	44.3	151	137	15
22	Pl	111.970	132.887	0.016	44.3	147	129	18
23	Pl	105.340	152.283	0.022	44.4	149	145	3
24	Pl	98.432	178.748	0.031	43.7	159	122	37
27	Pl	95.542	186.237	0.031	44.2	165	141	23
28	Pl	90.763	192.690	0.036	43.4	144	190	46
29	Pl	103.172	161.291	0.025	44.2	156	137	19
30	Pl	105.175	153.498	0.023	44.4	152	144	9
31	Pl	105.655	149.613	0.021	44.4	156	165	10
32	Pl	97.927	183.037	0.034	42.7	159	101	58
33	Pl	144.334	36.804	0.001	41.7	153	77	77
34	Pl	101.041	166.520	0.023	44.4	166	159	7
35	Pl	85.283	221.672	0.043	43.6	169	126	43

There were nine validation plots where the error was within 20 t/ha for conifer plots and five for deciduous plots. The σ for estimated biomass (conifer = 8.5 t/ha, deciduous =

10.2 t/ha) was considerably smaller than the σ of measured biomass (conifer = 43.0 t/ha, deciduous = 46.36). This suggested that the level of overall error (RMSE) was a result of low variance within validation data rather than any actual predictive power in the model (Figure 5.11, Figure 5.12).

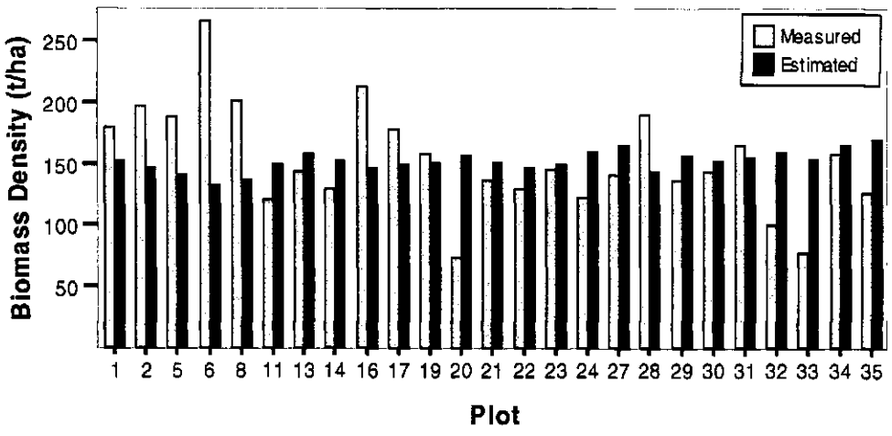

Figure 5.11– Measured biomass density and biomass density estimated with the NDVI linear regression model for conifer plots.

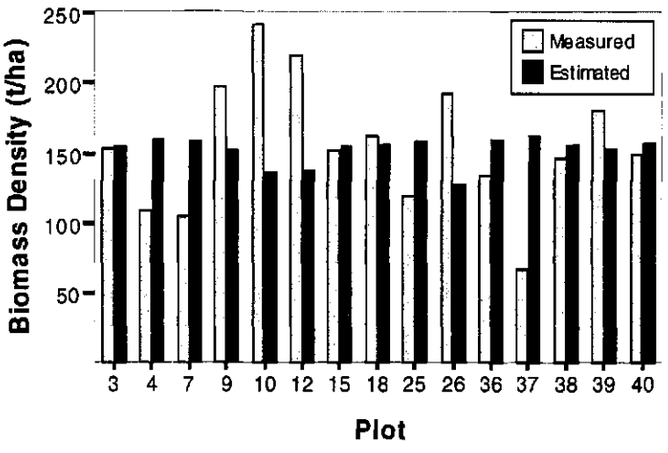

Figure 5.12- Measured biomass density and biomass density estimated with the NDVI linear regression model for deciduous plots.

5.6 SMA Endmember Fraction Linear Models

The relationship between biomass density and endmember fractions derived from SMA for sunlit canopy, shadow, and sunlit background was tested for the validation plots. As demonstrated in previous studies (e.g. Johnson et al., 2000) it is possible to improve the relationship between some sub-pixel components and biophysical parameters by removing factors that affect sub-pixel component abundance but are not directly related to canopy structure, such as the influence of topography on the relative positioning of trees within the canopy (Soenen et al., 2005). It is possible to remove the influence of topography to some extent by applying topographic correction (§2.4.2). The standard error and predictive strength for a linear regression between biomass density and topographically corrected and uncorrected data are displayed in Table 5.7.

Table 5.7 – Standard error and predictive strength for linear relationships between biomass and endmember abundance for sunlit canopy, shadow and sunlit background using uncorrected data and 6 topographic correction approaches.

		Coniferous		Deciduous	
Estimating Parameter		S.E.	r	S.E.	r
Uncorrected	Sunlit	40.4	0.39	48.1	0.02
	Shadow	41.0	-0.36	47.4	0.17
	Background	43.9	0.00	44.1	-0.38
Cosine	Sunlit	43.9	0.01	45.5	0.33
	Shadow	40.9	0.37	48.0	0.05
	Background	41.9	-0.30	45.5	-0.32
SCS	Sunlit	43.8	0.07	47.7	0.12
	Shadow	41.6	0.32	48.0	0.07
	Background	42.1	-0.29	44.6	-0.37
C	Sunlit	37.4	0.52	47.2	0.19
	Shadow	43.9	-0.01	47.4	0.17
	Background	43.1	-0.20	44.2	-0.39
SCS+C	Sunlit	42.7	0.24	47.7	0.12
	Shadow	43.2	0.19	48.0	0.07
	Background	39.5	-0.44	44.6	-0.37
Statistical	Sunlit	41.9	0.30	48.0	0.07
	Shadow	43.5	0.14	47.7	0.13
	Background	**34.4**	**-0.56**	**43.8**	**-0.41**
B-correction	Sunlit	41.2	0.35	47.5	0.15
	Shadow	42.9	0.22	48.0	0.04
	Background	37.0	-0.54	45.6	-0.32

There was a weak relationship between sunlit canopy area and biomass density for the uncorrected set of conifer validation plots. Conversely, there was a weak inverse relationship between shadow and calculated biomass density. However, once the topographic corrections were applied, the correlation with shadow became direct and there was a relationship between sunlit background and biomass density. The strongest relationship ($r^2 = 0.32$) was found between the sunlit background endmember abundance calculated using statistical-empirical corrected imagery. This observation was consistent with results reported for a boreal forest study, where background ($r^2 = 0.77$) and shadow fraction ($r^2 = 0.71$) were the strongest predictors of biomass density (Hall et al., 1995). The strength of the relationship, however, was less than reported in that boreal forest study. The results for deciduous validation plots were similar with the background endmember fractions from the corrected data yielding the strongest relationships. Again, the statistical-empirical corrected imagery yielded the endmember abundance with the strongest relationship ($r^2 = 0.17$). Therefore, the background endmember fraction extracted from the statistical-empirical imagery was most suitable for use within the linear regression model to predict biomass density.

Table 5.8 – SMA estimates of biomass and their difference from field validation values using regression parameters (b), coefficient of determination (r^2), and standard error (S.E.) from a cross-validation analysis for lodgepole pine (Pl), white spruce (Sw) and trembling aspen (Aw) validation plots.

Plot	Species	b_0	b_1	r^2	S.E.	Estimate (t/ha)	Measured (t/ha)	Difference (t/ha)
3	Aw	319.944	-772.709	0.218	44.3	109	154	45
4	Aw	270.086	-521.872	0.117	45.2	132	109	23
7	Aw	278.447	-553.499	0.158	43.8	151	105	46
9	Aw	292.229	-647.922	0.211	43.0	143	198	55
10	Aw	202.327	-239.667	0.025	42.2	167	243	76
12	Aw	264.559	-521.637	0.149	42.6	161	220	59
15	Aw	293.901	-632.548	0.182	45.3	172	152	20
18	Aw	287.444	-607.051	0.170	45.6	168	162	6
25	Aw	283.033	-578.088	0.166	44.6	153	119	34
26	Aw	323.196	-796.448	0.282	41.4	120	193	73
36	Aw	287.719	-602.672	0.176	45.1	159	134	25
37	Aw	297.477	-625.376	0.257	36.6	164	67	97
38	Aw	285.030	-595.995	0.169	45.6	153	147	6
39	Aw	280.272	-579.065	0.155	45.5	170	180	10
40	Aw	291.689	-622.664	0.180	45.3	168	149	19
2	Sw	289.472	-668.165	0.253	38.0	192	196	4
5	Sw	287.083	-660.394	0.276	37.6	164	188	24
6	Sw	262.990	-557.201	0.264	32.3	168	266	98
8	Sw	284.575	-650.769	0.275	37.2	164	201	37
1	Pl	291.984	-679.318	0.273	38.0	181	180	2
11	Pl	294.863	-686.183	0.300	37.1	159	120	38
13	Pl	291.352	-675.784	0.284	38.0	147	143	4
14	Pl	290.395	-669.077	0.280	37.9	143	129	14
16	Pl	289.520	-680.064	0.315	35.6	149	213	64
17	Pl	289.345	-670.935	0.284	37.7	157	179	21
19	Pl	292.237	-683.774	0.290	37.8	144	158	15
20	Pl	289.642	-653.140	0.311	34.4	150	73	77
21	Pl	300.785	-715.218	0.311	37.2	174	137	38
22	Pl	291.127	-671.628	0.284	37.8	148	129	20
23	Pl	292.948	-681.572	0.289	37.9	159	145	14
24	Pl	299.286	-706.443	0.314	36.8	167	122	45
27	Pl	292.735	-684.815	0.285	37.9	133	141	8
28	Pl	287.041	-658.382	0.266	37.9	175	190	15
29	Pl	290.993	-673.621	0.282	38.0	143	137	6
30	Pl	292.880	-681.106	0.289	37.9	159	144	15
31	Pl	290.803	-674.870	0.283	38.0	160	165	5
32	Pl	325.268	-850.622	0.261	37.4	57	101	44
33	Pl	291.189	-661.081	0.315	34.6	152	77	75
34	Pl	294.859	-698.347	0.297	37.7	135	159	24
35	Pl	297.460	-709.330	0.277	37.9	110	126	15

The absolute RMSE for biomass density was 38 t/ha for conifer validation plots and 48 t/ha for deciduous plots. The maximum difference between predicted and measured values occurred for plots with biomass density much higher or lower than the average for the validation plots. These high error plots were the same as those found in the NDVI error results. However, the size of the error for the SMA model was lower than

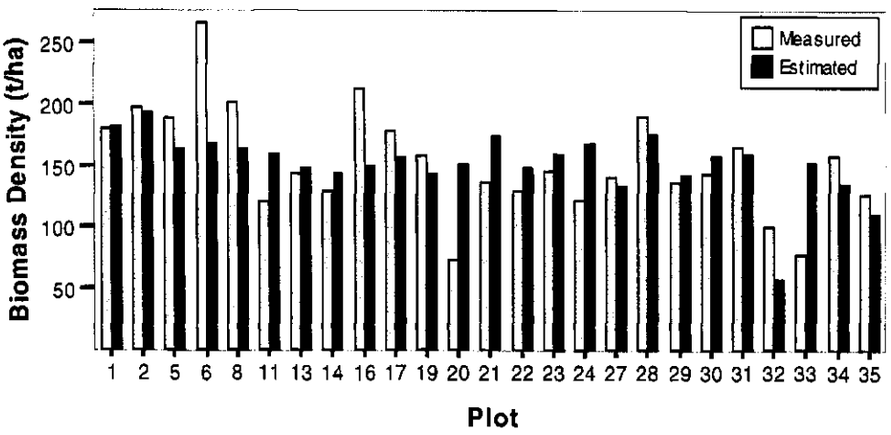

Figure 5.13– Measured biomass density and biomass density estimated with the sunlit background endmember abundance linear regression model for conifer plots.

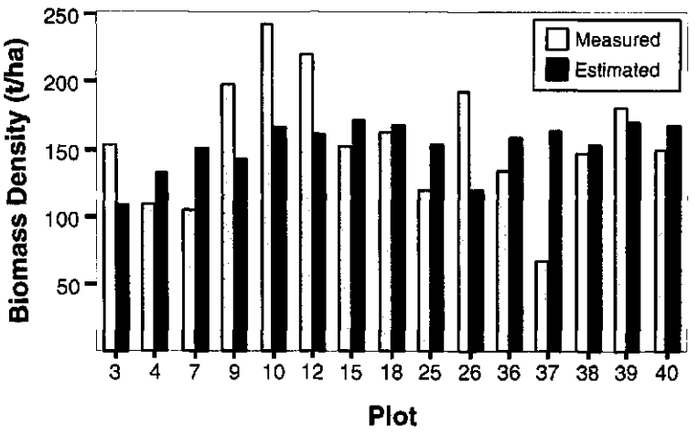

Figure 5.14- Measured biomass density and biomass density estimated with the sunlit background endmember linear regression model for deciduous plots.

that of the NDVI (Table 5.8). SMA was also able to more accurately model a larger range of the biomass density conditions found in the validation plots than NDVI (e.g. plot 2, plot 35). The estimated biomass values using SMA also showed more variation than those estimated using NDVI. For example, in plots 32 and 35, the estimated value was a

lower biomass density value and more consistent with the measured values (Figure 5.13) whereas with NDVI, the estimated biomass density was consistent with the average estimate.

5.7 Discussion

The MFM canopy reflectance model based method was suitable for making first-level estimates of forest stand biomass density, similar to other procedures using generalized forest inventory parameters (e.g. Fournier et al., 2003, Guindon et al., 2001). The MFM method can be considered an improvement to this method due to the ability to employ more refined parameter classes with flexible class ranges and increments, and further, that it also provides explicit structural information that has a variety of uses. Unfortunately, the GOMS model was not sensitive to stand height (Appendix A). As a result, it was unclear if this biomass estimation procedure was only applicable to even aged forest stands where canopy size is more a function of bole diameter. The addition of stand height to the empirical model, perhaps from another canopy reflectance model (e.g. GORT), or inventory data has potential to improve this method.

Considering the above statements, the new canopy reflectance model inversion based method for predicting biomass density using the GOMS model has shown some promising results. When comparing the results from the CRM based method with those from other empirical methods it is important to consider a number of factors: 1) the computational investment required for each method, 2) the *in situ* data requirements and the cost in time and resources, 3) the potential for algorithm and model improvement, 4) the potential for application within other ecosystems and forested environments, 5)

overall prediction accuracy or agreement with field measurements, and 6) the range of values that were accurately predicted.

5.7.1 Computation Time

Computation time is an issue of importance when applying these prediction methods to large areas or within studies with a temporal component. The quickest procedure is the NDVI method followed closely by SMA. The procedure to derive vegetation indices and endmember fractions has been optimized over many years of development and incorporated into many software packages and is very efficient. The canopy reflectance model method is still being developed and while computation time can be quite slow it is expected to increase with algorithm optimization and additional computational resources. Parallel computation and distributed computing (westgrid.ca, 2005), is a prospect currently being investigated.

5.7.2 *In Situ* Data Requirements

To construct an empirical model, the linear regression methods require a spatially representative sample of the structural parameter of interest be acquired from the field. For imagery covering large spatial extents, this requires a large amount of physical resources (i.e. personnel, transportation, logistical requirements) and time. For these large areas, there is a greater likelihood of large variation in the parameter of interest. Therefore, a large sample of the parameter is required.

Often, forestry studies occur over remote, inaccessible terrain or in areas with limited road access (Turner et al., 2004). In these cases it may not be feasible to collect an ideal sample size from these areas. However, with the canopy reflectance model inversion procedure, it is possible to operate with little or no field data providing that the

physical relationship between first-order canopy variables and the parameter of interest is defined. The minimum requirement for operation of the canopy reflectance model inversion method is spectral information for the primary overstory species, understory background, and shadowed vegetation. These components can be collected with minimum effort from any location within the study area, from spectral library data, from image endmember extraction, or through modelling (Peddle et al., 1999). It should also be noted that only general structural information is required to increase estimate accuracy by constraining input possibilities within the canopy reflectance model inversion method. This can be demonstrated by contrasting the MFM run 4 results with the MFM run 2 results.

5.7.3 Algorithm Improvement

While the empirical methods discussed here have reached maturity in terms of algorithm development, there is considerable potential for improvements to the canopy reflectance model method. A great deal of potential lies within the ability of this method to be applied to different canopy reflectance models. There have been considerable improvements in the field of canopy reflectance modelling (Chen et al., 2000). With these improvements come new, more detailed canopy reflectance models that, within this method, are invertible for a range of new parameters including other important biophysical parameters such as leaf area and gap fraction (Ni et al., 1999). Canopy reflectance modelling has also moved into the LiDAR domain, which presents new opportunities for obtaining physical parameters, such as height, that are difficult to obtain using multispectral methods (Ni-Meister et al., 2001).

5.7.4 Application to Other Ecotypes

Canopy reflectance modelling methods are able to be applied to both heterogeneous and homogeneous canopies. Thus, the canopy reflectance model inversion method should be applicable in a wide range of applications from agriculture to tropical forests. Empirical models may only be applicable to a smaller range of ecotypes as the parameters used, such as NDVI, have been shown to be less effective in dense canopies (Carlson et al., 1990; Steininger, 1996).

5.7.5 Summary of Biomass Prediction Error

Biomass estimate error was similar between the spectral domain canopy reflectance model inversion method and the methods using empirical relationships with NDVI and the SMA derived background endmember abundance (Figure 5.15). The prediction error for these methods was within 50 t/ha. This level of error is similar to validation RMSE of 37.6 t/ha reported by Hall et al. (2006) for a Boreal study area and less accurate than the 20t/ha difference reported by Hall et al. (1995) in another Boreal application and 18 t/ha in an Atlantic forest application reported by Peddle et al. (2003).

The absolute RMSE for all methods was higher than the error at the majority of the validation plots. This would indicate that there were a few plots with large differences between estimated and measured biomass density that increased the overall average.

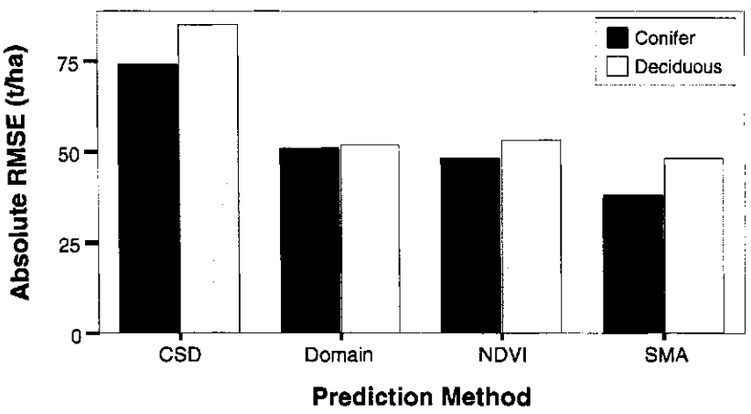

Figure 5.15– Summary of Absolute RMSE for biomass density prediction methods including closest spectral distance (CSD), spectral domain (Domain), NDVI and spectral mixture analysis background fraction (SMA).

5.7.6 Range of Accurately Predicted Biomass Density Values

Error levels for a minority of plots were considerably higher than average (Figures 5.16 and 5.17). In particular the prediction errors for plot 6, plot 20, and plot 16 were consistently high (> 60 t/ha) regardless of prediction method. The majority of the validation plots had error values less than 40 t/ha (Figure 5.16). It is interesting to note that many of the errors appear to be related. For example, when graphing structural estimate error from SMA and spectral domain methods, there are differences in the magnitude of the larger errors but they generally occur for the same plots (Figure 5.18). There were, however, a few exceptions. In plots 32 and 33, for example, the error for the MFM spectral domain method is significantly lower than the NDVI and SMA methods. These validation plots both had relatively low measured biomass densities, suggesting that the NDVI and SMA methods were unsuited to low biomass conditions. However, the canopy reflectance model based methods appeared to perform well across a greater range of forest stand types and conditions.

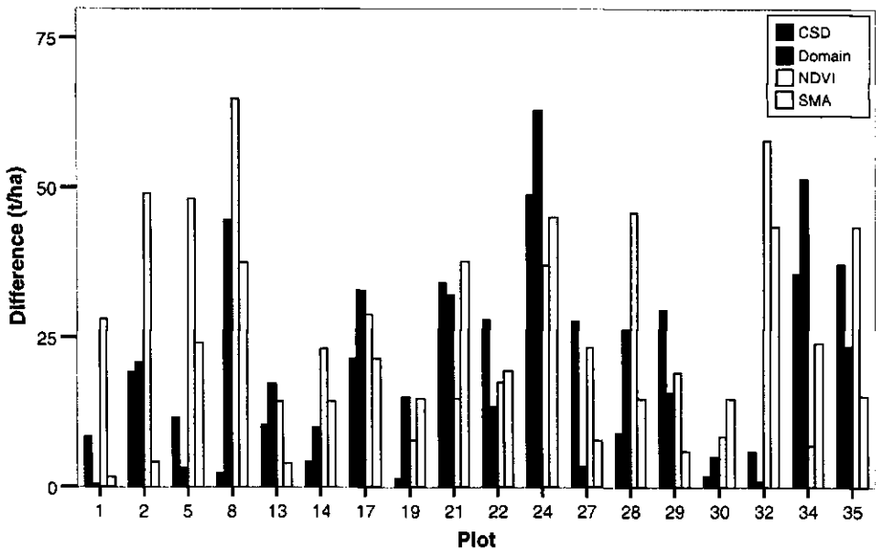

Figure 5.16– Absolute difference between estimated and measured biomass density for conifer plots. Plots within 70 t/ha difference (natural break).

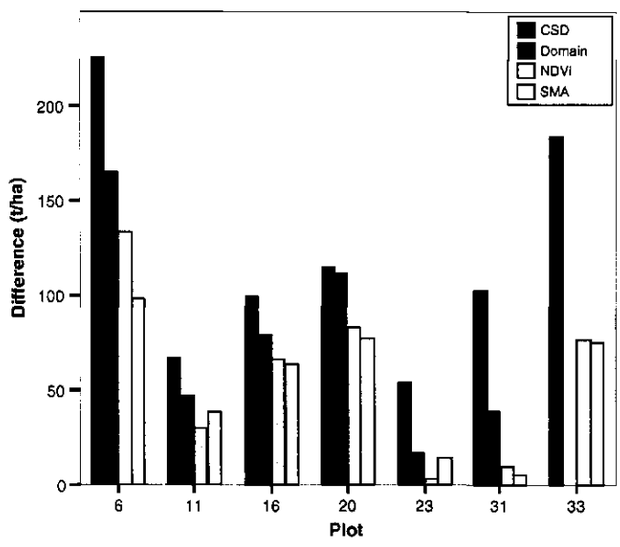

Figure 5.17– Absolute difference between estimated and measured biomass density for conifer plots. Plots where error exceeds 70 t/ha difference (natural break).

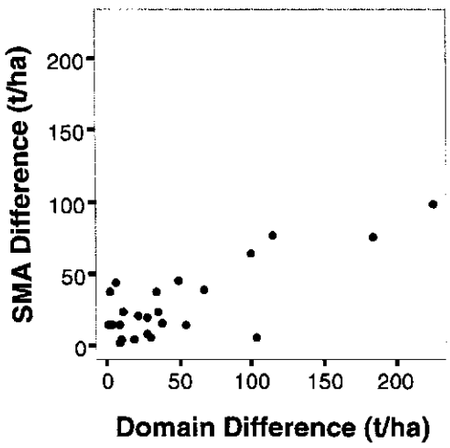

Figure 5.18– Scatterplot of error values for the SMA and spectral domain methods

Many of the interpretations made for conifer plots also applied to deciduous validation plots (Figure 5.19). There was some relationship between the magnitude of error at the plot level, but not to the extent evident in the conifer validation plots. The domain method also yielded the most accurate predictions for plots where measured biomass values were low (Plot 7, Plot 37), or high (Plot 10, Plot 12). However, in cases where individual plot biomass was near the average for all validation plots, the NDVI and SMA estimates showed slightly lower differences.

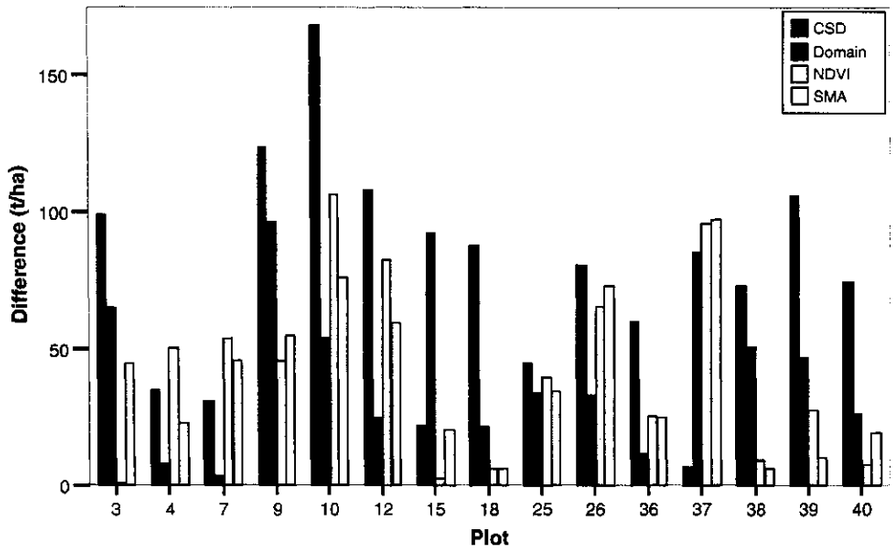

Figure 5.19– Absolute difference between estimated and measured biomass density for deciduous plots.

5.8 Summary

This chapter presented a new application of the MFM inversion method. The MFM method was used with empirical models based on crown volume for estimating biomass density. These were compared with two empirical models relating multispectral image derivatives to biomass density (SMA, NDVI). The ability to estimate biomass density was evaluated primarily on overall prediction error (absolute RMSE) and plot level prediction error among validation plots for each overstory species type.

Overall, the NDVI and SMA linear models and spectral domain MFM method had similar error. However, upon examination of the difference between measured and estimated reflectance for individual plots, it was found that the canopy reflectance model methods are more accurate at estimating lower and higher biomass values (i.e. located

outside of one σ from the average of the validation plots). This may indicate that there is some threshold at which the empirical models using SMA and NDVI become inappropriate.

The canopy reflectance model inversion method for estimating biomass density has shown potential when considering the error assessment as well as the potential for further improvements with respect to search algorithms, computational methods and more detailed canopy reflectance model development. It is expected that the canopy reflectance model inversion method has the potential to be more appropriate in areas with greater biomass density variability or studies with more detailed canopy reflectance models. The MFM inversion method also provides an explicit physical basis and produces first-order structural estimates. It is possible that other canopy reflectance models may also provide first-order parameters that may be more appropriate for empirical relationships with biomass (e.g. crown closure, LAI).

CHAPTER 6

Summary and Conclusions

6.1 Introduction

The ability to provide timely, reliable estimates of canopy structure and biomass is critically important. These data give an indication of the physical state of forests since they are related to tree physiological processes and carbon storage potential. This forest status information drives forest management, global climate change research, and policy decisions. Remote sensing methods, including the canopy reflectance model inversion method used in this research, are one of the most efficient methods for producing estimates of forest structure.

In this research, a method for predicting forest canopy structure and biomass density over large areas using multispectral imagery and a new canopy reflectance model inversion technique was developed and tested in the Canadian Rocky Mountains. This canopy reflectance model method has an advantage because it requires very little, or no, *in situ* data for direct operation. It should be noted, however, that *in situ* data are a requirement for validation of results. Another advantage to the canopy reflectance model method is that, along with biomass density, estimates of primary structural parameters as well as species type classification are produced. This method was evaluated by comparing its output to two existing empirical methods that require a significant amount of *in situ* data to produce estimates of biomass density.

This method was tested within a sub-alpine forest environment in the Front Range of the Canadian Rocky Mountains. The canopy reflectance model method was applied to

both conifer and deciduous dominant stands with variable density and canopy structure. Four different parameterization tests were implemented to evaluate the effect of input data structure on model output. Also, a series of algorithms for describing the model output were tested for cases where a number of potential solutions exist. Evaluation of the model was based on overall accuracy and prediction accuracy for individual field validation plots as well as broader issues of utility, particularly for large areas. In this chapter, a summary of the results from these tests is provided. Following this, conclusions are drawn based on the findings presented within this study. The contribution to the field of reflectance model inversion and biophysical parameter estimation research is then given followed by suggestions for future study.

6.2 Summary of Results

In this research, an indirect canopy reflectance model inversion for density, horizontal crown radius, vertical crown radius, height to crown center, height distribution and biomass, was performed using a series of input parameter sets and systems to describe multiple solutions. Four input parameter sets were used to generate MFM look-up tables (LUTs) of different size and detail. For each of these LUTs, two and four band reflectance data were employed corresponding to either SPOT band 2 and 3 or SPOT bands 1, 2, 3, and 4. These reflectance data were matched with modeled reflectance values using an exact match, spectral distance, or spectral domain method. Ancillary terrain derivative data were also incorporated for each LUT and image band combination. Potential solutions from the inversion were summarized using the mode and median of the solution distribution.

The ability to estimate canopy structure was dependant on the information content of the LUT. In general, overall prediction error decreased with increasing LUT information content. However, there was a threshold at which the improvement was less evident as a result of increasing potential solutions. When selecting from the LUT, the most effective method incorporated a reflectance domain. Use of reflectance equality also produced accurate predictions, but there were frequent cases where no solution was found. Also, when selecting from the LUT, use of four spectral information bands was more effective when selecting from less detailed LUTs and two spectral bands was more effective when selecting from more detailed LUTs. The inclusion of ancillary terrain data did not consistently increase prediction accuracy for any of the LUT test cases.

The lowest absolute RMSE over all conifer validation plots was 590 stems/ha density, 0.4 m horizontal crown radius, 0.6 m vertical crown radius, and 3.4 m height distribution. For deciduous validation plots the lowest RMSE was 320 stems/ha density, 0.4m horizontal crown radius, 0.7 m vertical crown radius, and 4.6 m height distribution. It was observed that the GOMS modeled reflectance was not sensitive to height to crown center for the illumination and canopy conditions found in this study area. As a result, solutions for height were invariant regardless of estimate method.

It was possible to invert the GOMS model for structural parameters not included within the primary parameter set, such as biomass, if this secondary parameter was derived from the primary model parameters. However, in the case of biomass density, it could not be accurately predicted since it relied on height estimates from the model. Instead, the model was inverted for biomass using the crown dimensions and density. Crown dimensions were transformed into canopy surface area; a variable which had a

reasonable correlation with tree-level biomass. The correlation strength was highest for pine ($r^2 = 0.63$) followed by aspen ($r^2 = 0.52$) and spruce ($r^2 = 0.48$).

The MFM method was an effective density predictor when using a spectral domain to develop a distribution of potential solutions and selecting the mode value from that distribution. In all cases, the most accurate estimates overall were those using 4 input spectral bands to select values from the detailed and constrained LUT (MFM run 4).

In the best case, the inversion procedure yielded estimates with an absolute RMSE for all validation plots of 51 t/ha for conifer stands and 52 t/ha for deciduous stands. These results were similar to those predicted using a linear regression with NDVI (48 t/ha conifer, 53 t/ha deciduous) and slightly higher than those predicted using a linear regression with SMA derived background fraction (38 t/ha conifer, 48 t/ha deciduous). However, upon examination of individual plot results, it appeared that the canopy reflectance model method was more effective for predicting lower biomass density values than the SMA method. All of the methods showed high error levels when predicting biomass density where the validation data exceeded 200 t/ha.

While empirical models using NDVI and SMA have reached a level of maturity in terms of development, the canopy reflectance model inversion method has potential for further improvement. This study showed that additional development of the indirect inversion selection criteria used within the MFM method can lead to improvements in overall accuracy. With further canopy reflectance model developments and advances in distributed computing architecture it is expected that there will be corresponding improvements in prediction accuracy and efficiency for the canopy reflectance model indirect inversion method. The MFM method also has the added advantage of an explicit

physical basis. Thus, the MFM method can provide the primary structural parameters in addition to any empirically derived parameters.

6.3 Conclusions

The main conclusions drawn from this research were:

- It was possible to estimate canopy structure and biomass density using a highly automated indirect canopy reflectance inversion modelling procedure with very few *in situ* data requirements. The accuracy of these estimates was similar to existing empirical multispectral methods.
- Prediction accuracy within the canopy reflectance model inversion was related to the detail of input parameter range and increment size used in the LUT creation stage.
- Using field data to constrain LUTs in the inversion process yielded more accurate structural estimates due to the removal of erroneous potential solutions.
- Using the median value when summarizing the distribution of potential solutions consistently lead to more accurate estimates of canopy structure.
- Canopy reflectance model inversion has potential for use in studies where gathering extensive *in situ* data for empirical modelling is costly, not feasible, or impossible.

6.4 Contribution to Research

In a broad context, this research has presented a new methodology for estimating biomass density using canopy reflectance models and satellite imagery. Knowledge of

biomass density and above ground total biomass is important in a number of fields. The relationship between biomass and stored carbon within forested areas is an important current research thrust in global climate change studies (Brown, 2002), specifically, within the context of afforestation, deforestation, and reforestation monitoring where aboveground biomass stocks for vast areas are of interest. The methods presented in this study are applicable to large spatial extents and also automated allowing for processing of large data sets including time-series imagery for temporal studies.

Within a forest management context, this new method can be used to supplement pre-existing inventory procedures. Parameters such as crown closure, biomass, and volume estimated with the inversion procedure can provide additional information for forest fire modelling, harvest potential and vegetation health. In fact, this information may also be of use to a range of ecologists within habitat studies where crown dimensions are of importance, or where canopy gap fraction dictates understory growth, habitat function, or wildlife mobility.

This MFM canopy reflectance model inversion method is physically based and provides an alternative to strictly statistical models using multispectral image derivatives. The methodology presented within this thesis has been automated to a high degree and implemented in software. The creation of this software was undertaken with flexibility in mind and as a result can easily be converted for use with new and more advanced canopy reflectance models or image data sets (e.g. MODIS). As an additional benefit, this new methodology can now be applied to other areas, forest types and eco-regions with little overhead, time, or expense relative to previous implementations. It is also now possible

to incorporate powerful canopy reflectance models in image processing methods like topographic correction (Soenen et al., 2005) and relative radiometric correction.

Within the field of canopy reflectance modelling, this work has advanced the understanding of parameterization for inversion and the potentials and limits of the indirect inversion method. It is of critical importance to understand the trade off between accuracy and computational efficiency when using indirect inversion methods. It has been shown here that there is a definite link between parameterization and estimate accuracy. Further, this work has shown that it is possible to invert a canopy reflectance model for parameters not directly included within the input parameter set providing there is some physical or statistical linkage to the primary parameters. This work has also examined the effect of multiple potential solutions to the inversion and presented methods to quantify and summarize these potential solutions. The idea of multiple potential solutions has also been examined from the aspect of error in modeled and measured reflectance. As a result of pursuing a greater understanding of these factors, the limits of prediction accuracy for indirect inversion of the GOMS model have been further defined.

Within this thesis, the canopy reflectance inversion procedure was also compared with existing multispectral methods. This comparison gave an indication of the relative effectiveness of the inversion procedure in its current implementation as well as additional decision criteria when weighing the importance of accuracy and efficiency. It was concluded that the inversion procedure is a promising research area since it is similar in accuracy to traditional empirical methods and outperforms these traditional methods in a variety of important ways.

6.5 Future Research

The inversion procedure shows significant promise not only in the realm of canopy structure prediction but also in other ways. The first suggestion is for the inversion procedure to use newer, more detailed canopy reflectance models. The GORT model (Ni et la., 1999) for example is a geometric optical radiative transfer hybrid that incorporates a more complex description of individual canopy elements and within-crown radiative transfer while maintaining the simplicity of parallel-ray geometry. The GOMS model involves a high level of abstraction of the canopy and is limited in its description of within-crown shadowing and gaps. The inclusion of within-canopy gap might increase the sensitivity of the model at higher densities as well as providing a more accurate representation of within-canopy light interaction. However, this occurs at a trade off with computational efficiency. In addition, LAI, a parameter of some significance, is a primary model variable.

A second area for further research is to determine if there is any relationship between the structural values from the distribution of potential inversion solutions and the measured distribution of the structural parameter. It is possible that canopy structural conditions are auto-correlated within a spectral domain. If this is true and the autocorrelation is similar to that found on the ground, then it may be possible to locate a spectral domain that yields a solution distribution similar to that found in the field.

An important area neglected by this study was transition zones between forest stands and areas of mixed forest. These areas are more complex and variable with respect to canopy structure. It would be necessary to apply a mixed empirical biomass model for

these areas. Mixed forest stands were not an emphasis in this study, thus further research is required toward predicting biomass density in mixed forest areas.

An area for further study outside the realm of biophysical parameter estimates is that of relative radiometric correction. Given a suitable canopy reflectance model and *in situ* information for a number of sites spatially distributed within an image, it may be possible to use modeled canopy reflectance to correct image reflectance. By comparing image reflectance and model reflectance at field sites it may be possible to derive a function to relate the two.

There are further forestry applications where the inversion method may also be of use. The first of these is within a forest fire modelling context. Canopy bulk density and canopy extent are important parameters within forest fire modelling (Riano et al., 2004). This study has shown that canopy dimensions can be accurately estimated. Other models may include canopy bulk density, or primary parameters that may yield canopy bulk density. The method presented within this study could also be applied to quantify the amount of biomass lost during a fire through temporal analysis. This could give some indication of the amount of above ground carbon stored in the forest overstory and released to the atmosphere.

REFERENCES CITED

Abuelgasim, A.A., and A.H. Strahler. 1994. Modelling Bidirectional Radiance Measurements Collected by the Advanced Solid-State Array Spectroradiometer (ASAS) over Oregon Transect Conifer Forests. *Remote Sensing of Environment.* 47: p. 261 – 275.

Adams, J., M. Smith, and A. Gillespie, 1993. Imaging Spectroscopy: Interpretation Based Upon Spectral Mixture Analysis. In, "Topics in Remote Sensing and Remote Geochemical Analysis: Elemental and Mineralogical Composition", Cambridge: Cambridge University Press. Ed. Pieters, C., and P. Englert. p. 145 – 166.

Atkinson, P.M., G.M. Foody, P.J. Curran, and D.S. Boyd, 2000. Assesing the Ground Data Requirements for Regional Scale Remote Sensing of Tropical Forest Biophysical Properties. *International Journal of Remote Sensing.* 21(13&14): p. 2571 – 2587.

Avery, T.E., G.L., Berlin, 1985. *Interpretation of Aerial Photographs.* Minneapolis, Minnesota: Burgess Publishing Company.

Baltzer, H. 2001. Forest Mapping and Monitoring with Interferometric Synthetic Aperture Radar (InSAR). *Progress in Physical Geography.* 25(2): p. 159 – 177.

Banfield, G.E., J.S. Bhatti, H. Jiang, M.J. Apps. 2002. Variability in Regional Scale Estimates of Carbon Stocks in Boreal Forest Ecosystems: Results from West-Central Alberta. *Forest Ecology and Management.* 169: p. 15 – 27.

Bannari, A., D. Morin, F. Bonn, and A.R. Huete, 1995. A Review of Vegetation Indices. *Remote Sensing Reviews.* 13: p. 95 – 120.

Baskerville, G.L. 1972. Use of Logarithmic Regression in Estimation of Plant Biomass. *Canadian Journal of Forestry.* 2: p. 49 – 53.

Bond-Lamberty B., C. Wang, and Gower, S.T., 2002. Aboveground and Belowground Biomass and Sapwood Area Allometric Equations for Six Boreal Tree Species of Northern Manitoba. *Canadian Journal of Forest Research.* 32: p. 1441 – 1450.

Brown, S., 2002. Measuring Carbon in Forests: Current Status and Future Challenges. *Environmental Pollution.* 116: 363 – 372.

Buckley, D.S., J.G. Isebrands, T.L. Sharik, 1999. Practical Field Methods of Estimating Canopy Cover, PAR, and LAI in Michigan Oak and Pine Stands. *Northern Journal of Applied Forestry*. 16 p. 25 – 32.

Bunnell, F.L., and D. J. Vales, 1989. Comparison of Methods for Estimating Forest Overstory Cover: Differences Among Techniques. *Canadian Journal of Forestry*. 20 p. 101 – 107.

Butler, D., and Q. Schiermeier, 2005. Grim but Determined – The G8 Reaches Accord on Africa and Climate. *Nature*. 436(7048): p. 156 – 157.

Carlson, T.N., E.M. Perry, and T.J. Schmugge, 1990. Remote Estimation of Soil Moisture Availability and Fractional Vegetation Cover for Agricultural Fields. *Agricultural and Forest Meteorology*. 52: p. 45 – 69.

Cavayas, F., and P.M. Teillet, 1985. Geometric Model Simulations of Conifer Canopy Reflectance. *Proceedings of the 3rd International Colloquium on Spectral Signatures of Objects in Remote Sensing, Les Arcs, France, 16 – 20 Dec.* p. 183 – 189.

Chen, J.M., 1996. Evaluation of Vegetation Indices and a Modified Simple Ratio for Boreal Applications. *Canadian Journal of Remote Sensing*. 22(3): p. 229 – 242.

Chen, J.M., X. Li, T. Nilson, A. Strahler. 2000. Recent Advances in Geometrical Optical Modelling and its Applications. *Remote Sensing Reviews*. 18: p. 227 – 262.

Civco, D.L., 1989. Topographic Normalization of Landsat Thematic Mapper Digital Imagery. *Photogrammetric Engineering and Remote Sensing*. 55(9): p. 1303-1309.

Colby, J.D., 1991. Topographic Normalization in Rugged Terrain. *Photogrammetric Engineering and Remote Sensing*. 57(5): p. 531- 537.

Colby, J.D. and P.L. Keating, 1998. Land Cover Classification Using Landsat TM Imagery in the Tropical Highlands: The Influence of Anisotropic Reflectance. *International Journal of Remote Sensing*. 19(8): p. 1479 - 1500.

Combal, B., F. Baret, M. Weiss, A. Tubuil, D. Mace, A. Pragnere, R. Myeni, Y. Knyazikhin, and L. Wang, 2002. Retrieval of Canopy Biophysical Variables from Bidirectional Reflectance Using Prior Information to Solve the Ill-Posed Inverse Problem. 84: p. 1 – 15.

Conese, C., M.A. Gilabert, F. Maselli, L. Bottai, 1993. Topographic Normalization of TM Scenes through the Use of an Atmospheric Correction Method and Digital Terrain Models. *Photogrammetric Engineering and Remote Sensing*. 59(12): p. 1745-1753.

De Jong, S.M., E.J. Pebesma, B. Lacaze, 2003. Above-Ground Biomass Assessment of Mediterranean Forests Using Airborne Imaging Spectrometry: The DAIS Peyne Experiment. *International Journal of Remote Sensing*. 24(7): p. 1505 – 1520.

Del Frate, F., D. Solimini, 2004. On Neural Network Algorithms for Retrieving Forest Biomass From SAR Data. *IEEE Transactions on Geoscience and Remote Sensing*. 42(1): p. 24 – 34.

Dong, J., R.K. Kaufmann, R.B. Myeni, C.J. Tucker, P.E. Kauppi, J. Liski, W. Buermann, A. Alexeyev, M.K. Hughes, 2003. Remote Sensing Estimates of Boreal and Temperate Forest Woody Biomass: Carbon Pools, Sources, and Sinks. *Remote Sensing of Environment*. 84: p. 393 – 410.

Dymond, J.R., J.D. Shepard, 1999. Comment on "Topographic Normalization of Landsat TM Images of Forest Based on Subpixel Sun-Canopy-Sensor Geometry," by Gu and Gillespie (*Remote Sens. Environ.* 64:166-175, 1998). *Remote Sensing of Environment*. 69:194.

Ekstrand, S., 1996. Landsat TM-Based Forest Damage Assesment: Correction for Topographic Effects. *Photogrammetric Engineering and Remote Sensing*, 1996. 62(2): p. 151 - 161.

Elvidge, C.D., R.J.P. Lyon, 1985. Influence of Rock-Soil Spectral Variation on the Assesment of Green Biomass. *Remote Sensing of Environment*. 17: p. 265 – 279.

Fournier, R.A., J.E. Luther, L. Guindon, M.C. Lambert, D. Piercey, R.J. Hall, and M.A. Wulder. Mapping Aboveground Tree Biomass at the Stand Level from Inventory Information: Test Cases in Newfoundland and Quebec. *Canadian Journal of Forest Research*. 33 p. 1846 – 1863.

Franklin, J., F.W. Davis, and P. Lefebvre. 1991. Thematic Mapper Analysis of Tree Cover in Semiarid Woodlands Using a Model of Canopy Shadowing. *Remote Sensing of Environment.* 36: p. 189 – 202.

Franklin, S.E., R.J. Hall, L.Smith, G.R. Gerylo, 2003. Discrimination of Conifer Height, Age, and Crown Closure Classes using Landsat-5 TM Imagery in the Canadian Northwest Territories. *International Journal of Remote Sensing.* 24(9): 1823 – 1834.

Fransson, J.E.S., G. Smith, J. Askne, and H. Olsson, 2001. Stem Volume Estimation in Boreal Forests Using ERS-1/2 Coherence and SPOT XS Optical Data. *International Journal of Remote Sensing.* 22(14): p. 2777 – 2791.

Frazer, G.W., R.A. Fournier, J.A. Trofymow, R.J. Hall, 2001. A comparison of Digital and Film Fisheye Photography for Analysis of Forest Canopy Structure and Gap Light Transmission. *Agricultural and Forest Meteorology.* 109: p. 249 – 263.

Gao, X., A.R. Huete, W. Ni, T. Miura, 2000. Optical-Biophysical Relationships of Vegetation Spectra without Background Contamination. *Remote Sensing of Environment.* 74: p. 609 – 620.

Gaveau, D.L.A., 2002. Modelling the Dynamics of ERS-1/2 Coherence with Increasing Woody Biomass over Boreal Forests. *International Journal of Remote Sensing.* 23(18): p. 3879 – 3885.

Gemmell, F. 1995. Effects of Forest Cover, Terrain, and Scale on Timber Volume Estimation with Thematic Mapper Data in a Rocky Mountain Site. *Remote Sensing of Environment.* 51: p. 291 – 305.

Gemmell, F. 1998. An Investigation of Terrain Effects on the Inversion of a Forest Reflectance Model. *Remote Sensing of Environment.* 65: p. 155 – 168.

Gerylo, G.R., R.J. Hall, S.E. Franklin, and L. Smith, 2002. Empirical Relations Between Landsat TM Spectral Response and Forest Stands near Fort Simpson, Northwest Territories, Canada. *Canadian Journal of Remote Sensing.* 28: p. 68 – 79.

Gougeon, F.A. 1995. A Crown-Following Approach to the Automatic Delineation of Individual Tree Crowns in High Spatial Resolution Aerial Images. *Canadian Journal of Remote Sensing.* 21: p. 274 – 284.

Gould, S.J., 1966. Allometry and Size in Ontogeny and Phylogeny. *Biological Review.* 41 p. 587 – 640.

Gruninger, J.A., J. Ratkowski, and M.L. Locke, 2004. The Sequential Maximum Angle Convex Cone (SMACC) Endmember Model. *Proceedings, SPIE Algorithms for Multispectral and Hyperspectral and Ultraspectral Imagery, Orlando, FL, April, 2004.* Vol. 5425-1.

Green, R., 1979. *Sampling Design and Statistical Methods for Environmental Biologists.* Toronto: Wiley.

Gu, D. and A. Gillespie, 1998. Topographic Normalization of Landsat TM Images of Forest Based on Subpixel Sun-Canopy-Sensor Geometry. *Remote Sensing of Environment.* 64 p. 166 - 175.

Gu, D., A.R. Gillespie, J.B. Adams, R. Weeks, 1998. A Statistical Approach for Topographic Correction of Sattelite Images by Using Spatial Context Information. *IEEE Transactions on Geoscience and Remote Sensing.* 37(1): 236 – 246.

Gu, D. and A. Gillespie, 1999. Response to Dymond and Shepard's Comment on "Topographic Normalization of Landsat TM Images of Forest Based on Subpixel Sun-Canopy-Sensor Geometry. *Remote Sensing of Environment.* 69: p. 195 - 196.

Guindon, L., J. Luther, R. Fournier, M-C. Lambert, D. Piercy, 2003. Mapping Forest Biomass Using Landsat TM and Forest Inventory Data: Test Case in Newfoundland. *Proceedings, 25th Canadian Symposium on Remote Sensing,* Montreal, PQ., Canada. (CD-ROM).

Hall, R.J. 2003. The Roles of Aerial Photographs in Forestry Remote Sensing Image Analysis. In M. Wulder & S. Franklin (Eds.), *Remote Sensing of Forest Environments: Concepts and Case Studies* (p. 47 -75). Boston: Kluwer Academic Publishers.

Hall, R.J., R.S. Skakun, E.J. Arsenault, B.S. Case, 2006. Modeling Forest Stand Structure Attributes using Landsat ETM+ data: Application to Mapping of Aboveground Biomass and Stand Volume. *Forest Ecology and Management.* 225: p. 378 – 390.

Hall, F.G., Y.E. Shimabukuro, K.F. Huemmerich, 1995. Remote Sensing of Forest Biophysical Structure using Mixture Decomposition and Geometric Reflectance Models. *Ecological Applications*. 5(4): p. 993 – 1013.

Hall, F.G., D.R. Peddle, and E.F. LeDrew, 1996. Remote Sensing of Biophysical Variables in Boreal Forest Stands of Picea Mariana. *International Journal of Remote Sensing: Letters*. 17(15): p. 3077 – 3081.

Hall, F.G., D.E. Knapp, and K.F. Huemmrich, 1997. Physically Based Classification and Satellite Mapping of Biophysical Characteristics in the Southern Boreal Forest. *Journal of Geophysical Research*. 102(D24): p. 29567 – 29580.

Hame, T., A. Salli, K. Andersson, A. Lohi, 1997. A New Methodology for the Estimation of Biomass of Conifer-Dominated Boreal Forest Using NOAA AVHRR data. *International Journal of Remote Sensing*. 18(15): p. 3211 – 3243.

Hernandez, R.P. and D. Lee, 2002. Terrestrial Ecosystems as Carbon Sources and Sinks. Occasional Paper. Environmental and Resource Studies, Department of Geography, Trent University. 15p.

Huete, A.R., 1985. Spectral Response of a Plant Canopy with Different Soil Backgrounds. *Remote Sensing of Environment*. 17: p. 37 – 53.

Hugli, H. and W. Frei, 1983. Understanding Anisotropic Reflectance in Mountainous Terrain. *Photogrammetric Engineering and Remote Sensing*. 49(5): p. 671 - 683.

Husch, B., T.W. Beers, and J.A. Kershaw, 2003. *Forest Mensuration*. Hoboken, New Jersey: John Wiley & Sons, Inc.

Itten, K.I. and P. Meyer, 1992. Geometric and Radiometric Correction of TM Data of Mountainous Forested Areas. *IEEE Transactions on Geoscience and Remote Sensing*. 31(4): p. 764 - 770.

Jasinski, M.F., and P.S. Eagleson, 1990. Estimation of Subpixel Vegetation Cover Using Red-Infrared Scattergrams. *IEEE Transactions in Geoscience and Remote Sensing*. 28(2): p. 253 – 267.

Jensen, J.R., M.E. Hodgson. 1985. Remote Sensing Forest Biomass: An Evaluation Using High Resolution Remote Sensor Data and Loblolly Pine Plots. *Professional Geographer.* 37(1): p. 46 – 56.

Johnson, R.L., D.R. Peddle, and R.J. Hall, 2000. A modeled-based sub-pixel scale mountain terrain normalization algorithm for improved LAI estimation from airborne casi imagery. *Proceedings, 22nd Canadian Symposium on Remote Sensing, Victoria, BC., Canada. August 21-25, 2000. Canadian Aeronautics and Space Institute, Ottawa, 2000*: p. 415 - 424.

Justice, C.O., S.W. Wharton, and B.N. Holben, 1981. Application of Digital Terrain Data to Quantify and Reduce the Topographic Effect on Landsat Data. *International Journal of Remote Sensing* 2(3): p. 213 - 230.

Kaufmann, M.R., C.A. Troendle, 1981. The Relationship of Leaf Area and Foliage Biomass to Sapwood Conducting Area in Four Subalpine Forest Tree Species. *Forest Science.* 27(3) p. 477 – 482.

Kellndorfer, J., W. Walker, L. Pierce, C. Dobson, J.A. Fites, C. Hunsaker, J. Vona, M. Clutter, 2004. Vegetation Height Estimation from Shuttle Radar Topography Mission and National Elevation Datasets. *Remote Sensing of Environment.* 93: p. 339 – 358.

Kimes, D.S. and J.A. Kirchner, 1981. Modelling the Effects of Various Radiant Transfers in Mountainous Terrain on Sensor Response. *IEEE Transactions on Geoscience and Remote Sensing.* GE - 19(2): p. 100 - 108.

Kimes, D.S., Y. Knyazikhin, J. Privette, A. Abuelgasim, and F. Gao, 2000. Inversion Methods for Physically Based Models. *Remote Sensing Reviews.* 18: p. 381 – 440.

Knyazikhin, Y. and Marshak, A. 1991. Fundamental Equations of Radiative Transfer in Leaf Canopies and Iterative Methods for their Solution. In: *Photon-Vegetation Interactions: Applications in Plant Physiology and Optical Remote Sensing,* edited by Myeni, R.B. and Ross, J. p 9 – 43, Springer – Verlag, New York.

Knyazikhin, Y., J.V. Martonchik, R.B. Myeni, D.J. Diner, and S.W. Running, 1998a. Synergistic Algorithm for Estimating Vegetation Canopy Leaf Area Index and Fraction of Absorbed Photosynthetically Active Radiation from MODIS and MISR data. *Journal of Geophysical Research.* 103: p. 32257 – 32275.

Knyazikhin, Y. J.V. Martonchik, D.J. Diner, R.B. Myeni, M. Verstraete, B. Pinty, and N. Gobron, 1998b. Estimation of Vegetation Canopy Leaf Area Index and Fraction of Absorbed Photosynthetically Active Radiation from Atmosphere Corrected MISR data. *Journal of Geophysical Research.* 103: p. 32239 – 32256.

Kuplich, T.M., V. Salvatori, and P.J. Curran, 2000. JERS-1/SAR Backscatter and its Relationship with Biomass of Regenerating Forests. *International Journal of Remote Sensing.* 21(12): p. 2513 – 2518.

Leblanc, S.G. and J.M. Chen, 2000. A Windows Graphic User Interface (GUI) for the Five-Scale model for Fast BRDF Simulations. *Remote Sensing Reviews.* 19: p. 293 – 305.

Lefsky, M.A., W.B. Cohen, D.J. Harding, G.G. Parker, S.A. Acker, S.T. Gower, 2002. LiDAR Remote Sensing of Above-Ground Biomass in Three Biomes. *Global Ecology and Biogeography.* 11: p.393 – 399.

Li, X. and A.H. Strahler. 1985. Geometric-Optical Modelling of a Conifer Forest Canopy. *IEEE Transactions in Geoscience and Remote Sensing.* GE-23 5: 705 – 721.

Li, X. and A.H. Strahler. 1992. Geometric-Optical Bidirectional Reflectance Modelling of the Discrete Crown Vegetation Canopy: Effect of Crown Shape and Mutual Shadowing. *IEEE Transactions on Geoscience and Remote Sensing.* 30(2): p. 276 – 292.

Lim, K., P. Treitz, M. Wulder, B. St-Onge, M. Flood, 2003. LiDAR Remote Sensing of Forest Structure. *Progress in Physical Geography.* 27(1): p. 88 – 106.

Lim, K.S. and P.M. Trietz, 2004. Estimation of Above Ground Forest Biomass from Airborne Discrete Return Laser Scanner Data Using Canopy-Based Quantile Estimators. *Scandanavian Journal of Forest Research.* 19: p. 558 – 570.

Lucas, R.M., M. Moghaddam, N. Cronin, 2004. Microwave Scattering From Mixed-Species Forests, Queensland, Australia. *IEEE Transactions on Geoscience and Remote Sensing.* 42(10): p. 2142 – 2159.

Luther, J.E., R.A. Fournier, R.J. Hall, C.H. Ung, L. Guindon, D.E. Piercey, M.C. Lambert and A. Beaudoin, 2003. A Strategy for Mapping Canada's Forest Biomass with Landsat TM Imagery. *Proceedings, 25th Canadian Symposium on Remote Sensing,* Montreal, PQ., Canada. (CD-ROM).

Malhi Y., P. Meir, And S. Brown, 2003. Forests Carbon and Global Climate. In, Capturing Carbon and Conserving Biodiversity, I. Swingland (Editor), Sterling, VA, Earthscan, p. 15 – 41.

McDonald, A.J., F.M. Gemmell, and P.E. Lewis, 1998. Investigation of the Utility of Spectral Vegetation Indices for Determining Information on Coniferous Forests. *Remote Sensing of Environment.* 66: 250 – 272.

Minnaert, M., The Reciprocity Principle in Lunar Photometry. *Astrophysical Journal,* 1941. 93: p. 403 - 410.

Meyer, P., K.I. Itten, T. Kellenberger, S. Sandmeier, R. Sandmeier. 1993. Radiometric Corrections of Topographically Induced Effects on Landsat TM data in an Alpine Environment. *ISPRS Journal of Photogrammetry and Remote Sensing.* 48(4): p. 17 - 28.

Moran, M.S., T.R. Clarke, J. Qi, E.M. Barnes, and P.J. Pinter, 1997. Practical Techniques for Conversion of Airborne Imagery to Reflectances. *Proceedings of the 16th Biennial Workshop on Videography and Color Photography in Resource Management, Weslaco, Texas April 29 – May 1, 1997.* p. 82 – 95.

Morsdorf, F., E. Meier, B. Kotz, K.I. Itten, M. Dobbertin, B. Allgower. 2004. LiDAR-Based Geometric Reconstruction of Boreal Type Forest Stands at Single Tree Level for Forest and Wildland Fire Management. *Remote Sensing of Environment.* 92: p. 353 – 362.

Natural Resources Canada, Canadian Forest Service. 2006. *The State of Canada's Forests: 2004 – 2005.* Ottawa: Author.

Ni, W., X. Li, C.E. Woodcock, M.R. Caetano, and A.H. Strahler, 1999. An Analytical Hybrid GORT Model for Bidirectional Reflectance Over Discontinuous Plant Canopies. *IEEE Transactions on Geoscience and Remote Sensing.* 37(2): p. 987 – 999.

Ni-Meister, W., D. Jupp, R. Dubayah, 2001. Modelling Lidar Waveforms in Heterogeneous and Discrete Canopies. *IEEE Transactions in Geoscience and Remote Sensing*. 39(9): p. 1943 – 1958.

Nichol, J., and C.M. Lee, 2005. Urban Vegetation Monitoring in Hong Kong using High Resolution Multispectral Images. *International Journal of Remote Sensing*. 26(5): p. 903 – 918.

Okuda, T., M. Suzuki, S. Numata, K. Yoshida, S. Nishimura, N. Adachi, K. Niiyama, N. Manokaran, M. Hashim. 2004. Estimation of Aboveground Biomass in Logged and Primary Lowland Rainforests using 3-D Photogrammetric Analysis. *Forest Ecology and Management.* 203: p. 63 – 75.

Parresol, B.R., 1999. Assesing Tree and Stand Biomass: A review with Examples and Critical Comparisons. *Forest Science*. 45(4): p. 573 – 593.

Patenaude, G., R.A. Hill, R. Milne, D.L.A. Gaveau, B.B.J. Briggs, T.P. Dawson, 2004. Quantifying Forest Above Ground Carbon Content Using LiDAR Remote Sensing. *Remote Sensing of Environment.* 93: p. 368 – 380.

Patenaude, G., R. Milne, T.P. Dawson, 2005. Synthesis of Remote Sensing Approaches for Forest Carbon Estimation: Reporting to the Kyoto Protocol. *Environmental Science and Policy.* (in Press).

Peddle, D.R., F.G. Hall, W. Wanner, E.F. LeDrew, 1995. Remote Sensing of Photosynthetic Activity in Boreal Forest Stands Using Spectral Mixture Analysis and Geometric-Optical Reflectance Models. *Proceedings, International Colloquium on Photosynthesis and Remote Sensing, Montpellier, France, 1995.* p. 159 – 170.

Peddle, D.R. 1998. Field Spectroradiometer Data Acquisition and Processing for Spectral Mixture Analysis in Forestry and Agriculture. *Proceedings, First International Conference on Geospatial Information in Agriculture and Forestry, Lake Buena Vista, Florida, June 1998.*

Peddle, D.R., 1999. Multiple Forward Mode (MFM) Reflectance Modelling: A New Approach to Obtaining Forest Physical-Structural Information by Radiative Transfer Inversion of Remote Sensing Imagery. *Unpublished Internal Document* – Department of Geography, University of Lethbridge, Alberta, February, 1999.

Peddle, D.R., F.G. Hall, E.F. LeDrew, 1999. Spectral Mixture Analysis and Geometric-Optical Reflectance Modelling of Boreal Forest Biophysical Structure. *Remote Sensing of Environement*. 67: p. 288 – 297.

Peddle, D.R., H.P. White, R.J. Soffer, J.R. Miller, E.F. LeDrew. 2001. Reflectance Processing of Remote Sensing Spectroradiometer Data. *Computers and Geosciences*. 27: 203 – 213.

Peddle, D.R., S.P. Brunke and F.G. Hall, 2001a. A Comparison of Spectral Mixture Analysis and Ten Vegetation Indices for Estimating Boreal Forest Biophysical Information from Airborne Data. *Canadian Journal of Remote Sensing*. 27(6): 627 – 635.

Peddle, D.R., P.M. Teillet, and M.A. Wulder, 2003a. Radiometric Image Processing, Chapter 7, in *Remote Sensing of Forest Environments: Concepts and Case Studies*, M.A. Wulder and S.E. Franklin, Editors. 2003, Kluwer Academic Press: London Dordrecht Boston Norwell, Massachusetts, USA. p. 181 - 208.

Peddle, D.R., S.E. Franklin, R.L. Johnson, M.A. Levigne, and M.A. Wulder, 2003b. Structural Change Detection in a Disturbed Conifer Forest Using a Geometric Optical Reflectance Model in Multiple Forward Mode. *IEEE Transactions in Geoscience and Remote Sensing*. 41(1): p. 163 – 166.

Peddle, D.R., J. E. Luther, N. Pilger, D. Piercey, 2003c. Forest Biomass Estimation Using a Physically-Based 3-D Structural Modelling Approach for Landsat TM Cluster Labeling. *Proceedings, 25th Canadian Symposium on Remote Sensing,* Montreal, PQ., Canada. (CD-ROM).

Peddle, D.R., R.L. Johnson, J.Cihlar, and R. Latifovic, 2004. Large Area Forest Classification and Biophysical Parameter Estimation Using the 5-Scale Canopy Reflectance Model in Multiple Forward Mode. *Remote Sensing of Environment. BOREAS Special Issue*. 89: p. 252 - 263.

Peddle, D.R., R.L. Johnson, J.Cihlar, S.G. Leblanc and J.M. Chen, 2006. MFM-5-Scale: A Physically Based Inversion Modelling Approach for Unsupervised Cluster Labelling and Independent Forest Landcover Classification. *Canadian Journal of Remote Sensing*. (accepted for publication).

Picard, G., T. Le Toan, S. Quegan, Y. Caraglio, T. Castel, 2004. Radiative Transfer Modelling of Cross-Polarized Backscatter from a Pine Forest Using the Discrete Ordinate and Eigenvalue Method. *IEEE Transactions on Geoscience and Remote Sensing.* 42(8): p. 1720 – 1730.

Pilger, N., D.R. Peddle and R.J. Hall, 2003. Forest Volume Estimation Using a Canopy Reflectance Model in Multiple-Forward-Mode. *Proceedings, 25th Canadian Symposium on Remote Sensing,* Montreal, PQ., Canada. (CD-ROM).

Pilger, N., D.R. Peddle, and J.E. Luther, 2002. Estimation of Forest Cover Type and Structure from Landsat TM Imagery using a Canopy Reflectance Model for Biomass Mapping in Western Newfoundland. In, *Proceedings, IEEE International Geoscience and Remote Sensing Symposium (IGARSS '02)/ 24th Canadian Symposium on Remote Sensing,* Toronto, ON., Canada. June 24-28, 2002. Institute for Electrical and Electronic Engineers, USA / Canadian Aeronautics and Space Institute, Ottawa. (CD-ROM).

Proy, C., D. Tanré, and P.Y. Deschamps, 1989. Evaluation of Topographic Effects in Remotely Sensed Data. *Remote Sensing of Environment.* 30: p. 21 - 32.

Riano, D., E. Chuvieco, J. Salas, and I. Aguado, 2003. Assessment of Different Topographic Corrections in Landsat-TM Data for Mapping Vegetation Types. *IEEE Transactions on Geoscience and Remote Sensing.* 41(5): p. 1056 - 1061.

Riano, D., E. Chuvieco, S. Condes, J. Gonzalez-Matesanz, S.L. Ustin. 2004. Remote Sensing of Environment. *Remote Sensing of Environment.* 92: p. 345 – 352.

Rosenqvist,A., A. Milne, R. Lucas, M. Imhoff, C. Dobson, 2003. A Review of Remote Sensing Technology in Support of the Kyoto Protocol. *Environmental Science & Policy.* 6: 441 – 455.

Rouse, J.W., R.W. Haas, J.A. Schell, D.W. Deering, J.C. Harlan, 1974. Monitoring the Vernal Advancement and Retrogradation (Greenwave Effect) of Natural Vegetation. NASA/GSFCT Type III Final Report, Greenbelt, MD, USA.

Roy, P.S., S.A. Ravan, 1996. Biomass Estimation Using Satellite Remote Sensing Data – An Investigation on Possible Approaches for Natural Forest. *Journal of Bioscience.* 21(4): 535 – 561.

Rudnicki, M., U. Silins, and V. J. Lieffers, 2004. Crown Cover is Correlated with Relative Density, Tree Slenderness, and Tree Height in Lodgepole Pine. *Forest Science*. 50(3) p. 356 – 363.

Scarth, P., S. Phinn, 2000. Determining Forest Structural Attributes Using an Inverted Geometric-Optical Model in Mixed Eucalypt Forests, Southeast Queensland, Australia. *Remote Sensing of Environment*. 71: p. 141 – 157.

Schaff, C.B., Li, X., Strahler, A.H., 1994. Topographic Effects on Bidirectional and Hemispherical Reflectances Calculated with a Geometric-Optical Canopy Model, *IEEE Trans. Geoscience Remote Sens.*, 32(6):1186-1193.

Schaaf, C.B. and A.H. Strahler. 1994. Validation of Bidirectional and Hemispherical Reflectances from a Geometric-Optical Model Using ASAS Imagery and Pyranometer Measurements of a Spruce Forest. *Remote Sensing of Environment.* 49: p. 138 – 144.

Schott, J.R., C. Salvaggio, W.J. Volchok, 1988. Radiometric Scene Normalization Using Pseudoinvariant Features. *Remote Sensing of Environment*. 26: p. 1-16.

Shabanov, N. V., Y. Knyazikhin, F. Baret, and R. Myeni. 2000. Stochastic Modelling of Radiation Regime in Discontinuous Plant Canopies. *Remote Sensing of Environment.* 74: p. 125 – 144.

Shaw, D.T., T.J. Malthus, J.A. Kupiec. 1998. High Spectral Resolution Data for Monitoring Scots Pine (*Pinus Sylvestris* L.) Regeneration. *International Journal of Remote Sensing.* 19(13): p. 2601 – 2608.

Shimabukuro, Y. and J. Smith, 1994. The Least Squares Mixing Models to Generate Fraction Images derived from Remote Sensing Multispectral Data. *IEEE Transactions on Geoscience and Remote Sensing*. 29: p. 16 – 20.

Singh, T., 1982. Biomass Equations of the Prairie Provinces. Information Report NOR-X-242. Northern Forest Research Centre, Canadian Forest Service, Environment Canada. Internal Publication.

Smith, J.A., T.L. Lin, and K.J. Ranson, 1980. The Lambertian Assumption and Landsat Data. *Photogrammetric Engineering and Remote Sensing*. 46(9): p. 1183 - 1189.

Snell, J.A.K., and J.K. Brown, 1978. Comparison of Tree Biomass Estimators – DBH and Sapwood Area. *Forest Science*. 24(4) p. 455-457.

Soenen, S.A., D.R. Peddle and C. Coburn, 2003. Topographic correction of remote sensing imagery using a canopy reflectance model. In, *Proceedings, 25th Canadian Symposium on Remote Sensing*, Montreal, PQ., Canada. Oct. 14-17, 2003. Canadian Aeronautics and Space Institute, Ottawa. (10 p., CD-ROM)

Soenen, S.A., D.R. Peddle and C. Coburn, 2005. SCS+C: A Modified Sun-Canopy-Sensor Topographic Correction in Forested Terrain. *IEEE Transactions on Geoscience and Remote Sensing*. 43(9): p. 2148 - 2158.

Spencer, J.W., 1971. Fourier Series Representation of the Position of the Sun. *Search*. 2(5), 172.

Steininger, M.K., 1996. "Secondary Forest Regrowth in the Amazon: Age, Area, and Change Estimation with Thematic Mapper Data. *International Journal of Remote Sensing*. 41(11): p. 2557 – 2567.

Stennes, B., E. Krcmar-Nozic, and G.C. van Kooten, 1998. Climate Change and Forestry: What Policy for Canada? *Sustainable Forest Management Network Working Paper 1998-2*. 13p.

Strahler, A.H., 1980. Systems Theory in Physical Geography. *Physical Geography*. 1(1): p. 1 – 27.

Strahler, A.H., C.E. Woodcock, J.A. Smith. 1986. On the Nature of Models in Remote Sensing. *Remote Sensing of Environment*. 20: p. 121 – 139.

Strahler, A.H., 1997. Vegetation Canopy Reflectance Modelling – Recent Developments and Remote Sensing Perspectives. *Remote Sensing Reviews*. 15: p. 179 – 194.

Suits, G.H. 1972. The Calulation of the Directional Reflectance of a Vegetative Canopy. *Remote Sensing of Environment*. 2: p. 117 – 125.

Teillet, P.M., B. Guindon, and D.G. Goodenough, 1982. On the Slope-Aspect Correction of Multispectral Scanner Data. *Canadian Journal of Remote Sensing*. 8(2): p. 84 - 106.

Temps, R.C., Coulson, K.L., 1977. Solar Radiation Incident Upon Slopes of Different Orientations, *Solar Energy*, 19:179-184.

Thenkabail, P.S., N. Stucky, B.W. Griscom, M.S. Ashton, J.Diels, B.Van Der Meer, E. Enclona, 2004. Biomass Estimations and Carbon Stock Calculations in the Oil

Palm Plantations of African Derived Savannas Using IKONOS Imagery. *International Journal of Remote Sensing*. 25(23): p. 5447 – 5472.

Tobler, W.R., 1979. *Cellular Geography, Philosophy in Geography*. Gale and Olsson, Eds., Dordrecht, Reidel.

Tokola, T., J. Sarkeala, and M.V.D. Linden, 2001. Use of Topographic Correction in Landsat TM-Based Forest Interpretation in Nepal. *International Journal of Remote Sensing*. 22(4): p. 551 - 563.

Treuhaft, R.N., B.E. Law, and G.P. Asner, 2004. Forest Attributes from Radar Interferometric Structure and Its Fusion with Optical Remote Sensing. *Bioscience*. 54(6): p. 561 – 571.

Tsolmon, R., T. Tateishi, and J.S.S Tetuko, 2002. A Method to Estimate Forest Biomass and its Application to Monitor Mongolian Taiga using JERS-1 SAR Data. *International Journal of Remote Sensing*. 23(22): p. 4971 – 4978.

Tucker, C., 1979. Red and Photographic Infrared Linear Combinations for Monitoring Vegetation. *Remote Sensing of Environment*. 8: p. 127 – 150.

Turner, D.P., S.V. Ollinger, and J.S. Kimball. 2004. Integrating Remote Sensing and Ecosystem Process Models for Landscape- to Regional-Scale Analysis of the Carbon Cycle. *BioScience*. 54(6): p. 573 – 584.

UNFCCC, 1997. Kyoto Protocol to the United Nations Framework Convention on Climate Change. ***http://unfccc.int***.

van Leeuwen, W.J.D., A.R. Huete, 1996. Effects of Standing Litter on the Biophysical Iterpretation of Plant Canopies with Spectral Indices. *Remote Sensing of Environment*. 55: p. 123 – 138.

Walter, J-M. N., E.F. Torquebiau, 2000. The Computation of Forest Leaf Area Index on Slope Using Fish-Eye Sensors. *Life Sciences*. 323: p. 801-813.

Wanner, W., 1994. Geometric Optical Mutual Shadowing model (GOMS): Users Manual. Unpublished document. Boston University.

Weiss, M., F. Baret, R.B. Myneni, A. Pragnere, Y. Knyazikhin. 2000. Investigation of a Model Inversion Technique to Estimate Canopy Biophysical Variables from Spectral and Directional Reflectance Data. *Agronomie*. 20: p. 3 – 22.

West, G.B., J.H. Brown, B.J. Enquist. A general Model for the Origin of Allometric Scaling Laws in Biology. *Science*. 276: p. 122 – 126.

Woodcock, C.E., J.B. Collins, V.D. Jakabhazy, X. Li, S.A. Macomber, and Y. Wu. 1997. Inversion of the Li-Strahler Canopy Reflectance Model for Mapping Forest Structure. *IEEE Transactions on Geoscience and Remote Sensing*. 2: p. 405 – 414.

Woods, K.D., A.H. Feiveson, D.B. Botkin, 1991. Statistical Error Analysis for Biomass Density and Leaf Area Index Estimation. *Canadian Journal of Forest Research*. 21: p. 974 – 989.

Wu, Y., A. H. Strahler, 1994. Remote Estimation of Crown Size, Stand Density, and Biomass on the Oregon Transect. *Ecological Applications*. (4)2: p. 299 – 312.

Wulder, M.A., 1998. Optical Remote Sensing Techniques for the Assesment of Forest Inventory and Biophysical Paramters. *Progress in Physical Geography*. 22: p. 449 -476.

Zheng, D., J. Rademacher, J. Chen, T. Crow, M. Bresee, J. Le Moine, S. Ryu, 2004. Estimating Aboveground Biomass using Landsat 7 ETM+ Data Across a Managed Landscape in Northern Wisconsin, USA. *Remote Sensing of Environment*. 93: 402 – 411.

Nonperiodical Internet Links

Environment Canada Weather Office (n.d.) Retrieved February, 2004 from: *http://www.climate.weatheroffice.ec.gc.ca/climate_normals/results_e.html?Province=ALL&StationName=Kananaskis&SearchType=BeginsWith&LocateBy=Province&Proximity=25&ProximityFrom=City&StationNumber=&IDType=MSC&CityName=&ParkName=&LatitudeDegrees=&LatitudeMinutes=&LongitudeDegrees=&LongitudeMinutes=&NormalsClass=A&SelNormals=&StnId=2402&&lang=ENG&pageid=2*

Western Canada Research Computing Grid (n.d.) Retrieved October, 2005 from – **http://www.westgrid.ca**

Appendix A – GOMS Model Sensitivity Analysis

This appendix details the results of a simple sensitivity analysis applied to the GOMS model to examine the effect of the height parameters on resulting model reflectance. It was expected that the model had little sensitivity to the height to crown parameter at low solar zenith angles in medium to high density stands such as those observed in the Kananaskis study area. Conversely, it was expected that the height distribution had an effect on modeled reflectance regardless of density and solar zenith angle as shadowing was dependant on relative, not absolute, crown positioning in the vertical dimension.

The tests were based on forward mode GOMS model runs where all parameters were held constant with the exception of height to crown center in the first set of tests and height distribution in the second set of tests. Height to crown center was varied between 7m and 17m while height distribution was varied between 5m and 15m (Tables A-1 and A-2). The remaining crown structural parameters were held constant at values representing values observed in the field. Illumination parameters were similar to those observed for the SPOT image acquisition time, with the exception of the last test in each set where the solar zenith angle was set to a lower value. Density was also varied for each test.

Table A-1 – Model input variables for height to center sensitivity analysis

Test #	density (trees/ha)	r (m)	b (m)	dh (m)	SZA	SAZ	VZA	VAZ
1	3000	1	2	10	37	157	7	15
2	1500	1	2	10	37	157	7	15
3	500	1	2	10	37	157	7	15
4	100	1	2	10	37	157	7	15
5	1500	1	2	10	5	157	7	15

Table A-2 – Model input variables for height distribution sensitivity analysis

Test #	density (trees/ha)	r (m)	b (m)	h (m)	SZA	SAZ	VZA	VAZ
6	3000	1	2	12	37	157	7	15
7	1500	1	2	12	37	157	7	15
8	500	1	2	12	37	157	7	15
9	100	1	2	12	37	157	7	15
10	1500	1	2	12	5	157	7	15

The results from the sensitivity analysis showed that model reflectance was not sensitive to the height to center parameter regardless of the stand density variation tested here (Figure A-1). However, model reflectance did vary with height in instances of lower solar zenith angles as can be seen in the results of Test 5. The results from the height distribution tests showed that modeled reflectance was sensitive to the height distribution parameter in higher density stands (Figure A-2). At lower density the modeled reflectance varied little with variation in the height distribution parameter.

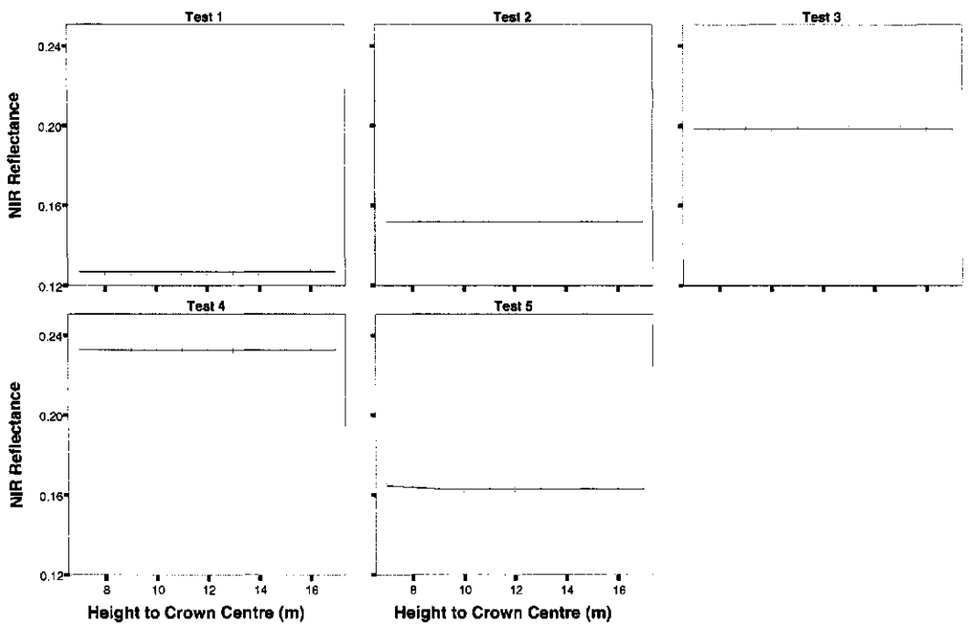

Figure A-1 – Sensitivity of GOMS modeled reflectance to the height to crown center parameter

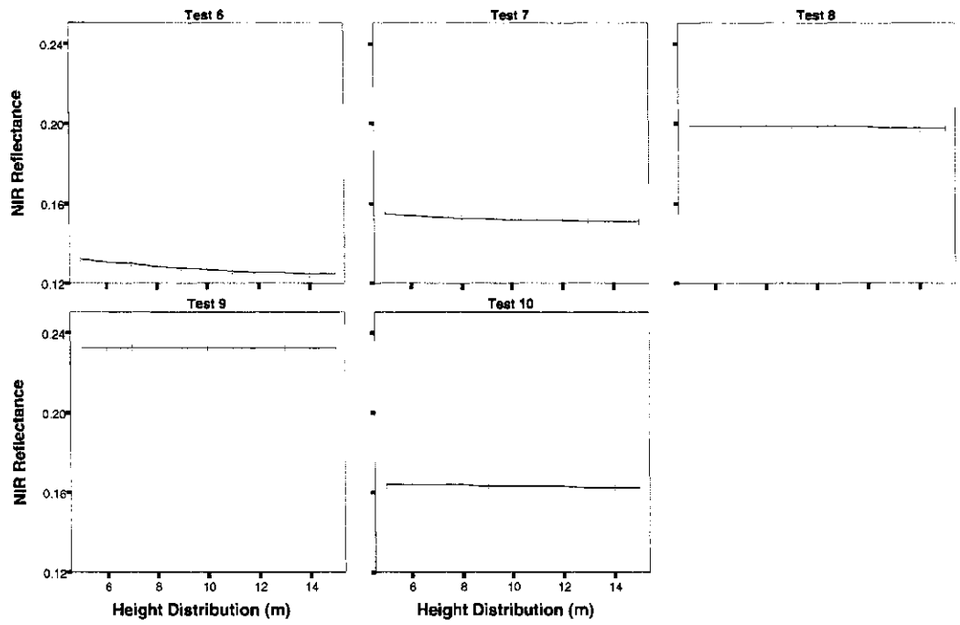

Figure A-2 – Sensitivity of GOMS modeled reflectance to the height distribution parameter

In Summary, the GOMS model had little sensitivity to the height to center parameter. This fact had significant implications within the inversion context discussed in this thesis. Since there was no variation in output reflectance when the height to center parameter was varied it was impossible to invert the model for height. This explained the lack of variation in predicted values (§ 5.4). However, the fact that height has little effect on pixel level reflectance made physical sense when examining forest stand BRDF for only one view angle close to nadir. Projected shadow area, whether it was on neighboring crowns or on the background, varied little with changes in overall canopy height. The relative positioning of the crowns within the canopy would have a greater effect on projected shadow as these changes would alter the observed texture of the canopy.